



Universität Hamburg  
DER FORSCHUNG | DER LEHRE | DER BILDUNG



CHyN  
Centre for Hybrid Nanostructures

# OPTIMIZING GOLD NANOPARTICLES UPTAKE FROM IN VITRO TO IN VIVO

## Dissertation

zur Erlangung des Doktorgrades

der Naturwissenschaften

(Dr.rer.nat)

dem

Fachbereich Chemie

der Universität Hamburg

vorgelegt von

**Yalan Huang**

Aus

Hubei, China

Hamburg, 2022

The presented work was conducted under the supervision of Prof. Wolfgang J. Parak and Dr. Neus Feliu at the Center for Hybrid Nanostructures (CHyN) of the University of Hamburg, Germany from June 2018 to June 2022.

First Evaluator: Prof. Dr. Wolfgang Parak

Second Evaluator: Prof. Dr. Wrenger Carsten

Disputation date: 07. Oct. 2022

Examination commission members:

Prof. Dr. Wolfgang Parak (Chair)

Prof. Dr. Wolfgang Maison

Prof. Dr. Neus Feliu Torres

Date: 24. April. 2023

## Index

1. Introduction.....	11
1.1 A review of the four endocytosis pathways of NPs.....	11
1.2 The effect of cell lines and cell status on the endocytosis of Au NPs .....	13
1.3 Effect of NPs size and shape on the endocytosis of Au and Ag NPs .....	14
1.4 The necessity of uptake study in a dynamic environment .....	17
1.5 In vivo distribution of Au NPs.....	18
1.6 Motivation for Study.....	19
2. The uptake of different sizes of Au NP/NRs in Hela cells in four incubation systems...22	
2.1 Introduction.....	22
2.2 Major reagents .....	23
2.3 Abbreviations.....	24
2.4 Key instruments .....	26
2.5 Materials and Methods.....	26
2.5.1 Synthesis of Au NPs and Au NRs.....	26
2.5.2 Interfacial tension (IFT) measurement.....	34
2.5.3 Cell Culture.....	35
2.5.4 Description of the four incubation systems .....	36
2.5.5 Cell viability of Hela cells incubated with different concentrations of Au NP/NRs in Static system .....	38
2.5.6 Cell viability of Hela cells incubated with Au NPs/NRs in Static, Dynamic, and Fluid systems .....	39
2.5.7 Dead/Live staining for Hela cells incubated with Au NPs/NRs in Static, Dynamic, and Suspension systems.....	40
2.5.8 Growth curve of cells in different systems .....	42
2.5.9 Static system cell uptake study: Adhered Hela cells exposed to Static Au NPs/NRs .....	42

2.5.10	Dynamic system cell uptake study: Adhered HeLa cells exposed to periodically dynamic Au NPs/NRs .....	43
2.5.11	Fluid system cell uptake study: adhered HeLa cells incubated with the continuous uni-directional flow of Au NP/NRs .....	43
2.5.12	Separation of suspended HeLa cells with free Au NPs/NRs .....	44
2.5.13	Suspension system cell uptake study: suspended HeLa cells exposed to dynamic Au NP/ NRs .....	45
2.6	Results and discussions.....	45
2.6.1	Characterization of Au NP/NRs.....	45
2.6.2	IFT at the Au NP/NRs colloid-toluene interface .....	54
2.6.3	Cell viability.....	56
2.6.4	Growth curve of cells in different systems .....	61
2.6.5	Uptake of Au NP/NR into adhered HeLa cells incubated in Static system .....	62
2.6.6	Uptake of Au NP/NR into adhered HeLa cells incubated in Dynamic system.....	65
2.6.7	Uptake of Au NP/NR into adhered HeLa cells incubated in Fluid system .....	68
2.6.8	Separation of suspended HeLa cells with free Au NPs/NRs .....	70
2.6.9	Uptake of Au NP/NR into suspended HeLa cells incubated in Suspension system	73
2.6.10	Uptake results discussion.....	75
3.	Uptake of different sizes Au NPs in Red blood cells.....	83
3.1	Introduction.....	83
3.2	Major reagents .....	83
3.3	Abbreviations.....	84
3.4	Key instruments .....	85
3.5	Materials and Methods.....	85
3.5.1	Au NPs synthesis and characterization .....	85
3.5.2	RBCs uptake experiment .....	85
3.6	Results and discussions.....	87
3.6.1	Characterization of Au NPs .....	87

3.6.2	The effect of cell density on the uptake of 4 nm Au NP into RBCs.....	94
3.6.3	The effect of Au NP concentration on the uptake of Au NP into RBCs .....	95
3.6.4	The effect of Au NP size on the uptake of Au NP into RBCs.....	97
4.	The intake and metabolism of Au NP and BSA-Eu in mosquitoes.....	99
4.1	Introduction.....	99
4.2	Major reagents .....	99
4.3	Abbreviations.....	100
4.4	Key instruments .....	102
4.5	Materials and Methods.....	102
4.5.1	synthesis of 4 nm Au NP .....	102
4.5.2	labeling of BSA with Eu .....	102
4.5.3	mosquito feeding, anesthetizing, and digestion for ICP-MS measurement.....	109
4.6	Results and discussion .....	110
4.6.1	The optimized food mixture for mosquitoes.....	110
4.6.2	The intake and metabolism of Au NP, BSA-Eu, and Iodine ion in mosquitoes...	113
5.	Summary and Outlook .....	118
5.1	The uptake of different size Au NP/NRs in Hela cells in different incubation systems .....	118
5.2	The uptake of different size Au NPs in RBCs .....	119
5.3	Ingestion and metabolism of Au NPs in mosquito .....	120
5.4	The novelties of our study.....	121
5.5	Future perspectives .....	121
6.	References.....	123
7.	Publications.....	132
8.	Acknowledgements.....	133
9.	List of hazardous substances.....	134

## **Abstract**

The effect of size/shape, the concentration of Au NPs, and the incubation time on the uptake of Au NPs in adhered cells in a Static incubation system has already been extensively investigated and some discussions were given based on the assumption of evenly distributed Au NPs in the incubation space and also the unchanged concentration of Au NPs during the incubation time. However, the finding of the higher concentration of big Au NPs (approximate size larger than 50 nm level) at the bottom of the cell culture flask or plate compared to the upper zone due to the gradual gravity-inducing-sedimentation might challenge former understandings of uptake study. But in this thesis, in the three incubation systems except for the Static system, the gradual gravity-inducing-sedimentation of Au NPs has been disrupted by continuous mixing. In addition, the Dynamic and uni-directional Fluid incubation systems in this thesis simulate the *in vivo* dynamic environment encountered by Au NPs, which can provide direct references, for example, the optimized dose and size of Au NPs, for *in vivo* applications of Au NPs. Based on ICP-MS (Inductively Coupled Plasma - Mass Spectrometry) combined with cell counting, the internalized Au mass per cell instead of Au NP number per cell was used as the exclusive standard to compare the size/shape-dependent, Au concentration-dependent, and incubation time-dependent uptake behavior of Au NPs in all these four systems and also analyze the effect of incubation systems on the uptake behavior. Our results indicated the much higher uptake induced by twice the concentration of Au NPs and also the gradually increased uptake with prolonged incubation time in all these four systems, regardless of the Au NP/NRs size/shape, Au NPs motions, and also Hela cell status changes in these four systems. Besides, compared to other smaller Au NPs (5, 25 nm Au NPs and 40 nm Au NRs), the uptake of 50 nm and 100 nm Au NPs was to a larger extent negatively affected by the incubation changing from Static to Dynamic and Fluid. For example, the 24 h uptake of 50 nm and 100 nm Au NPs in the Dynamic system is less than 50% of the 24 h uptake in the Static system, and the 4 h uptake of 50 nm and 100 nm Au NP in the Fluid system is even less than 10% of the 4 h uptake in Dynamic system, inferring the strong adverse effect of Au NP motions on the uptake and providing a reference for the dose used in *in vivo* applications. Another interesting finding is the common uptake behavior in Static, Dynamic, and Fluid systems that the internalized Au mass per cell of larger Au NPs (50 nm, 100 nm Au NP, and 100 nm Au NR) is much higher than that of smaller Au NPs (5 nm, 25 nm Au NPs, and 40 nm Au NR) disappeared in the Suspension system in which both Au NPs and Hela cells were suspended. This can be attributed to the higher contact possibility between smaller Au NPs and suspension

Hela cells compared to bigger Au NPs due to the much faster Brownian motion and also the higher penetration ability of smaller Au NPs into the Hela cell tumor sphere compared to larger Au NPs in the Suspension system.

Extensive studies on the cellular uptake of Au NPs have been limited to adherent eukaryotic cells, and a very small number of investigations have addressed the uptake of Au NPs into red blood cells (RBCs), the most readily available cells in the bloodstream, potential future homologs Drug or NPs carriers with longer circulation times in the bloodstream. There is currently a debate as to whether endocytosis can occur in RBCs. In this thesis, ICP-MS was used to study the uptake of Au NPs in RBCs and with this method, those Au NPs attached to the RBCs surface without truly entering the RBCs can also be included as the internalized Au mass. Using the internalized Au mass per cell as a standard for uptake comparison, the concentration-dependent and size-dependent uptake behavior were also demonstrated in the RBCs, but no evident time-dependent behavior was observed under the designed experimental parameters. And the higher uptake of 4 nm Au NPs in RBCs compared to the 25 nm and 50 nm Au NPs was partly attributed to the hinderance for the endocytosis of 25 nm and 50 nm to a larger extent compared to the 4 nm Au NPs due to the mesh of the spectrin-actin network skeleton of the RBCs cell membrane.

In the third part of this thesis, the mosquito, a simplified animal model with also endothelial systems in the different organs, was chosen to study the ingestion and metabolism of 4nm Au NPs, Europium labelled Bovine serum albumin (BSA-Eu), and Iodine (I) ions in mosquitoes with ICP-MS, to provide a reference for the study of in vivo fate of Au NPs in other animals. According to our observation, the Iodine was excreted the fastest compared to Au NPs, BSA-Eu and we can observe the excretion of Iodine immediately after feeding. Besides, both the Iodine ions and Au NPs have been completely excreted after 6 days of metabolism, while there is still a small amount of BSA-Eu remaining in the mosquito.

## **Zusammenfassung**

Der Einfluss von Größe/Form, Konzentration von Au NPs und Inkubationszeit auf die Aufnahme von Au NPs in adhärenente Zellen im statischen Inkubationssystem wurde ausführlich untersucht, und einige Diskussionen wurden auf der Grundlage der Annahme gleichmäßig verteilter Au NPs im durchgeführt Inkubationszone und auch unveränderte Konzentration von Au NPs während der Inkubationszeit. Die Feststellung der höheren Konzentration großer Au NPs (ungefähre Größe größer als 50 nm) am Boden des Zellkulturkolbens oder der Platte im Vergleich zur oberen Zone aufgrund der allmählichen Schwerkraft-induzierenden Sedimentation könnte jedoch frühere Ergebnisse dieser Aufnahmestudie in Frage stellen. Aber in dieser Arbeit wurde in den drei anderen Inkubationssystemen als dem statischen System die allmähliche Schwerkraft-induzierende Sedimentation von Au NPs durch kontinuierliches Mischen gestört. Darüber hinaus simulieren die dynamischen und uni-direktionalen Flüssigkeitsinkubationssysteme in dieser Arbeit die dynamische In-vivo-Umgebung, der Au NPs ausgesetzt sind, und liefern direkte Referenzen, wie die optimierte Dosis und Größe von Au NPs, für zukünftige In-vivo-Anwendungen von Au NPs. Basierend auf ICP-MS (Massenspektrometrie mit induktiv gekoppeltem Plasma) in Kombination mit Zellzählung wurde anstelle der Au-NP-Anzahl pro Zelle die internalisierte Au-Masse pro Zelle als einziger Standard zum Vergleich der größen/form-abhängigen, Au Konzentration-abhängiges und inkubationszeit-abhängiges Aufnahmeverhalten von Au NPs in all diesen vier Systemen und analysieren auch den Einfluss von Inkubationssystemen auf das Aufnahmeverhalten. Unsere Ergebnisse zeigten die höhere Aufnahme, die durch die doppelte Konzentration von Au NPs induziert wurde, und auch die allmählich erhöhte Aufnahme mit verlängerter Inkubationszeit in all diesen vier Systemen, unabhängig von der Größe/Form der Au NPs/NRs, den Bewegungen der Au NPs und auch die Zustandsänderungen der Hela-Zellen dieser vier Systeme. Selbst wenn die Inkubation von statisch auf dynamisch und flüssig umgestellt wurde, war die Aufnahme von 50 nm und 100 nm großen Au NPs stärker reduziert als bei anderen kleineren Au NPs (5, 25 nm Au NPs und 40 nm Au NRs). Beispielsweise beträgt die 24-Stunden-Aufnahme von 50 nm und 100 nm Au NPs in einem dynamischen System weniger als 50 % der 24-Stunden-Aufnahme in einem statischen System, und die 4-Stunden-Aufnahme von 50 nm und 100 nm Au NPs in einem flüssigen System machen durchweg weniger als 10 % der 4-stündigen Aufnahme im dynamischen System aus, was auf die stark nachteilige Wirkung der Au NP-Bewegung auf die Aufnahme hinweist und auch eine Referenz für das In-vivo-Dosierübungsdesign darstellt. Ein weiterer interessanter Befund ist das gemeinsame



Aufnahmeverhalten in Statischen, Dynamischen und Flüssigen systemen, dass die internalisierte Au-Masse pro Zelle größerer Au NPs (50 nm, 100 nm Au NP und 100 nm Au NR) viel höher ist als die kleinerer Au NPs (5 nm, 25 nm Au NP und 40 nm Au NR) verschwanden in dem Suspensions system, in dem sowohl Au NPs als auch Hela-Zellen suspendiert waren. Dies kann auf die höhere Möglichkeit des Kontakts zwischen kleineren Au NPs und Suspensions-Hela-Zellen im Vergleich zu größeren Au-NPs aufgrund der viel schnelleren Brownschen Bewegung und auch auf die vergleichsweise höhere Fähigkeit kleinerer Au NPs, in die Tumorsphäre von Hela-Zellen einzudringen, zurückzuführen sein. im Vergleich zu größeren Au NPs im Suspensionssystem.

Umfangreiche Studien zur zellulären Aufnahme von Au NPs waren auf adhärenente eukaryotische Zellen beschränkt, und eine sehr kleine Anzahl von Untersuchungen befasste sich mit der Aufnahme von Au NPs in rote Blutkörperchen (RBCs), die am leichtesten verfügbaren Zellen im Blutstrom, potenzielle Zukunft Homologe Wirkstoff- oder NPs-Träger mit längeren Zirkulationszeiten im Blutkreislauf. Derzeit wird diskutiert, ob bei Erythrozyten eine Endozytose auftreten kann. In dieser Arbeit wurde ICP-MS verwendet, um den Einbau von Au NPs in RBCs zu untersuchen, und diese Methode kann auch jene Au NPs einkapseln, die an der RBC-Oberfläche befestigt sind, ohne tatsächlich in die RBCs einzudringen. Unter Verwendung der internalisierten Au-Masse pro Zelle als Standard für die Aufnahme wurde das konzentrations- und größenabhängige Aufnahmeverhalten auch in den RBCs demonstriert, aber unter den entworfenen experimentellen Parametern wurde kein offensichtliches zeitabhängiges Verhalten beobachtet. Und die höhere Aufnahme von 4-nm-Au-NPs in Erythrozyten im Vergleich zu den 25-nm- und 50-nm-Au-NPs wurde teilweise der Hemmung der Endozytose von 25-nm- und 50-nm-Au-NPs zugeschrieben, die dem Maschenwerk des Spektrin-Aktin-Netzwerkskeletts von zugeordnet ist die RBCs-Zellmembran im Vergleich zu den 4-nm-Au-NPs stärker.

Im dritten Teil dieser Arbeit wurde eine Mücke, ein vereinfachtes Tiermodell mit ebenfalls endothelialen Systemen in den verschiedenen Organen, ausgewählt, um die Aufnahme und den Metabolismus von 4 nm Au NPs, Europium-markiertem Rinderserumalbumin (BSA-Eu) und zu untersuchen Jod (I)-Ionen in Moskitos unter Verwendung von ICP-MS, um eine Referenz für die Untersuchung des In-vivo-Schicksal von Au NPs in anderen Tieren bereitzustellen. Aus unserer Beobachtung wurden die Jodionen im Vergleich zu Au NPs, BSA-Eu, am schnellsten ausgeschieden, und wir können die Jodausscheidung unmittelbar nach der Fütterung beobachten. Außerdem werden sowohl die Jod-Ionen als auch die Au NPs nach 6 Tagen

Stoffwechsel vollständig ausgeschieden, während eine kleine Menge BSA-Eu noch in der Mücke verbleibt.

# 1. Introduction

## 1.1 A review of the four endocytosis pathways of NPs

The inherent physicochemical properties of Au NPs have made them possible for a variety of promising biomedical applications including the basic drug carrier [1, 2], bio-imaging contrast[3-5], photodynamic therapy (PDT) [6-9], photo-thermal therapeutic medicines (PTT) [9-13] and also vaccines.[14, 15]

Cellular internalization of NPs is the major mechanism involved in the biomedical applications of NPs, no matter for the delivery of the intracellular biologically active substance to exert their therapeutic effects in the cytoplasm or other specific organelles, such as nucleus and mitochondria, or for PDT or PTT based on the intracellular accumulation of NPs, etc., even though some NPs can exert the beneficial effects without true entrance into cells.[16-21] These four types of endocytosis are the most common internalization pathway: Clathrin-mediated endocytosis, Caveolae mediated endocytosis, Phagocytosis, Pinocytosis/Macropinocytosis. All these four types of endocytosis shared a common process, the cell membrane invagination or pseudopodia and engulfing of the NPs into an endocytic vesicle and then the endocytic vesicle separation from the cell membrane and enters the cytoplasm, while the endocytic vesicle will merge with lysosome or endosomal escape and vesicle related secretion can also happen. There is also another type of endocytic pathway, the Clathrin/ Caveolae independent endocytic pathway, which happens in cells devoid of both clathrin and caveolae.[22] Besides, the non-endocytic internalization of NPs such as passive diffusion, hole formation, direct microinjection, and electroporation was also reported.[23, 24]

Except for the shared process, these four endocytic pathways have also their respective characteristics, and here we just focus on the initiation of endocytosis and also the unique size of the endocytic vesicle of these most common four types of endocytic pathways. The Clathrin-mediated endocytosis was driven by the assembly of proteins, including clathrin, clathrin-adaptor proteins and scaffold proteins, and other proteins, at the endocytic site from soluble cytosolic protein pools, forming the endocytic vesicle diameter of typical 100 nm in mammals.[25] Caveolae-mediated endocytosis is Clathrin-independent endocytosis, and the protein caveolin instead of Clathrin integrates itself within the cholesterol rafts encouraging the membrane curvature and leading to the formation of vesicles of 60-80 nm[26]. Phagocytosis exists in all cells, but the efficiency is much higher in phagocytes. Phagocytosis was mainly activated by the recognition of opsonins such as immunoglobulins and complement

proteins which coat the cargos, whereas, the cooperation between opsonins with non-opsonic receptors (e.g., mannose and scavenger receptors) expressed by the phagocytes can also happen and influence the phagocytosis efficiency.[27-30] The vesicle formed during phagocytosis is usually larger than 500 nm. And pinocytosis (cell drinking) is a non-specific route where the cell membrane invaginates and engulfs the foreign materials and formed a vesicle of between 0.5-5  $\mu\text{m}$ .

Currently, transmission electron microscopy (TEM), Atomic Force Microscope (AFM), and Confocal laser scanning microscopy (CLSM) were used combined with specific inhibitor treatment to investigate the specific endocytic pathway undertaken. Sometimes, several endocytic pathways cooperate together for the uptake of specific NPs, while it can also happen that a specific endocytic pathway is predominant. For example, He B. et al. confirmed the uptake of Au NPs in B16 (mouse melanoma) and A549 (human lung adenocarcinoma) by Clathrin-mediated endocytosis, macropinocytosis, and also micropinocytosis under TEM based on the 4 °C incubation uptake and also treatment with chlorpromazine, filipin, genistein, cytochalasin D, 5-N-ethyl-N-isopropylamiloride [EIPA], and dynasore.[31] Rothen-Rutishauser, B et al. found the predominant uptake via caveolae-mediated endocytosis in human alveolar epithelial cells (A549) for fluorescently labeled polymer-coated 13.3 nm Au NP based on the usage of chlorpromazine and methyl-beta-cyclodextrin via LSM and TEM observations.[32] Hao X. et al. used the same inhibition chemical methyl-beta-cyclodextrin (M beta CD) and also confirmed the predominant uptake via caveolae-mediated endocytosis of small-size AuNPs (4,5 nm Au-cysteine conjugates labeled with amine-reactive Cy5 dye), which was further supported by the non-effect of the sucrose which disrupts the formation of clathrin-mediated endocytosis.[33] Yang LX et al's work with dynasore found the clathrin-mediated endocytosis and macropinocytosis internalization of water solubilized, lipoic acid-protected Au Nanoclusters (AuNCs) with a hydrodynamic diameter of 3.3 nm into Hela cells combined with a lesser extent contribution of the caveolin-mediated pathway, but they also observed the non-effect of Dynasore on the membrane-associated uptake part.[34] Jiang LQ. found both the clathrin- and caveolin-mediated endocytosis pathways were undertaken by chitosan-based NPs (CsNps) released from RAW264.7 cells to enter Hepa1-6 cells.[35] Chatterjee, M et al. confirmed the 60 nm PLGA-Tg (a hydrophobic drug, 6-thioguanine (Tg), Poly (d, L-lactide-co-glycolide) (PLGA),) NPs into HeLa cells was through pinocytosis according to AFM observation of the 2.3  $\mu\text{m}$  depth pit on the cell membrane treated with PLGA-Tg NPs compared to the pit depth of 700 nm on the control cell.[36]

And it has been proved that the NPs composition, size[37], shape[38], surface modification[39], surface charge[40], and cell lines[41] cooperate to determine which kind of endocytosis pathway the NPs will undertake.

## **1.2 The effect of cell lines and cell status on the endocytosis of Au NPs**

Here we narrow our discussion to mammalian cells, which can also be classified into different categories, Prokaryotic (cells without a true nucleus) and Eukaryotic (cells with a nucleus), normal tissue cells and cancer cells, adherent cells and suspension cells, professional phagocytes, and non-professional phagocytes.

The NPs internalization difference in normal tissue cells and cancer cells laid the foundation for targeting therapy and enormous studies have been done to compare the uptake in normal cells and cancer cells to find the nanoparticles with good targeting properties.[42-44] For example, Dhar S. et al. observed the gellan gum-reduced Au NPs internalization in cancer cells (LN-229) with no uptake observed in normal mouse embryonic fibroblast cells (NIH3T3).[45]

The efficiency of phagocytosis in professional phagocytes including macrophages, neutrophils, monocytes, dendritic cells, and osteoclasts can be higher than in non-professional phagocytes, however, it has been generally accepted that phagocytosis can also happen in non-professional phagocytes but in a lower efficiency such as in Fibroblasts, epithelial cells, and endothelial cells.[46-48]

The predominant endocytosis pathway undertaken by different cell lines can also vary even incubated with the same Au NPs. For example, Rattanapinyopituk, K et al. observed both an increase of endocytic vesicles in the cytoplasm and also clathrin immunopositivity in syncytiotrophoblasts and fetal endothelial cells by electron microscopy (EM), while the caveolin-1 immunopositivity was observed exclusively in the fetal endothelium in the maternal-fetal barrier of mice treated with 20 nm and 50 nm Au NPs.[49]

Except for cell lines, cell status can also play an important role in the internalization of Au NPs. For example, MacParland, S. A. et al. reported the higher uptake of 15, 60, and 100 nm PEGylated and Alexa Fluor 750 dye decorated Au NPs in Human monocyte-derived macrophages' "regulatory" M2 phenotype compared to the subtypes (M2c > M2 > M2a > M2b > M1)[50], MacParland, S. A. et al.'s finding was also reported by Chakraborty R. et al. that the intake of polyallylamine hydrochloride (PAH) coated Au NRs (PAH-Au NRs) by M2 cells was

greater than by M1, which laid the technical basis for the human health status prediction based on the ratio of different phenotypes of Macrophages.[51] Besides, MacParland, S. A. et al. also found a significantly higher uptake of Au NPs in Kupffer cells expressing higher levels of M2 markers (CD163) compared to Kupffer cells expressing lower levels of surface CD163.[50]

However, many of the previous publications about the uptake of Au NPs were narrowed to adherent cells, and there was very little research about the uptake of Au NPs in suspension cell lines, nor in mature RBCs, the suspended Prokaryotic cells, which can interact with NPs in the blood vessels, thus largely affect the distribution of NPs in blood. Currently, there is debate about whether endocytosis can happen in RBCs. One argument is that fluid phase or receptor-mediated endocytosis seems to be absent in Mature, normal human RBCs, because of the prohibition of the dense spectrin/actin membrane skeleton and the densely packed hemoglobin in these Mature, normal human RBCs.[52] Immature or diseased RBCs or reticulocytes, however, may perform endocytosis. But some observations of the uptake of NPs in RBCs have also been reported, which might undertake a non-endocytic pathway. For example, Janetanakit, W et al. observed the existence of hollow Silica nano golf balls (Au@SiO<sub>2</sub>, HGBs) inside RBCs with AFM after 30 min incubation and they also found the morphology change of RBCs into much flatter, disappearing of bicave and also increased of diameter after the uptake.[53] While some researchers reported the association or attachment of Au-based NPs to RBCs without damage to the cell membrane.[54, 55] Abo-Zeid, Y et al. reported a negligible uptake of polymer NPs loaded with ribavirin by RBCs compared to human hepatoma cells Huh7.5 cells based on Spectro-photo fluorometry and flow cytometry quantification measurement.[56]

### **1.3 Effect of NPs size and shape on the endocytosis of Au and Ag NPs**

The size, shape, and surface functionalization of the NPs and also the cell status collaborate to determine which endocytic pathway to undertake, thus the size is not the exclusive filter to judge the endocytic pathway. As reported in some publications, it seems that the size increase of NPs will cause the change of endocytosis from Clathrin-mediated endocytosis to caveolin-mediated endocytosis or macropinocytosis. For example, Ding L. et al. found that the 15 nm Au NPs, the 45 nm Au NPs, and the rod-shaped Au NRs enter cells via a dynamin-dependent endocytosis pathway, however, the 80 nm Au NPs mainly enter the cells by macropinocytosis pathway due to the big size.[57] Rejman, J et al. reported that the internalization of Fluorescent microspheres involves clathrin-coated pits when the microsphere diameter was lower than 200

nm, and with increased size, the internalization gradually transfers to caveolae-mediated internalization, and the caveolae-mediated internalization was even dominant when the particles reach 500 nm in size.[58] However, the actual case is that even small NPs can also enter cells through phagocytosis which was hypothesized to be because of the aggregation of these small NPs after opsonization.[48, 59] Small sizes of NPs can also undertake clathrin-mediated endocytosis and pinocytosis, for example, the pinocytosis of 3-8 nm Au-lys-PLL-FITC (Au-lysine-14-poly-l-lysine-fluorescein isothiocyanate) NPs in RAW 264.7 macrophages cells has been observed by Shukla, R et al..[60] The macropinocytosis of 5 nm polymer coated Au NPs in Hela cells and HUVECS (Human Umbilical Vein Endothelial Cells) has also been reported.[61]

The different membrane curvature force and the different number of involved proteins required by the different size NPs can result in the different uptake rates of different size cargo, however, in practical experiments, other concomitant factors can cover up this effect. The higher concentration of larger NPs induced by sedimentation of the larger NPs in static incubation can increase the contact possibility between NPs and cells and result in higher uptake even though the energy required for the endocytosis of larger NPs is higher than smaller Au NPs. For example, MacParland, SA et al. Observed the increased uptake of PEGylated and Alexa Fluor 750 dye decorated Au NPs in both monocyte and derived macrophages with an increase of diameter from 15 nm to 50 nm and 100 nm.[50] Wu MY et al. found the size-dependent uptake of Ag NPs in B16 mouse melanoma cell line (B16), with the 20 nm of the lowest uptake efficiency and 100 nm Ag NPs of the highest uptake efficiency among the 5 nm, 20 nm, 50 nm, and 100 nm Ag NPs after incubation for 12 h and 24 h.[62] Yang, Y et al. found that the 50 nm Au nanocages transmembrane transporting needs smaller force and shorter duration with a much faster speed compared to 100 nm Au nanocages, but both sizes of Au nanocages transmembrane transporting depend on the combination of caveolin-mediated endocytosis, clathrin-mediated endocytosis and macropinocytosis.[63] However, this endocytosis selection also depends on the cell line and it has to be noticed that NPs even smaller than 100 nm can also enter some cell lines through clathrin-mediated endocytosis and also macrophages through phagocytosis.[64]

In some cases, the higher uptake of NRs than spherical NPs is partly due to the easier actin polymerization during the phagocytosis [65], and also the NRs have a greater surface curvature at the ends of the NPs, which will affect the energy the membrane needs to wrap the NRs.[37] Christie, C et al. reported the twice uptake amount by Macrophages of pegylated AuNRs (45

nm length and 15 nm diameter ) compared to pegylated AuNS of larger size,[10] which cannot be just attributed to the shape change without a discussion about the important role of the size of the Au NRs and the Au NS in this uptake amount difference.

When we compare the uptake of spherical Au NPs to Au NRs or Au nanostars (NS), no universally applicable conclusion can be achieved perhaps because it is almost impossible to just change the shape without changing the size and surface chemistry of the NPs, besides, the trend might vary in different size range. For example, Huang X. L. et al.'s work with mesoporous nanoparticles presented that the NPs of highest area ratio (AR) AR=4 showed the largest uptake compared to the other two NPs of the same composition, same zeta potential, and the only different AR=1 and AR=2.[66] While, Meng H. et al. used flow cytometry and confocal microscopy to compare the uptake of four types of mesoporous silica nanoparticles in HeLa cells and A549 cells, which has also similar chemical composition, pore size, and the same sedimentation speed, but different aspect ratio (AR) and found that the uptake of the spherical NPs was the lowest compared to the other three rods NPs and the uptake of NRs firstly increased with the increasing of AR and then decreased and the NR of AR 2.1-2.5 was mostly favored and of the highest uptake amount, 40 times the uptake of the spherical NP in HeLa cells.[67] When the shape of NPs becomes worm-like whose AR>20, the uptake will become again negligible compared to spherical NPs, and the explanation given is that the actin polymerized only at the contacting point without enough energy to wrap the NPs.[65, 68] It can be inferred that the shape of the NPs will not only affect the uptake amount, but also the endocytosis pathway undertaken will be different for different shapes of NPs.

Other factors including the surface physicochemical property of NPs [69-72]and also the protein corona[73, 74] will also play an important role in the uptake of Au NPs. Some publications inferred the suppressed uptake of Au NPs and Au NRs caused by the protein corona perhaps because of the block of the caveolin-mediated endocytosis in some cells[73], however, this suppression effect of protein corona also varies among different cell types, and Au NPs sizes. Cheng X. J. et al. found a more significant inhibition effect of protein corona on the uptake of large-sized Au NPs by phagocytic cells than that of small-sized Au NPs by nonphagocytic cells.[74] Ding L. found that when the fetal bovine serum (FBS) was absent from the media, the endocytosis pathway of 15 nm and 45 nm Au NPs, and star-shaped Au nanomaterials changed from receptor-mediated endocytosis to macropinocytosis pathway and Au NRs changes from receptor-mediated endocytosis to clathrin and caveolin-independent pathway.[57]



## **1.4 The necessity of uptake study in a dynamic environment**

The failure of many therapeutic NPs in in vivo applications was mainly due to the low dose of NPs which truly arrived at the targeted area. The actively in vivo targeting of NPs involves 4 dynamic steps: the transport of NPs in blood vessels, transvascular transport of NPs, transport of NPs in the tumor interstitial matrix, and entry of NPs into tumors, all of which are happening in a dynamic environment, much more complicated than the normal in vitro static incubation of NPs with cells.[75, 76] Besides, complicated factors including the size, shape, stiffness of NPs, the geometry of vessels, shear rate distribution, vascular permeability, and also the blood cells in the vessels would affect the NPs adhesion to the vessel wall and also the transvascular movement of NPs.[77] Thus, uptake study for NPs in in vitro dynamic environment is urgent, which should be closer to in vivo environment compared to the traditional in vitro static incubation, however, simulation experiments seem to run much slower than theoretical simulation by computational fluid dynamics (CFD) method. Based on the CFD method, some basic understanding has been got based on simplified models, but also discrepancy results have came out because of the different models used.[77-80]

Here, I just make a summary of the theoretical simulation investigations about the effect of the size, and shape of NPs on their accumulation near the vessel wall, which is only the first step on the way to targeting cancer cells. It has been extensively reported that Rod-shape NPs have a higher binding probability to the vascular wall than spherical NPs.[80-83] But Tan et al. [84] have pointed out that the high binding rate of rod-shaped NPs to the vascular wall depends on the initial contact and orientation to the vascular wall, and the rod-shaped NPs with a larger longitudinal and transverse ratio may not have a higher binding force. Both Liu[83] and Shah[81] did not consider the initial contact and orientation of NPs to the wall in their simulation, but Tan's simulation has also its limitation in that it was based on the assumption that the long axis of aspheric particles is aligned with the contact wall, bringing out the maximum adhesion force and maximum contact area.[77] However, this ideal situation does not always occur in vivo. Regarding the effect of the size of NPs on the binding of NPs to vessel wall, some simulations thought that the smaller size binds faster than bigger NPs because of a faster diffusion rate,[79, 83, 85] while another work pointed out that the submicron particles should be the first choice for vascular targeted therapy based on the emphasis of the effect of micro-level cell-free layer interaction with NPs on the NPs accumulation near the vessel wall.[86] Besides, the existence of blood cells such as RBCs also influences the distribution of NPs by rejecting the NPs to a smaller vessel at the bifurcation vessels or pulling

volume extension effect on the NPs.[78, 87, 88] Blood rheological parameters or vascular permeability parameters can also affect the longitudinal diffusion of NPs in blood vessels.

Most of the above CFD simulations were based on simplified mathematical models and need the incorporation of more advanced in vitro dynamic experiments to achieve a better prediction of the NPs fate in vivo. There have already been advanced in vitro models with the implementation of physiological fluids, immune elements, physiologically relevant dynamic flow, and co-culture of human alveolar epithelial and macrophage to study the silver NPs adhesion behavior and toxicity compared to the traditional in vitro model.[89, 90] Besides, there have already been organ-on-a-chip systems with both endothelial cells and cardiac tissue featured to gain a mechanistic understanding of nanoparticle-induced cardiac dysfunction.[91-93] The simulation of the human circulatory system used to determine the retention of magnetic nanoparticle carriers when exposed to an external magnetic field has also been reported.[94] However, mechanically understanding the uptake of NPs in the physiological circulation system still requires a large amount of study of advanced in vitro model which is both practical and also close to the in vivo environment.

## **1.5 In vivo distribution of Au NPs**

The bio-distribution of NPs affects both their efficacy and safety, which determines whether a nanoparticle-based technology can be successfully used in the clinic.[95] Metal-containing particles raise biodistribution and toxicity concerns because they generally accumulate in the reticuloendothelial system (RES), such as the liver, lung, and spleen, which decreases the possibility of NPs transportation to the target area and can be also poisonous to the RES cells after large accumulation. The recognition by many phagocytes in the RES increased the accumulation of NP in the RES even though the NPs can also be taken up by many non-phagocytes in the liver such as endothelial cells partly because of the characteristic of the discontinuous endothelial in the vessels surrounding the liver and spleen and NPs can also accumulate in the kidney where there are also blood vessels with fenestrated endothelia.[96] Many factors including the administration route, nanoparticle physicochemical properties, the injection dose, and the in vivo model will affect the bio-distribution of the NPs.[97, 98] Here we just limit the discussion to intravenous administration of Au NPs conjugated with different coatings. One basic design was ‘stealth’ Au NPs to escape the recognition by the RES and get prolonged circulation time in the blood to transfer to the targeted site, for example, through conjugation with PEG[99], but these ‘stealth’ NPs can still end up in RES. Lin Z. et al. have

reviewed many publications about the blood half-life, bio-distribution of Au-based NP in plasma, liver, spleen, heart, brain, and other organs, and also the renal and biliary excretion of the Au-based NPs.[100] Some general trends have been reported even though the understanding of the bio-distribution of Au NPs in vivo is still preliminary, for example, the widespread of Au NPs in the organs was greater for small Au NPs compared to larger NPs although the majority of the Au NPs accumulate in the RES regardless of the size. [101, 102] De Jong et al. detected 10 nm Au NP in blood, liver, spleen, kidney, testis, thymus, heart, lung, and brain, whereas the larger particles were only detected in blood, liver, and spleen 24 h after the intravenous injection.[101] Another common trend is that the passage through the blood-brain barrier can also be size-dependent with the enhanced penetration ability of the smaller Au-based NP. [102, 103] However the clearance of Au NPs from blood and distribution in the organs depend not only on the size but also on the surface charge and ligand decoration. [104, 105] Frigell Jens et al. achieved the brain uptake of Au NPs through the incorporation of small, modified neuropeptides onto the Au NPs surface.[106]. And the protein corona binding to the Au NPs can also largely affect the distribution of the Au NPs. For example, Hirn S. et al reported a higher spleen accumulation of 2.8 nm Au NP coated with carboxyl groups compared to any of the Au NP (1.4, 5, 18, 80, and 200 nm) conjugated with mono-sulfonated triphenylphosphine (TPPMS) and they assumed the difference to be caused by the different protein binding to the Au NP coated with carboxyl groups.[107]

## **1.6 Motivation for Study**

Au NPs, due to their attractive physicochemical properties, has raised many investigations on their promising biofunctions including imaging, photothermal therapy, photodynamic therapy, and also as drug carriers. Uptake of Au NPs, the basic interaction with cells majorly determines the following functions of Au NPs in cells and has achieved enormous research concerns including the investigation of the endocytosis mechanism of Au NPs in different cell lines and also the uptake difference caused by size, shape and surface charge and surface function. However, it is difficult to achieve a strict universal conclusion owing to the following facts. 1) many complicated factors that influenced the Au NPs cellular internalization work together rather than the only factor designed by the researcher. For example, when the size of the Au NPs was changed, the surface protein corona binding onto the NPs and the surface curvature might also vary. 2) the uptake quantification method and also the initial dose vary in different works. Some of the studies quantified the uptake based on TEM observation which was only limited to several cells while some quantitative works were based on ICP-MS. And the uptake

amount can be judged by the internalized Au NPs number per cell and also the Au atoms per cell. And the initial incubation dose of Au NPs might be calculated based on the UV-vis spectra or the ICP-MS and the error between these two methods can also add to the study. No standard method makes it difficult to compare conclusions in different works. 3) Whether the wash step was enough to remove the excess free Au NPs and the Au NPs attached to the surface of the cells still requires more proof. 4) The colloidal stability of Au NPs after exposure to high-ion concentration and protein-rich media was not reported in many works. And the Au NPs can aggregate after exposure to the media and result in altered surface chemical properties. Thus we still need a more precise, systematic, and persuasive investigation of the uptake behavior.

Besides, another two drawbacks of the current uptake studies were 1) the static incubation, which is completely different from the actual flow bloodstream which the Au NPs will encounter in the in vivo environment. According to our understanding, the flowing bloodstream will change the movement of the Au NPs thus affecting the contact possibility between Au NPs and cells. 2) Most studies were only limited to the uptake of Au NPs in adherent cells. But several reasons necessitate the investigation of the Au NPs in suspension cells. Firstly, in the bloodstream, there are also enormous suspension cells such as RBCs, and interaction between Au NPs and these suspension cells will also largely influence the in vivo fate of the Au NPs. Secondly, the different interaction surface area between adherent/suspension cells and Au NPs provides a different contact possibility and might result in different uptake behavior. Thirdly, according to the endocytosis mechanism, the curvature energy required for the cell membrane plays an important role in the uptake rate. And the surface tension of adherent cells and suspension cells are different and thus the curvature energy required for adherent and suspension cells can be different from each other, which might consequently affect the uptake speed of Au NPs in these two types of cells.

All these drawbacks required a more systematical investigation of the uptake study including a persuasive quantification method, dynamic incubation, and also uptake study of Au NP in suspension cells, which can be a more meaningful reference for the uptake of Au NP in vivo.

RBCs have attracted much interest to be used as a drug or NP carrier because of their large amount in the bloodstream, high surface area to volume ratio, and long circulating time. But there is a debate about whether endocytosis can happen in RBCs. It is generally accepted that the nucleus is absent in matured RBCs and there is only a very small amount of clathrin in RBCs, thus most people believe that endocytosis can not happen in mature RBCs. However

several publications reported the existence of NPs inside RBCs after some time of incubation. Besides, currently, there are also many works on several manmade methods to manipulate NPs into RBCs. Thus it requires more investigations on whether RBCs can uptake NPs and what is the route for NPs to enter RBCs. And because NPs will encounter large amounts of RBCs after intravenous injection, it is even more necessary to investigate the uptake of Au NPs in ex vivo incubation to get a reference for in vivo investigations.

After injection into animals, the interaction with the abundant proteins might alter the surface physiochemical properties of Au NPs. Currently, the most serious problem is the accumulation of Au NPs in the RES, which shorted the circulation time of Au NPs in the bloodstream and makes it difficult for the Au NPs to be transferred to the target area. Up until now, there is no effective method to overcome this problem since the NPs can still end up in the RES even after decoration with a 'stealth' coat such as PEG. All these problems required more studies on the in vivo bio-distribution of Au NPs. The mosquito is a very simplified animal model which has also a digestive tract composed of the foregut, anterior gut, posterior gut, and hindgut. The Malpighian tubules and hindgut are the renal excretory tissues of mosquitoes. Besides, there are also many endothelial cells in mosquitoes, which are similar to other animals. Thus we investigate the ingestion and metabolism of Au NPs in mosquitoes and also detect the bio-distribution of Au NPs inside mosquitoes and wish to provide a reference for other in vivo research.

## **2. The uptake of different sizes of Au NP/NRs in HeLa cells in four incubation systems**

### **2.1 Introduction**

Cell uptake is a very important step during the NPs-organs interaction, which largely affects the labeling efficiency of target cells with NPs and also the lowest dose of NPs required for significant imaging, drug delivery, photodynamic therapy, and photo-thermal therapeutic effects. Thus, many *in vitro* models have been designed to simulate the interaction between NPs and the physiology environment to study the cellular uptake of NPs. Currently, the most studied model was cell lines *in vitro* static incubation of NPs, which was used to investigate the effect of physicochemical properties of NPs, cell lines, incubation time on the uptake of NPs in cell lines and to deeply understand the corresponding endocytosis path for NPs to enter cells.[37, 38, 71, 108] But this *in vitro* static incubation model neglected the fluid flow characteristic of the blood stream in the actual physiology environment, which would not only influence the distribution of NPs, but also the cell response is different in fluid condition compared to static incubation.[109, 110] For example, 100 nm Au NPs would sediment because of gravity after some time of static incubation and thus increase the contact possibility between these 100 nm Au NPs and cells at the bottom of the flask, but the distribution of this 100 nm Au NPs can alter in the flow blood stream.[109-112] And also the flow shear in the actual bloodstream would affect the uptake property of NPs in the endothelial cells since these cells are mechanically responsive.[113, 114] What's more, the flow shear is even varying in the context of the tumor vasculature.[115]

In this chapter, four incubation systems were designed and were described as Static, Dynamic, Fluid, and Suspension systems. In these four systems, the Au NP/NRs will be in different motion styles including static incubation, periodically dynamic shaking, and continuous unidirectional flow respectively. And the HeLa cells were in adherent or suspension status, which can represent the two common cell statuses in the actual organs and bloodstream. These four systems can better cover the actual dynamic environment encountered by NPs exposure *in vivo*. A detailed description of these four systems is presented in chapter 2.5.4. After a quantitative study of the uptake of Au NP/NRs in HeLa cells in these four systems, a better understanding of the kinetics of the Au NP intracellular internalization can be achieved.

## 2.2 Major reagents

Name	Purity	Company	Function
Gold(III) chloride trihydrate	≥99.9%	Sigma Aldrich	Au NPs and NRs synthesis
Tetraoctylammonium bromide	98%	Sigma Aldrich	Au NPs synthesis
Toluene	100.0 %	VWR	Au NPs synthesis and also Interfacial tension measurement
Sodium borohydride	≥98.0%	Sigma Aldrich	Au NPs and NRs synthesis
Hydrochloric Acid	TraceMetal™ Grade	Fisher Scientific	Au NPs synthesis and also ICP sample preparation
Sodium Hydroxide	≥99%	Carl Roth	Au NPs and NRs synthesis
1-dodecanethiol		Sigma Aldrich	
Methanol	100.0 %	VWR	Au NPs synthesis
Chloroform	100%	VWR	Au NPs and NRs synthesis
poly(isobutylene-alt-maleic anhydride)		Sigma Aldrich	Au NPs and NRs synthesis
1-dodecylamine	97%	Alfa Aesar	Au NPs and NRs synthesis
Sodium citrate dihydrate	99%	Sigma Aldrich	Au NPs synthesis
CH <sub>3</sub> O-PEG-SH, 2000 Dalton		PAPP POLYMERE	Au NPs and NRs synthesis
Hexadecyltrimethylammonium bromide	≥98%	Sigma Aldrich	Au NRs synthesis
Sodium salicylate	≥99.5%	Sigma Aldrich	Au NRs synthesis

Sodium oleate	> 97%	TCI	Au NRs synthesis
L-Ascorbic acid	> 99%	Sigma Aldrich	Au NRs synthesis
Silver nitrate	≥99.0%	Sigma Aldrich	Au NRs synthesis
Tetrahydrofuran	≥99.5%	Carl Roth	PMA-g-dodecyl synthesis
Nitric Acid (TraceMetal™ Grade),	67 to 70% (HNO <sub>3</sub> , w/w)	Fisher Scientific	ICP sample preparation
Phosphate buffered saline		Invitrogen	For cell culture
Dulbecco's modified eagle medium		Thermofisher	For cell culture
Fetal bovine serum		Biochrom	For cell culture
Penicillin/streptomycin		Sigma-Aldrich	For cell culture
Trypsin –EDTA (0.05%)		Thermofisher	For cell culture
Resazurin	≈80%	Sigma-Aldrich	For cell viability test
LIVE/DEAD™ Viability/Cytotoxicity Kit for Mammalian Cells		Thermofisher	For cell dead/live staining

## 2.3 Abbreviations

HAuCl <sub>4</sub>	tetrachloroauric acid
TOAB	Tetraoctylammonium bromide
NaBH <sub>4</sub>	Sodium borohydride
HCl	Hydrochloric Acid
NaOH	Sodium Hydroxide
DDT	1-dodecanethiol
DDA	dodecylamine
PMA	an amphiphilic polymer which is based on a backbone of poly(isobutylene-alt-maleic anhydride), functionalized with dodecylamine, yielding dodecylamine



	hydrophobic side chains through formation of amide bonds upon reaction with the maleic anhydride rings (PMA).
PMA-g-dodecyl	an amphiphilic polymer which is based on a backbone of poly(isobutylene-alt-maleic anhydride), functionalized with dodecylamine, yielding dodecylamine hydrophobic side chains through formation of amide bonds upon reaction with the maleic anhydride rings (PMA).
EP	Eppendorf
Au	Gold
NP	nanoparticle
SPR	surface plasmon resonance
RT	Room temperature
NR	nanorod
CTAB	Hexadecyltrimethylammonium bromide
NaOL	Sodium oleate
AgNO <sub>3</sub>	Silver nitrate
Au NPs@ TOAB	Au NPs capped with TOAB
Au NPs@ DDT	Au NPs capped with DDT
Au NPs@PMA	Au NPs capped with PMA
Au NPs@cit	Au NPs capped with citrate
Au NPs@PEG	Au NPs capped with CH <sub>3</sub> O-PEG-SH
Au NPs@PEG@DDA	Au NPs capped with mixture of CH <sub>3</sub> O-PEG-SH and DDA
Au NRs@CTAB	Au NRs capped with CTAB
Au NRs@PEG	Au NRs capped with CH <sub>3</sub> O-PEG-SH

## 2.4 Key instruments

Name	Model	Company	Function
Inductively coupled plasma mass spectrometry (ICP-MS)	7700 series	Agilent	Element concentration measurement
Transmission electron microscopy (TEM)	JEM-1400PLUS	JEOL	Au NPs core size measurement
Dynamic light scattering (DLS)	NANO ZS	Malvern	Au NP hydrodynamic diameter measurement and zeta potential measurement
Fluorescence meter	Fluorolog-3	Horiba Jobin Yvon	Cell viability measurement
UV-Vis Spectrophotometer	Cary 60	Agilent	UV-Vis absorbance spectra Measurement
Drop shape analyzer DSA25	Pendant drop	KRÜSS	Interfacial tension measurement
Confocal Microscopy	LSM510	CarlZeiss	Cell Dead/Live staining measurement

## 2.5 Materials and Methods

### 2.5.1 Synthesis of Au NPs and Au NRs

The protocol for the 4 nm, 25 nm, 50 nm, and 100 nm Au NPs synthesis and ligand exchange and polymer coating process have been reported by J Hühn et al.[116]

#### 2.5.1.1 Synthesis of 4 nm Au NPs@PMA

The 4 nm Hydrophobic Au NPs were synthesized based on the Brust-Schiffrin two-phase method[117] with modifications[118]. 0.9 mmol HAuCl<sub>4</sub> were dissolved in 25 mL Milli-Q water. 2.170 g TOAB was dissolved in 80 mL toluene. Then the above two solutions were mixed in a separation funnel and shaken vigorously for 5 minutes. After about 3 minutes natural settlement, it can be observed that the mixture prepared above separated into two layers with

the upper layer in deep orange color and the bottom aqueous phase colorless, which is because the  $\text{AuCl}_4^-$  ions has been transferred into the organic toluene phase and changing into tetraoctylammonium tetrachloroaurate ion pairs ( $\text{N}(\text{C}_8\text{H}_{17})_4^+\text{AuCl}_4^-$ ). Next, the bottom aqueous phase was discarded and the organic phase was transferred to a 250 mL round flask. Then 334 mg  $\text{NaBH}_4$  was dissolved in 25 mL Milli-Q water by several seconds shaking and must be used before decomposition, which can be suggested by the occurrence of many bubbles. The 25 mL fresh  $\text{NaBH}_4$  solution was immediately added dropwise to the organic phase in the flask within 1 minute under vigorous stirring. Once adding the  $\text{NaBH}_4$  solution, the mixture in the flask immediately changed into red-violet color, which is because of the reduction of  $\text{Au}^{3+}$  into  $\text{Au}^0$ . Then, the stirring was kept for one hour at RT. Afterward, the mixture was transferred to a separation funnel and the aqueous phase was discarded after the organic phase completely separates from the aqueous phase which takes about 3 minutes natural settlement. Later, 25 mL of 10 mM  $\text{HCl}$  (aq) was added to the organic phase and the mixture was shaken for 3 minutes to wash away some remaining ions. Wait for some minutes natural sedimentation until the organic phase separated from the aqueous phase, and then the aqueous phase at the bottom was discarded. Then 25 mL of 10 mM  $\text{NaOH}$  (aq) was added to the organic phase remaining in the separation funnel and the mixture was again shaken for about 3 min. Again, the bottom aqueous phase was discarded after the two phases separates from each other after some minutes natural sedimentation. Then the organic phase remaining in the separation funnel was washed three times with 25 mL of Milli-Q water by shaking similarly to the former two steps and the aqueous phase was discarded every time after the organic phase separates from the aqueous phase. These washing steps were essential to get rid of residual precursors and salts. Then, the organic phase was transferred to a 250 mL round flask and stirred overnight, which is an Ostwald ripening [119-121] process for the Au NPs@ TOAB. Then 10 mL DDT was added to the organic phase in the flask and the mixture was heated to 65 °C under stirring for 2 hours. During this process, the ligand on the Au NPs surface was changed from TOAB to DDT. Until this step, Au NPs@ DDT around 4 nm was achieved, but it is still polydisperse and further purification steps were taken to get rid of too small or too big Au NPs@ DDT. The detailed purification steps are as below: Au NPs@ DDT was transferred to centrifuge tubes and centrifuged at 900 rcf 5 mins and the larger Au NP agglomerates at the bottom of the tube were discarded and the upper supernatant was kept. Afterward, some volume of Methanol at an approximate volume ratio of Methanol: Toluene = 1:1 was added to the upper supernatant until the mixture changed from transparent to turbid and the occurrence of some visible dots. Then this mixture was centrifuged at 900 rcf for 5 mins and the upper supernatant was discarded and

the bottom pellet was collected. After that, chloroform was added to disperse the bottom pellet and it can be observed that the pellet dispersed very well in the chloroform and the almost monodisperse 4 nm Au NPs@ DDT formed red-violet colloid.

To make the Au NPs hydrophilic, further polymer coating was conducted to the already purified Au NPs@ DDT. For the polymer coating of the Au NPs@ DDT, firstly the Au NPs@ DDT was mixed with a certain amount of PMA-g-dodecyl in some milliliters of chloroform in a flask, and the amount of PMA-g-dodecyl required was calculated according to Equation 2-1, which was reported by J Hühn et al[116]. In Equation 2-1, the number of polymer monomers per nm<sup>2</sup> of the effective surface area of Au NPs (RP/Area) depends on the Au NP core size with RP/Area =100 for 4 nm Au NP, RP/Area = 3000 for 25 nm and 50 nm Au NP and RP/Area =4000 for 100 nm Au NPs. All these parameters and detailed steps for polymer coating have been written by J Hühn et al[116]. The calculation of the effective surface area of Au NPs@ DDT per NP ( $A_{eff}$ ) was according to the sphere surface area equation and molar concentration of Au NP (CNP) was calculated according to UVvis absorbance intensity at 450 nm and the molar concentration of PMA-g-dodecyl (CP) was known according to the synthesis of the PMA-g-dodecyl process reported by J. Hühn et al[116]. It is worthy of attention that the volume of chloroform added must ensure a suitable concentration level of Au NPs, otherwise, the Au NPs might aggregate during this polymer coating process if the concentration of Au NPs is too low. According to our experience, the suitable concentration level of Au NPs is usually 0.1-1  $\mu$ M for 4 nm Au NPs@ DDT, 1 nM for 25 nm Au NPs@ DDA, 0.1 nM for 50 nm Au NPs@ DDA and 0.01 nM for 100 nm Au NPs@ DDA. Then this mixture of Au NPs and PMA-g-dodecyl in chloroform in the flask was shaken and sonicated for about 1 minute, afterwards the flask was connected to an evaporator and the mixture was evaporated under suitable level of vacuum at 40 °C until there was very small amount of liquid left (the pressure can be reduced with decreased volume of remaining liquid), during which process, the PMA-g-dodecyl was forced to cover the surface of the Au NPs forming polymer capped Au NPs. Then again, the same volume of chloroform was added to disperse the polymer capped Au NPs and the mixture was evaporated again under the same condition as the first evaporation process. This step was repeated again and after this third evaporation, the mixture was completely dry and a film of polymer-coated Au NPs can be seen on the surface of the flask. Then some volume of 0.1 M NaOH (aq) instead of chloroform was added to disperse the polymer-coated Au NPs and sonication can be used to accelerate the dissolution if necessary and this colloid was kept overnight just to ensure complete hydrolysis. During this process, the remaining anhydride

rings of PMA-g-dodecyl get hydrolyzed in alkaline conditions resulting in carboxylate groups that allow reconstitution in water thus providing Au NPs with excellent colloidal stability.[116] After this step, 4 nm Au NPs@PMA was completed.

$$V_{P\_sol} = (R_{P/Area} \times A_{eff} \times c_{NP} \times V_{NP\_sol}) / c_P \quad \text{Equation 2-1}$$

Then the 4 nm Au NPs@PMA was ultra-centrifuged at 214200 rcf for 30 min and the supernatant was discarded. This ultracentrifugation was repeated twice just to remove the excess free PMA-g-dodecyl. Finally, the PMA-coated Au NPs were filtered with a 0.22  $\mu$ m PES membrane filter and stored afterward in a 2 mL autoclaved EP tube.

### **2.5.1.2 Synthesis of 25, 50, and 100 nm Au NPs@PMA**

#### **Synthesis of 14 nm Au NPs@cit seed**

The 1st step of the synthesis of 25 nm, 50 nm, and 100 nm Au NPs@PMA was to synthesize the 14 nm citrate-capped Au NPs (Au NPs@cit) seed. The synthesis of Au NPs@cit seed was conducted according to a modified protocol reported by Bastus et al.[122] Firstly, 25 mM HAuCl<sub>4</sub> solution and 60 mM Sodium citrate solution were prepared separately. Then 3.3 mL 60 mM Sodium citrate solution and 146.7 mL Milli-Q water were mixed in a 250 mL round flask so that the solution inside the flask was 150 mL 1.32 mM Sodium Citrate solution. The flask was connected with a condenser and heated up until boiling under stirring and refluxing. After 5 min of boiling, 1.5 mL 25 mM HAuCl<sub>4</sub> solution was injected into the boiling solution quickly, and immediately after the injection, the solution changed into light blue and gradually the solution changed to soft purple and then soft red. After further boiling for 10 min, the solution was cooled down to RT temperature. And the corresponding peak SPR wavelength of this Au NPs@cit seed was approximately 518 nm according to UV-vis absorbance spectroscopy and the hydrodynamic diameter of this Au NPs@cit seed is about 14 nm according to DLS measurement.

#### **Growth of 14 nm Au NPs@cit seed to required size 25 nm, 50 nm, and 100 nm**

Then this flask of Au NPs@cit seed was heated up to 90 °C under stirring and refluxing, which condition was always maintained during all the following growth steps. Afterward, 1 mL 25 mM HAuCl<sub>4</sub> solution was injected into the Au NPs@cit seed and this 0.025 mmol HAuCl<sub>4</sub> was almost consumed after a 30 min reaction. Then the injection of 1 mL 25 mM HAuCl<sub>4</sub>

solution and the following 30 min interval reaction time were repeated twice. After this process, Au NPs@cit marked as generation 0 (G0) was achieved. Then 55 mL G0 colloid was extracted and a mixture of 2 mL 60 mM Sodium citrate solution and 53 mL Milli-Q water were poured into the flask, thus the G0 colloid was diluted. Wait about 15 min under stirring and refluxing until the temperature was back to 90 °C. Then make three consecutive injections of 1 mL 25 mM HAuCl<sub>4</sub> solution and each injection was followed by 30 min interval. After this, Au NPs@cit marked as generation 1 (G1) was achieved. Using the same procedure, G2, G3, G4, G5..... G8, G9 can be achieved. After each generation, 55 mL of that generation Au NPs@cit was extracted and the mixture of 2 mL 60 mM Sodium citrate solution and 53 mL Milli-Q water was poured into the flask instead. And until the temperature was increased again to 90 °C, three consecutive injections of 1 mL 25 mM HAuCl<sub>4</sub> solution and the following 30 mins time interval for the reaction were conducted. To know the size of each generation Au NPs@cit, 1 mL Au NPs@cit was taken out and UV-vis absorbance spectra was measured after it cools down to RT. Usually, the peak wavelength of G1, G4, and G9 is 525-530 nm, 537-542 nm, and 575-585 nm respectively and the corresponding diameter of the Cit-Au NP core is approximately 25 nm, 50 nm, and 100 nm respectively. If the temperature of the solution is a little higher than 90 °C (for example 92 °C), then the growth can be slower, and if the temperature is a little lower than 90 °C (for example 86 °C), then the growth can be faster. But the temperature can't be largely different from 90 °C. When the peak wavelength measured from UVvis absorbance reached the expected value corresponding to 25 nm, 50 nm, and 100 nm, the growth was stopped.

### **Ligand exchange from citrate ligand to CH<sub>3</sub>O-PEG-SH and later to a mixture of CH<sub>3</sub>O-PEG-SH and DDA**

To change the citrate ligand to PMA-g-dodecyl ligand, the Au NPs@cit was first transferred to CH<sub>3</sub>O-PEG-SH capped Au NPs (Au NPs@PEG), which exists because of the strong Au-S bond and then the ligand was partially changed into DDA and finally, the PMA-g-dodecyl was capped onto the surface of the Au NPs to form polymer coated Au NPs (Au NPs@PMA). The methods are as below: CH<sub>3</sub>O-PEG-SH with a molecular weight of 2000 Dalton was dissolved in Milli-Q water to form a concentration of normally 10-100 mg/mL. Then excess CH<sub>3</sub>O-PEG-SH solution was added to the Cit-Au NP colloid and stirred overnight at RT. The amount of CH<sub>3</sub>O-PEG-SH required was calculated according to Table 2-1. After this step, the Au NPs@cit will completely change to Au NPs@PEG. Afterward, DDA was dissolved in chloroform to form a concentration of 0.2 M. To transfer PEG-Au NP from water to chloroform

and also make DDA coating to the PEG-Au NPs at the same time, the 0.2 M DDA chloroform solution was added to the Au NPs@PEG colloid with a volume ratio of 1:1, which ensures that the DDA amount was in large excess and much more than the required amount listed in Table 2-1. At the beginning of this phase transfer process, the Au NPs@PEG will be at the upper layer presenting the color of the Au NPs and the transparent DDA chloroform solution will be at the bottom layer. After vigorous stirring, the PEG-Au NPs can be dragged to the bottom layer of chloroform. 4 hours of stirring was usually kept to get Au NPs with CH<sub>3</sub>O-PEG-SH and DDA firmly attached, which is the basis for the later polymer coating. Then the upper aqueous phase including free citrate and excess PEG was discarded and the bottom Au NPs with CH<sub>3</sub>O-PEG-SH and DDA firmly attached were collected. The Au NPs after this step can be described simply as Au NPs@PEG@DDA.

### **Purification steps to remove the excess CH<sub>3</sub>O-PEG-SH and DDA**

The above-synthesized Au NPs@PEG@DDA was centrifuged twice with chloroform to remove the excess CH<sub>3</sub>O-PEG-SH and DDA. The centrifugation speed for the 25 nm, 50 nm, and 100 nm Au NPs are 8000 rcf, 3354 rcf, and 536 rcf respectively and the centrifugation time of 20 -30 min is selected for all these three sizes of Au NPs. Every time after centrifugation, the supernatant was discarded and the pellet was collected and dispersed in chloroform. The centrifugation speed should be the lowest speed which can settle most Au NPs to the bottom without obvious aggregation.

### **Polymer coating**

After this purification step, the polymer coating was conducted and the methods were completely the same as the polymer coating for the 4 nm Au NPs and have been already written in the polymer coating for the 4 nm Au NPs and the amount of PMA-g-dodecyl added was according to the Equation 2-1. And the number of polymer monomers per nm<sup>2</sup> of the effective surface area of Au NPs (RP/Area) varies with the Au NP core size as RP/Area =3000 for 25 nm and 50 nm Au NP and RP/Area =4000 for 100 nm Au NPs and these parameters have been reported by J Hühn et al.[116] After the same polymer coating steps as having been written for the polymer coating for 4 nm Au NPs@PMA, centrifugation three times at 8000 rcf, 3354 rcf, and 536 rcf for about 20-30 mins were used for 25 nm, 50 nm, and 100 nm Au NPs respectively to remove the excess polymer with the supernatant discarded and the bottom Au NP pellet dispersed in Milli-Q water. In the end, the PMA-Au NPs were filtered with a 0.22 μm PES membrane filter and stored afterward in 2 mL autoclaved EP tubes separately.

Table 2-1 Phase transfer of Au NPs@Cit with different core diameters.

Au NP d <sub>c</sub> [nm]	C <sub>PEG</sub> /C <sub>NP</sub>	C <sub>DDA</sub> /C <sub>NP</sub>
25	3 × 10 <sup>4</sup>	13 × 10 <sup>6</sup>
50	20 × 10 <sup>4</sup>	20 × 10 <sup>6</sup>
100	50 × 10 <sup>4</sup>	40 × 10 <sup>6</sup>

CNP in Table 2-1 and Equation 2-1 refers to the molar concentration of Au NPs, which can be calculated from their UVvis absorbance intensity at 450 nm according to chapter 9.2 of J Hühn et al[116]. And CPEG, and CDDA refer to the molar concentration of CH<sub>3</sub>O-PEG-SH and DDA respectively.

### Synthesis of Au NRs@CTAB of 40 nm and 100 nm length.

The synthesis of Au NRs with a length of 40 nm and 100 nm follows the methods reported by Ye X. et al[123] and J Hühn et al[116]. Both the synthesis of 40 nm length and the synthesis of 100 nm length Au NRs contain the seed preparation and growth solution preparation processes. And the seed for both 40 nm long and 100 nm length Au NRs is the same. The seed synthesis method is as below: Dissolve CTAB in about 5 mL 50 °C Milli-Q water to form a CTAB solution of 0.2 M concentration and this solution was then cooled down to RT temperature. Mixed the 5 mL 0.2 M CTAB solution with 5 mL 0.5 mM HAuCl<sub>4</sub> solution under stirring at RT. After about tens of seconds stirring, 0.6 mL 0.01 M freshly prepared NaBH<sub>4</sub> solution was injected to the mixture under vigorous stirring. For the seed of 100 nm length Au NRs, the 0.6 mL 0.01 M freshly NaBH<sub>4</sub> solution was firstly diluted with 0.4 mL milliq water to make 1 mL of 0.006 M NaBH<sub>4</sub> solution and then this 1 mL of 0.006 M NaBH<sub>4</sub> solution was injected. There should not be many bubbles in the NaBH<sub>4</sub> solution before injection, otherwise, the NaBH<sub>4</sub> has decomposed. After the injection of NaBH<sub>4</sub> solution, the solution color immediately changes from yellow to brownish yellow. Keep stirring for 2 minutes and then the Au NP seed capped with CTAB has been synthesized and can be stored at 25 °C for half to one hour to experience Ostwald ripening [119-121] and make the seed stable for further use in the following Au NR growth.

The preparation of growth solution for 40 nm length Au NRs and 100 nm length Au NRs vary from each other. To prepare the growth solution for the 40 nm length Au NRs, 9.0 g CTAB and 0.8 g Sodium Salicylate were dissolved in 250 mL warm water (50-60 °C) under stirring. It takes some time for all the CTAB and Sodium salicylate to dissolve. After they completely dissolved, the solution was cooled in flow water to reach 30 °C. Then 6 mL 4 mM freshly prepared AgNO<sub>3</sub> was added and after 30 S gentle stirring, the solution was kept undisturbed



for 15 min at 30 °C. After that, 250 mL 1 mM HAuCl<sub>4</sub> solution was added and gentle stirring was kept for 15 min. Then 1 mL 64 mM ascorbic acid was added under stirring for about 30 S. Then 0.8 mL Au NPs seed was added under gentle stirring for about 20 S and then the mixture was kept undisturbed at RT overnight. The Au NRs@CTAB of 40 nm length has been achieved after this process.

To prepare the growth solution for the 100 nm length Au NRs, 7.0 g CTAB and 1.234 g Sodium oleate were dissolved in 250 mL warm water (50-60 °C) under stirring. It takes some time for all the CTAB and Sodium Oleate to dissolve. After they completely dissolved, the solution was cooled in flow water to reach 30 °C. Then 24 mL 4 mM freshly prepared AgNO<sub>3</sub> was added and after 30 S gentle stirring, the solution was kept undisturbed for 15 min at 30 °C. After that, 250 mL 1 mM HAuCl<sub>4</sub> solution was added and gentle stirring was kept for 90 min. During this 90 min stirring, the solution color changed from yellow to colorless. Then 2.4 mL HCl (aq) was added to adjust the solution pH from an initial 6.05 to finally 1.32. After the pH adjustment, the solution was gently stirred for 15 min. Then 1.25 mL 64 mM ascorbic acid was added under stirring for about 30 S. Then 0.4 mL Au NPs seed was added under gentle stirring for about 20 S and then the mixture was kept undisturbed at RT overnight. Au NRs@CTAB of 100 nm length has been synthesized.

### **Ligand exchange and polymer coating of the 40 nm and 100 nm Au NRs**

To make 40 nm Au NRs and 100 nm Au NRs@CTAB stable in biological media, PMA-g-dodecyl was coated to the Au NRs. And the complete processes were similar to the polymer coating for 25 nm, 50 nm, and 100 nm Au NPs, which have already been written. Thus, here just briefly describe the methods. Firstly, the CATB capped 40 nm Au NRs@CTAB and 100 nm Au NRs@CTAB were centrifuged at 8000 rcf for 20 mins and 2146 rcf for 20 mins respectively to remove the excess free CTAB. After the centrifugation, both the supernatant and also the white powder, which was precipitated CTAB, occurring at the bottom and the inside surface of the tube should be discarded. Then Milli-Q water was added to disperse the Au NRs@CTAB pellet. And this centrifugation wash step was repeated one time and then water was again added to disperse the Au NRs@CTAB pellet. CH<sub>3</sub>O-PEG-SH with a molecular weight of 2000 Dalton was dissolved in Milli-Q water to prepare a concentration of about 10-100 mg/mL. Then a certain amount of that CH<sub>3</sub>O-PEG-SH solution according to Table 2-2 was added and stirring was kept for about 20 hours. Then centrifugation twice at 8000 rcf for 20 mins was conducted for 40 nm Au NRs@PEG and centrifugation at 2146 rcf for 20 mins was

conducted for 100 nm Au NRs@PEG just to remove the free CH<sub>3</sub>O-PEG-SH and CTAB with the supernatant discarded and the bottom pellet dispersed in Milli-Q water. Then 0.4 M DDA chloroform solution was added to the Au NRs@PEG colloid with a volume ratio of chloroform: Au NPs colloid =1:2 and stirring was kept overnight. After that, the Au NRs can be transferred to chloroform and the organic phase changed from colorless to the color of light green and brownish for 40 nm and 100 nm length Au NRs@PEG@DDA respectively. Then centrifugation twice at 8000 rcf for 20 mins was conducted for 40 nm Au NRs@PEG@DDA and 2146 rcf for 20 mins twice was conducted for 100 nm Au NRs@PEG@DDA to remove the free CH<sub>3</sub>O-PEG-SH and DDA with the supernatant discarded and the bottom pellet dispersed in chloroform. After the purification, the polymer coating was conducted and the methods were completely the same as the polymer coating for the 4 nm Au NPs and have been written before and the amount of PMA-g-dodecyl added was according to Equation 2-1. And the number of polymer monomers per nm<sup>2</sup> of the effective surface area of Au NPs (RP/Area) was 3000 for Au NRs of both 40 nm and 100 nm length and these parameters have been reported by J Hühn et al[116]. After that, centrifugation three times at 8000 rcf, and 2146 rcf for 20 mins were used for the 40 nm Au NRs@PMA and 100 nm Au NRs@PMA respectively to remove the free polymer with the supernatant discarded and the bottom Au NP pellet dispersed in Milli-Q water. In the end, the PMA-Au NPs were filtered with a 0.22 μm PES membrane filter and stored afterward in 2 mL autoclaved EP tubes separately.

*Table 2-2 Phase transfer of CTAB-Au NRs with different lengths.*

length [nm]	C <sub>PEG/CNP</sub>	C <sub>DDA</sub> [M]
40	$8 \times 10^4$	0.4
100	$8 \times 10^4$	0.4

All the Au NP/NRs used in the following experiments are the ones coated with PMA-g-dodecyl if not specialized.

### **2.5.2 Interfacial tension (IFT) measurement**

The dynamic interfacial tension (IFT) at the Au NPs colloid-toluene interface was determined by the pendant drop tensionmetry using a Drop shape analyzer (DSA25, Krüss, Germany). The measurement procedure was the same as reported by Del Pino P et al..[124] Au NPs colloid was filled in the Hamilton syringe and the concentration of AuNPs (C<sub>Au</sub> and C<sub>NP</sub>) used was presented in Table 2-7 and the molar concentration of AuNPs was calculated from UVvis measurement according to the Lam-beer rule and the corresponding Au mass concentration was converted from the molar concentration of AuNPs based on the molar mass of Au NPs/NRs

described in Table 2-3. This Hamilton syringe plugged into a stainless steel needle (diameter 1.85 mm) immersed in the toluene phase was used to produce a sample droplet of 50  $\mu\text{L}$  at a dosing rate of 200  $\mu\text{L}/\text{min}$ . The IFT upon time of the droplet was recorded by an ultra-fast camera (Krüss, Germany). The IFT at the pure water-toluene interface was used as a control. The droplet volume for this IFT measurement for all sizes of Au NPs colloid was 50  $\mu\text{L}$ . IFT was determined using the analysis software package (Krüss, Germany) by fitting the droplet shape with the Young-Laplace equation:

$$\gamma = \frac{\Delta\rho \cdot g \cdot d_e}{H} \quad \text{Equation 2-2}$$

Where the  $\Delta\rho=0.128 \text{ g/mL}$  is the density difference between pure water and toluene ignoring the tiny density difference caused by the existence of Au NP/NRs. And,  $g=9.81 \text{ m/S}^2$  is the gravitational acceleration,  $d_e$  is the largest horizontal diameter of the droplet, and  $H$  is a function of  $S_n (=dn/d_e)$ , in which  $dn$  is the horizontal diameter at a distance equal to  $d_e \cdot (n/10)$  from the bottom of the drop. The dynamic IFT was measured for 30 mins and the measurement frequency is 1 per second. For each size of AuNP, at least three parallel drops were measured and the results are shown in Figure 2-7. The plots are representative of triplicate measurements.

### 2.5.3 Cell Culture

The Human cervical adenocarcinoma cells (Hela cell CCL2) were purchased from American Type Culture Collection (ATCC, Manassas, USA). Briefly, cells were maintained in complete cell culture media, which is Dulbecco's Modified Eagle's Medium (DMEM high glucose content, pyruvate, Gibco<sup>TM</sup>, Germany) complemented with 10% of fetal bovine serum (FBS, Biochrom, Germany), and 1% of (penicillin-streptomycin (p-s), Fisher Scientific, Germany). Cells were incubated at 37°C in a 5% CO<sub>2</sub> humid air atmosphere incubator. When cells reach approximately 90% confluency, usually two days after cell passaging, cells were passaged, firstly cells were washed one time with 10 mL of phosphate buffered saline (PBS without Ca<sup>2+</sup> and Mg<sup>2+</sup>, Biochrom, Germany), and then dissociated with 1 mL of trypsin ethylenediaminetetraacetic acid (Trypsin-EDTA, 0.05%) solution (Fisher Scientific, Germany) after the removal of the PBS. When the cells have been detached, the dissociation process was finalized by adding of 10 mL complete cell culture media. Then cells were gently pipetted and centrifuged at 300g for 5 min. After that, cells were suspended in complete cell culture media and then counted and seeded in flasks for cell passaging or seeded in culture plates for performing the in vitro experiments including cell viability test, cell Dead/live staining and cell uptake experiments, etc.. ( note: the volumes used in this cell sub-culturing protocol

corresponds to cells grown in a 75 cm<sup>2</sup> flask).[125] And all the cell media used in this chapter 2 is always the same complete cell culture media if not specialized.

#### **2.5.4 Description of the four incubation systems**

As shown in Figure 2-1, the four incubation systems were Static, Dynamic, Fluid, and Suspension systems respectively. The 1st system is called ‘Static’, which is just adhered HeLa cells in static incubation with Au NP/NRs colloid. In this Static system, the sedimentation of big Au NP/NRs (50 nm and 100 nm Au NPs and 100 nm Length Au NRs) would happen during the incubation, which would only exist in this Static system and will be disturbed in the other three systems. The 2nd system is called ‘Dynamic’, which is adhered HeLa cells exposed to the periodically dynamic flow of Au NP/NRs. In this ‘Dynamic’ system, the flask rotates around an axis at 10 rpm, and because the rotation speed is so slow that the Au NP/NRs colloid always stayed at the lowest height of the flask owing to gravity, and thus that there is a relative motion between Au NP/NRs colloid and the adhered cells and also the flask surface. Consequently, the Au NP/NRs colloid was continuously mixed in the whole incubation process and the sedimentation of Au NPs induced by gravity was avoided in this way. Besides, the adhered HeLa cells will experience an alternate exposure to just CO<sub>2</sub> and complete Au NP/NRs because cells only adhered to one surface of the flask, which constituted only about 1/3 of the total side areas of the flask and thus, the status where cells were immersed in the Au NP/NRs exposure occupying only 1/3 of the incubation time and the time when cells exposed to just CO<sub>2</sub> occupied the remaining 2/3 of the incubation time considering the constant rotation speed. But even when the cells were exposed to just CO<sub>2</sub> without any liquid flowing above the cell surface during 2/3 of the incubation time, there was actually still a “thin film” of Au NP/NRs covering the cells and can enter cells during this time period, and this “thin film” of Au NP/NRs was those that contacted cells in the passed 1/3 incubation time and was not completely taken away by the rotation because of the very low rotation speed. The uptake behavior of HeLa cells in this 1/3 time was assumed to be the same as in the Static system ignoring the neglectable effect of the 100 rpm rotation. The 3rd system is called ‘Fluid’, which is adhered HeLa cells seeded in  $\mu$ -slides I 0.2 Luer and connected to a Perfusion Set pump to make a continuous unidirectional flow of Au NP/NRs over the adhered cells. This Fluid system is completely different from the Dynamic system even though the cell status adheres in both these two systems. In the Dynamic system, there is only approximate 1/3 incubation time when the dynamic Au NPs exposure can flow over the cells, while in the other 2/3 incubation time, the cells were exposed to just CO<sub>2</sub>, and the remaining “thin film” of Au NP/NRs touching the cells

without any strong disturbance. But in the Fluid system, the flow is always continuous throughout the whole incubation time and there is a possibility that the flow shear will possibly hinder Au NPs endocytosis by taking Au NP/NRs away before they have been bound to the cell membrane or possibly to the contrary, creating a higher possibility for Au NP/NRs to touch cells by moving the Au NP/NRs towards cells. But which would be the dominant effect still needs to be judged according to our experimental results. The 4th system is called 'Suspension', which is suspended HeLa cells together with Au NP/NRs were incubated in a 15 mL falcon tube that rotates around the axis at 10 rpm. The HeLa cells and Au NP/NRs mixture will always be at the lowest position of the falcon tube just like in the Dynamic system, thus there will be a gentle relative motion between the falcon tube surface and the inside Au NP/NRs and cells mixture so that the Au NP/NRs colloid can be shaken during the whole incubation time and gravity-inducing sedimentation of big Au NP/NRs can be avoided and cells will also be softly mixed continuously. The only difference between the 'Suspension' system and 'Dynamic' system is the status of HeLa cells, while HeLa cells were always immersed and suspended in the Au NP/NRs colloid in the 'Suspension' system during the whole incubation time. In this Suspension system, suspended HeLa cells were initially in well dispersed spheres and after 8 h incubation, HeLa cells will form macroscopic accumulated tumor spheres, which is completely different from the normal adhered morphology in the other three systems.

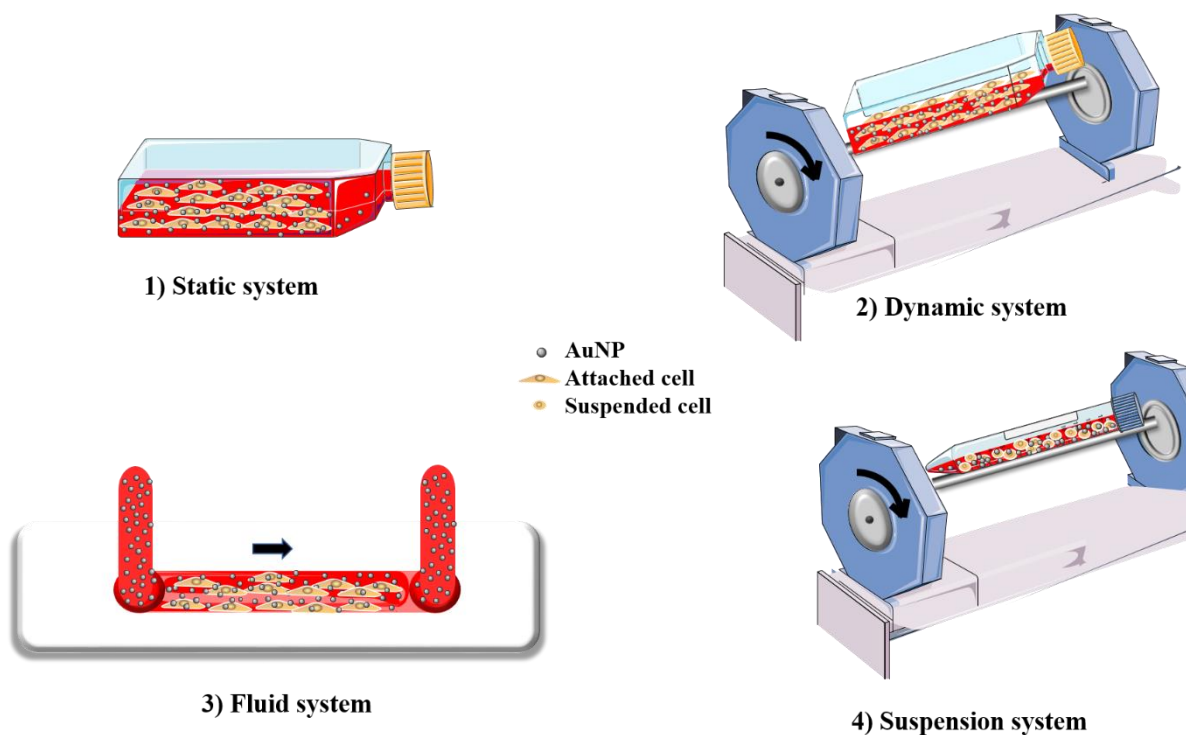


Figure 2-1 Schematic graphs of the 4 incubation systems

### 2.5.5 Cell viability of Hela cells incubated with different concentrations of Au NP/NRs in Static system

To perform the resazurin assay, 7500 cells in complete cell culture media ( $V=100\ \mu\text{L}$ ) were seeded per well in 96 well plates. Cells were kept overnight in a  $37^\circ\text{C}$  humid incubator containing 5%  $\text{CO}_2$  for attachment. The next day, the media was discarded and cells were exposed to  $100\ \mu\text{L}$  Au NP/NRs of different mass concentrations in terms of Au element for 24 and 48 h, while the control samples were exposed to  $100\ \mu\text{L}$  fresh complete media. This mass concentration was converted from the molar concentration of Au NP/NRs as described in chapter 2.6.1.2. The concentration series of Au NP/NRs were prepared by mixing a certain volume of highly concentrated aqueous Au NP/NRs colloid with enough volume of complete media (The volume of complete media exceeds nine times the volume of the highly concentrated aqueous Au NP/NRs colloid). After the desired time, Au NP/NRs exposure was removed and every sample was washed twice with  $100\ \mu\text{L}$  PBS, and then stained with  $100\ \mu\text{L}$  of  $0.025\ \text{mg/mL}$  resazurin solution for each well, which was prepared using 10% V/V Resazurin solution of  $0.25\ \text{mg/mL}$  concentration (Sigma-Aldrich, R7017) mixed with 90% V/V complete media. After 4 h incubation, the plates were read directly in a Fluorescence meter (Fluorolog-3, from Jobin Yvon inc, USA). Samples were excited at 560 nm, and the emission spectra was collected from 580 nm to 600 nm. Cell viability was calculated according to the following equation:

$$V [\%] = \frac{F_x - F_b}{F_c - F_b} \times 100 \quad \text{Equation 2-3}$$

In Equation 2-3,  $F_b$ ,  $F_c$ , and  $F_x$  refer to the fluorescence intensity from the well of blank, control, and Au NP/NR samples at the emission peak wavelength respectively with the wavelength varying from 580 nm to 582 nm.

### **2.5.6 Cell viability of HeLa cells incubated with Au NPs/NRs in Static, Dynamic, and Fluid systems**

To further clarify the HeLa cell viability after Au NP/NRs exposure in Static, Dynamic, and Fluid systems, Resazurin assay was performed as previously reported[126]. Cells were cultured completely following the same procedures as in the uptake study and then the Resazurin assay was conducted. Briefly,  $3 \times 10^5$  cells in 3 mL complete cell media were seeded in the T12.5 flasks for both the Static and Dynamic systems,  $1 \times 10^5$  cells in 100  $\mu$ L complete cell media were seeded in the  $\mu$ -slides I 0.2 Luer (Ibidi GmbH, Martinsried, Germany) for the Fluid system. These cells were incubated in the cell incubator overnight for attachment. The next day, cells were exposed to Au NP/NRs at the concentration of 20  $\mu$ g/mL in terms of Au element for 24h and the volume of the exposure was 3 mL for Static, 3 mL for Dynamic system, and 6 mL for the Fluid system. During this 24 h incubation, the incubation conditions were static, periodically dynamic flow, and continuous uni-directional flow respectively for Static, Dynamic, and Fluid systems, which is completely the same as presented in the schematic Figure 2-1 and described in chapter 2.5.4 and completely the same as its corresponding uptake experiment settings. This 20  $\mu$ g/mL Au NP/NRs exposure was prepared by mixing a certain volume of highly concentrated aqueous Au NP/NRs colloid with enough volume of complete media (The volume of complete media exceeds nine times the volume of the highly concentrated aqueous Au NP/NRs colloid). No NPs samples are HeLa cells of the same passage and exposed to complete cell media instead of Au NP/NRs and cultured in the same Static, Dynamic, and Fluid systems respectively for 24 h as the other samples. After this 24 h incubation, all the sample cells were washed separately and detached using the same parameter as they were treated in the uptake study and the No NPs samples were treated in the same way as the sample cells incubated in the same system, and then a suitable volume of Media was added to finalize the detachment. After that, cells were centrifuged at 300rcf for 5mins and the supernatant was discarded. Then cell pellet was redispersed in 1 mL complete media and counted and then diluted with a certain amount of complete media to reach a cell density of

$1.5 \times 10^5$  cell/mL. After that, 15000 cells in 100  $\mu$ L of complete cell media were seeded per well of 96 well plates with triplicate wells and incubated for several hours until cells attached to the well (usually takes about 5 h) and then media was discarded and 100  $\mu$ L 0.025 mg/mL resazurin were added per well. After 4 hours of incubation, plates were read directly by a Fluorescence meter.

The control sample was for cells of the same passage number as other samples and these control cell samples were suspended in complete cell media directly after trypsin detachment treatment from the flask. Then this cell suspension was immediately seeded in 96 well plates with a density of 7500 cell/well and incubated for 24 h and then every well was washed twice with 100  $\mu$ L PBS and treated with 100  $\mu$ L 0.025 mg/mL resazurin assay for 4 h and then analyzed by Fluorescence meter.

And the cell viability data was from three independent experiments with cells of three passage numbers.

### **2.5.7 Dead/Live staining for Hela cells incubated with Au NPs/NRs in Static, Dynamic, and Suspension systems**

The LIVE/DEAD (FisherScientific, L3224) assay was diluted with PBS solution and the two individual components were mixed to achieve a solution of Calcein AM concentration 2  $\mu$ M and Ethidium homodimer-1 concentration 4  $\mu$ M, which is the final assay used for the Dead/Live staining.

In the case of Static and Dynamic systems, Hela cells in complete cell media were seeded in Ibidi ( $\mu$ -slide 8 well plate) at the density of 10000 cells/well with a volume of 300  $\mu$ L/well and kept in the cell incubator overnight for cell attachment. The next day, cells with three parallel wells were exposed to AuNP/NRs at the concentration of 20  $\mu$ g/mL in terms of Au element (the volume of the exposure was 300  $\mu$ L per well for Static and Dynamic) and cultured in the Static and Dynamic system for 24 h respectively, which is just the same as presented in the schematic Figure 2-1 and described in chapter 2.5.4 and completely the same as its corresponding uptake experiment settings. For the control 1 (Ctrl1) and control 2 (Ctrl2), during this 24 h incubation, cells were just exposed to complete cell media without Au NP/NRs, but the incubation conditions were still the same as presented in the schematic Figure 2-1 and described in chapter 2.5.4. After 24 h exposure, for all the cells except the Ctrl 2 sample, the exposure was removed and cells were washed three times with PBS  $V=100$   $\mu$ L, and then cells were exposed to 100  $\mu$ L of LIVE/DEAD assay reagents per well and incubated for 45 min at



room temperature (RT). For the Ctrl2 samples, the media was firstly discarded and then the cells were first exposed to 75% ethanol  $V = 100 \mu\text{L}$  for 20 min, then the ethanol was removed and cells were then washed twice with  $100 \mu\text{L}$  PBS and then cells were exposed to  $100 \mu\text{L}$  of LIVE/DEAD assay reagents per well for 45 min at RT. Afterward, all the images were captured under confocal microscopy (Karl Zeiss LSM 510, Germany). The cell viability data was from three independent experiments with cells of three passage numbers.

In the case of the Suspension system,  $3 \times 10^5$  cells were suspended in 6 mL media in 15 mL Falcon tubes, then an appropriate amount of AuNP/NRs was added with a final concentration of  $20 \mu\text{g/mL}$  in terms of Au element. For Ctrl1 and Ctrl2 samples, cells were only exposed to 6 mL of complete cell media without AuNP/NRs. All these falcon tubes also including the Ctrl1 and Ctrl2 samples were installed on the Tube revolver (Thermo Scientific<sup>TM</sup>) in a  $37^\circ\text{C}$  incubator and rotated around an axis at a speed of 10 rpm for 24h just the same as presented in the schematic Figure 2-1 and described in chapter 2.5.4. Afterward, for all samples except the Ctrl2 samples, cells were firstly centrifuged at 300 rcf 5 mins and then the cell pellet was washed twice with 1 mL PBS by centrifugation at 300 rcf 5 mins and afterward, the cell pellet was dispersed in 0.5 mL LIVE/DEAD assay. For the Ctrl2 sample, the cells were firstly centrifuged at 300 rcf for 5 mins, and then the supernatant was discarded and cells were redispersed in 1 mL 75% ethanol for 20 mins and again centrifuged at 300 rcf for 5 mins with the supernatant ethanol discarded and the cell pellet was redispersed in 1 mL PBS and again centrifuged at 300 rcf for 5 mins and afterwards the supernatant was discarded and cells were redispersed in 0.5 mL LIVE/DEAD assay. After that, all the cells also including the Ctrl1 and Ctrl2 were counted separately and diluted with a certain amount of LIVE/DEAD assay to get a density of  $3 \times 10^5$  cell/mL. Then  $3 \times 10^4$  cells in  $100 \mu\text{L}$  LIVE/DEAD assay reagents were seeded in one well of Ibidi  $\mu$ -slide 8 well with three parallel wells and incubated for 45 min at room temperature. Finally, images were captured under confocal microscopy (Karl Zeiss LSM 510, Germany). The data was from three independent experiments with cells of three passage numbers.

The cell viability was calculated according to Equation 2-4.

$$V [\%] = \frac{N_1}{N_1 + N_2} \times 100 \quad \text{Equation 2-4}$$

In Equation 2-4,  $N_1$  is the number of live cells which were marked with green color and  $N_2$  is the number of dead cells marked with red color.

### **2.5.8 Growth curve of cells in different systems**

To investigate the effect of the incubation systems on cell growth, the cell growth curve was plotted over time. For the Static and Dynamic cell systems,  $3 \times 10^5$  cells were seeded in the T12.5 cm<sup>2</sup> culture flasks with a Volume of 3 mL or 6 mL. For the Fluid system, the cells were seeded in the  $\mu$ -slides I 0.2 Luer (Ibidi GmbH, Martinsried, Germany) at the cell density of 24000 cells/cm<sup>2</sup>. After attachment, the cell number was counted and marked as Day 0, which was normalized to 1. Then cells were exposed to 3 and 6 mL of fresh complete cell media respectively and were put in Static, Dynamic, and Fluid systems respectively for further incubation. All the cell incubation conditions corresponding to each system followed the parameters described in chapter 2.5.4 and presented in Figure 2-1. Every 24h, cells in all of these different systems were collected and counted respectively. For the Suspension system,  $3 \times 10^5$  cells in 3 mL or 6 mL media were seeded in 15 mL falcon tubes, this is Day 0 for the Suspension system and then cells were incubated in the Suspension system and collected and counted every 24h. Finally, the growth curve in different systems was plotted as shown in Figure 2-12. This Growth curve measurement of HeLa cells was conducted by Xing Sun.

### **2.5.9 Static system cell uptake study: Adhered HeLa cells exposed to Static Au NPs/NRs**

HeLa cells were seeded in a T12.5 cm<sup>2</sup> flask with the density of  $3 \times 10^5$  cells in V=3 mL complete cell media. After desired time to attach to the surface of the flask, cells were exposed to Au NP/NRs to achieve concentrations of 10  $\mu$ g/mL and 20  $\mu$ g/mL in terms of Au element mass concentration.

For each concentration, two volumes were given, 3 and 6 mL. Cells were incubated with Au NP/NRs for 4, 8, and 24 h in the Static system as presented in the schematic Figure 2-1 and described in chapter 2.5.4. After respective incubation, Cells were washed twice with 1 mL DPBS (Dulbecco's phosphate-buffered saline) containing Ca<sup>2+</sup> and Mg<sup>2+</sup> and 1 time with 1 mL PBS, then cells were detached by adding 0.3 mL of trypsin. Then 1 mL of DPBS containing Ca<sup>2+</sup> and Mg<sup>2+</sup> was added inside to disperse the cells. Afterward, cells were counted and the cell pellet was got by centrifugation at 300 rcf for 5 min and the supernatant was discarded. The internalized Au in the cell pellet was measured by ICP-MS. To prepare ICP-MS samples, the cells pellet was firstly digested with 50  $\mu$ L of HNO<sub>3</sub> (aq, 67 wt%) overnight, and then 100  $\mu$ L of HCl (aq, 35 wt%) was added inside, to further dissolve the Au NP/NRs inside. Then this digested sample was diluted with 2 mL of 2% V/V HCl (prepared by mixing 2 mL 35 wt% HCl

aq. With 98 mL Milli-Q water) and afterward kept for ICP-MS measurement. The Au concentration in each sample was measured by ICP-MS and the corresponding cell number was used to calculate the internalized Au mass per cell.

#### **2.5.10 Dynamic system cell uptake study: Adhered HeLa cells exposed to periodically dynamic Au NPs/NRs**

HeLa Cells were seeded in a T12.5 flask with the density of  $3 \times 10^5$  cells in 3 mL cell media. After cell attachment to the flask surface, cells were exposed to Au NP/NRs to achieve concentrations of 10  $\mu\text{g/mL}$  and 20  $\mu\text{g/mL}$  in terms of Au element mass. For each concentration, two volumes were given, 3 and 6 mL. Cells were incubated with NP/NRs for 4, 8, and 24 h in a Dynamic system where the flasks were rotated around an axis at a speed of 10 rpm, the same as presented in the schematic Figure 2-1 and described in chapter 2.5.4. After the designed time incubation in the rotary condition, cells were washed twice with 1 mL DPBS and 1 time with 1 mL PBS, then cells were detached by adding 0.3 mL of trypsin. Then 1 mL of DPBS was added inside to disperse the cell pellet. Cells were counted and cell pellets were got by centrifugation at 300 rcf for 5 min and the supernatant was discarded. To prepare ICP-MS samples, the cells pellet was firstly digested with 50  $\mu\text{L}$  of  $\text{HNO}_3$  (aq, 67 wt%) overnight, and then 100  $\mu\text{L}$  of  $\text{HCl}$  (aq, 35 wt%) was added inside, to dissolve the NPs inside. Then the ICP-MS sample preparation and the corresponding internalized Au mass per cell calculation method were completely the same as those used for the Static system.

#### **2.5.11 Fluid system cell uptake study: adhered HeLa cells incubated with the continuous uni-directional flow of Au NP/NRs**

100  $\mu\text{L}$  HeLa cells with a density of  $10^6$  cells/mL, were cultured in  $\mu$ -slides I 0.2 Luer (Ibidi GmbH, Martinsried, Germany). After about 7 hours of static culture to reach good cell attachment, the slides were installed in the Ibidi pump system. The cells were subject to homogeneous unidirectional laminar flow of 6 mL DMEM complete cell media and 0.498 Pa shear stress overnight. Afterward, cells were cultured in 6 mL unidirectional laminar flow of DMEM complete cell media containing AuNP/NRs with the concentration of 10 and 20  $\mu\text{g/mL}$  in terms of Au element mass concentration for 4, 8, and 24 hours respectively. For control, cells were only exposed to complete cell media. To pay special attention, bubbles should be avoided in the  $\mu$ -slides I 0.2 Luer. After the designed timepoints incubation, experiments were stopped and cells were washed three times with 100  $\mu\text{L}$  PBS, after that cells were detached with 100  $\mu\text{L}$  trypsin and then 500  $\mu\text{L}$  complete media was used to finalize the detachment and

disperse the cells. After counting via Neubauer Chambers (Celeromics Technologies, València, Spain), cells were centrifuged at 300 rcf for 5 mins and the supernatant was discarded and the cell pellet was collected for ICP-MS measurement. The ICP-MS sample preparation protocol and the internalized Au mass per cell calculation method are completely the same as those used for the Static and Dynamic systems.

### **2.5.12 Separation of suspended HeLa cells with free Au NPs/NRs**

To separate cells from free NP/NRs in the Suspension system, a pretest was conducted assuming that the sedimentation behavior of Au NP/NRs in this pretest was the same as they were after some time incubation with HeLa cells in the Suspension system. According to our knowledge, Au NP/NRs especially big Au NP/NRs like 100 nm AuNPs can settle down to the bottom of tubes at speed of 130 rcf (1000 rpm, rotator radius 120 mm). Therefore, a lower speed and more washing steps were used to separate the free NPs and cells. Thus 34 rcf (500 rpm, rotator radius 120 mm) 5 min centrifugation was used to separate cells and free Au NP/NRs. Firstly, 300000 cells were suspended in 6 mL cell culture media containing 20 µg/mL NPs in 15 mL falcon tubes, and then 34 rcf (500 rpm, rotator radius 120 mm, minimal speed of the centrifugation rotor) 5 min was used. This is marked as washing time #1. And the supernatant was collected for ICP-MS measurement and the cell pellet was collected and the cell number was counted after resuspension in 1.2 mL PBS (marked as washing time #1). We find that after this 1st-time centrifugation, more than 90% of the cells could be collected, which added feasibility for the separation. And then the centrifugation and counting were repeated three times (marked as washing time #2, #3, and #4). 50 µL of the supernatants from each step were taken out for ICP-MS measurement. In the last step, after the cell counting, the cell was again centrifuged and the cell pellet was collected for further measurement. Based on the Au mass in the supernatants, the proper washing times in this experiment were determined. For ICP-MS measurement, the 50 µL supernatant was digested overnight with 200 µL fresh Aqua Regia and then diluted with 1.8 mL 2% (V/V) HCl (prepared by mixing 2 mL 35 wt% HCl aq. With 98 mL Milli-Q water). And the cell pellet preparation for ICP-MS measurement completely followed the protocol used for the Static, Dynamic, and Fluid system uptake samples.

### **2.5.13 Suspension system cell uptake study: suspended HeLa cells exposed to dynamic Au NP/ NRs**

In 15 mL Falcon tubes,  $3 \times 10^5$  HeLa cells were dispersed in 3 mL and 6 mL complete cell media respectively, then a calculated amount of Au NP/NRs was added inside to make a homogeneous Au NP/NRs suspension of Au mass concentration of 10 and 20  $\mu\text{g/mL}$ . These Falcon tubes were afterward fixed on the Tube revolver (Thermo Scientific<sup>TM</sup>). Cells were incubated in a dynamic condition with the speed of 10 rpm for 4, 8, and 24h respectively as presented in schematic Figure 2-1 and described in chapter 2.5.4. Later on, the mixture of cells and Au NP/NRs suspension were centrifugated at 500 rpm for 5 min, and the supernatant was discarded. In the following steps, the cell pellet was washed four times with 1 mL PBS in a 2 mL Eppendorf tube by centrifugation at 500 rpm for 5 min. At the last wash step, the cell was counted before centrifugation and the cell pellet was collected for ICP-MS measurement after centrifugation. The ICP-MS sample preparation protocol and the internalized Au mass per cell calculation method are completely the same as those used for the Static, Dynamic, and Fluid systems.

## **2.6 Results and discussions**

### **2.6.1 Characterization of Au NP/NRs**

#### **2.6.1.1 Transmission electron microscopy**

Transmission electron microscopy (TEM) images were used to investigate the shape and size distribution of all NP/NRs as previously shown[116]. To determine the size distribution of the core diameter  $d_c$  of the different Au NP/NRs,  $d_c$  was calculated by counting 100 NP/NRs in each TEM image using the ImageJ software. Illustrative TEM images of the Au NP/NRs are displayed in Figure 2-2 and the obtained size distribution histograms and further characterization can be seen in Figure 2-3 and Table 2-3.

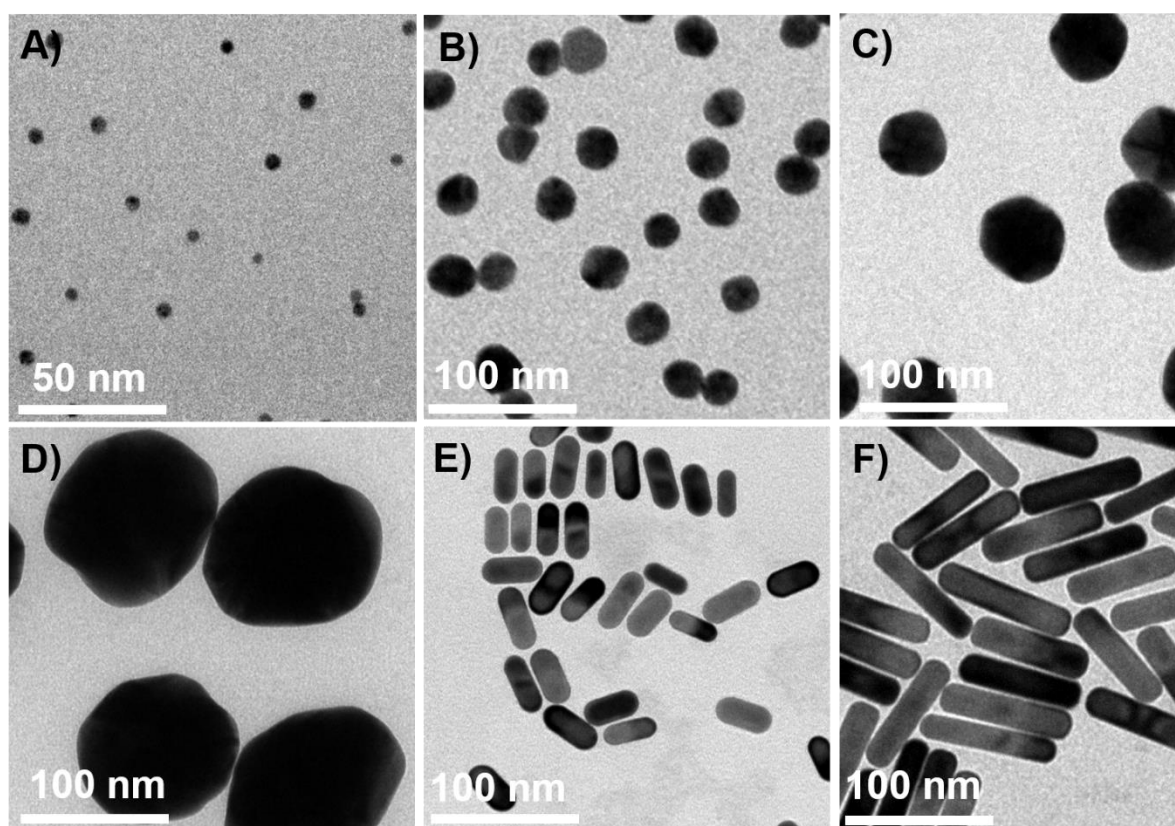


Figure 2-2 Representative TEM images of Au NP/NRs. A) 5, B) 25, C) 50, D) 100 nm AuNPs and E) 40, F) 100 nm AuNRs respectively. Additional detailed information of NPs is shown in Table 2-3.

Table 2-3 Characterization of 5, 25, 50, 100 nm AuNPs and 40, 100 nm AuNRs. Surface plasma resonance peak ( $\lambda_{SPR}$ ), core diameter ( $d_{TEM}$ ), core length ( $L_{TEM}$ ), hydrodynamic diameter ( $d_{h(N)}$ ), zeta potential ( $\zeta$ ), and molecular weights ( $M_w$ ) of the NP is shown. Data points are given as mean value  $\pm$  standard deviation (SD).

NPs	$\lambda_{SPR}$ [nm]	$d_{cTEM}$ [nm]	$L_{cTEM}$ [nm]	$d_{h(N)}$ [nm]	PdI	$\zeta$ [mV]	$M_w$ [g/mol]
5 nm AuNPs	517	4.7 $\pm$ 1.0	-	15.5 $\pm$ 0.3	0.26 $\pm$ 0.04	-31.8 $\pm$ 2.3	6.3 $\times$ 10 <sup>5</sup>
25 nm AuNPs	526	24.5 $\pm$ 3.7	-	30.6 $\pm$ 3.5	0.23 $\pm$ 0.01	-40.6 $\pm$ 1.9	8.9 $\times$ 10 <sup>7</sup>
50 nm AuNPs	543	49.8 $\pm$ 7.8	-	47.9 $\pm$ 2.2	0.20 $\pm$ 0.00	-38.9 $\pm$ 0.9	7.5 $\times$ 10 <sup>8</sup>
100 nm AuNPs	578	101.4 $\pm$ 12.8	-	109.4 $\pm$ 8.7	0.11 $\pm$ 0.03	-47.1 $\pm$ 2.1	6.3 $\times$ 10 <sup>9</sup>
40 nm AuNRs	665	15.7 $\pm$ 1.9	39.3 $\pm$ 2.5			-39.1 $\pm$ 2.1	8.8 $\times$ 10 <sup>7</sup>
100nm AuNRs	870	25.2 $\pm$ 1.4	99.3 $\pm$ 3.9			-41.0 $\pm$ 3.0	5.8 $\times$ 10 <sup>8</sup>

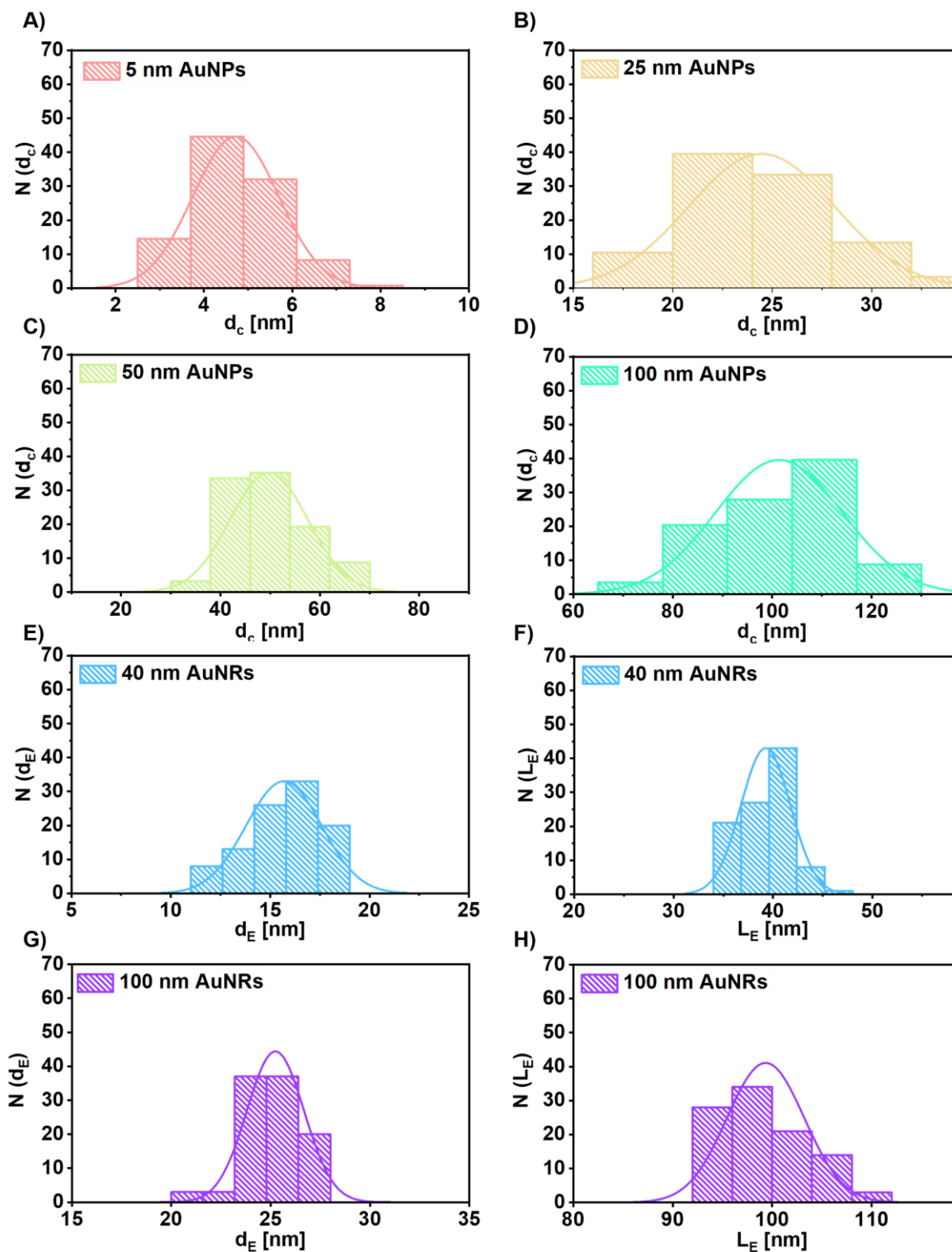


Figure 2-3 Size distribution histogram and size distribution Gaussian fitting of the Au NP/NRs. A) 5, B) 25, C) 50, D) 100 nm AuNPs, E), F) 40, and G), H) 100 nm AuNRs respectively based on the analysis of TEM images. Mean values were calculated from 100 NP/NRs. This graph was done by Xing Sun.

Detailed information was shown in Table 2-3.

### 2.6.1.2 Calculation of Au NP/NR mass concentration in terms of Au element $C_{(Au)}$

The mass concentrations of Au NPs/NRs in terms of Au element exposed in all our experiments including 20  $\mu\text{g/mL}$ , 10  $\mu\text{g/mL}$ , and series of concentrations used for cell viability test and also the mass concentration 112  $\mu\text{g/mL}$  used for the Interfacial tension measurement were all converted from the molar concentration of NP/NRs, which was calculated from UV-vis absorbance at 450 nm according to Beer Lambert law as previously reported, combined with the molar mass of Au NP/NRs.[116] The molar mass  $M_w$  of the NPs and NRs was calculated as previously reported[116]. Briefly, the 5, 25, 50, and 100 nm AuNPs were assumed to be perfect solid spheres, and their volume ( $V_{NP}$ ) was calculated based on Equation 2-5. In the case of 40 and 100 nm Au NRs, NRs were assumed to be cylinders, and their volume ( $V_{NR}$ ) was calculated based on the Equation 2-6. The average diameter ( $d_c$ ) of the NPs and the length ( $L$ ) of the NRs used were taken from the calculated TEM values as shown in Table 2-3. The volume of one NP/NR is described as follow:

$$V_{NP} = \frac{4}{3} \cdot \pi \cdot \left(\frac{d}{2}\right)^3 \quad \text{Equation 2-5}$$

$$V_{NR} = \pi \cdot \left(\frac{d}{2}\right)^2 \cdot L \quad \text{Equation 2-6}$$

The density of bulk Au ( $\rho_{Au}$ ), and Avogadro number ( $N_A$ ) are known, and thus the molar weight  $M_w$  of the NP and NR cores are calculated as:

$$M_{NP/NR} = V_{NP/NR} \cdot \rho_{Au} \cdot N_A \quad \text{Equation 2-7}$$

The molar concentration of Au NP/NRs ( $C_{NP/NR}$ ) can be calculated from the mass of Au ( $m_{Au}$ ) and the volume of solution ( $V_{solution}$ ) used, which was presented as

$$C_{NP/NR} = \frac{m_{Au}}{V_{solution} \cdot M_{NP/NR}} \quad \text{Equation 2-8}$$

Besides, the molar concentration of NP/NRs can also be calculated from the UVvis absorbance at 450 nm according to the Beer-Lambert law as reported.[167]



$$C_{\text{NP/NR}} = \frac{A_{450}}{\epsilon_{450} \cdot l} \quad \text{Equation 2-9}$$

Thus, the mass concentration of Au NP/NRs in terms of Au element  $C_{\text{Au}}$  can be transferred from the UVvis absorbance at 450 nm, but to make it simply, here we just list the molar concentration of Au NPs/NRs  $C_{\text{NP}}$  and the converted mass concentration of Au NP/NRs in terms of Au element  $C_{\text{Au}}$  in Table 2-4 and the initially measured UVvis absorbance at 450 nm was not listed here. This mass concentration of 20  $\mu\text{g/mL}$  was used for the Au NP/NRs exposure instead of the mass concentration measured by ICP-MS, and the other mass concentrations of Au NPs/NRs used in this work were also based on the conversion from molar concentrations of Au NP/NRs.

*Table 2-4 The concentration conversion between the mass concentration Au ( $C_{\text{Au}}$ ) = 20  $\mu\text{g/mL}$  used in the experiments and the equivalent number of NPs/NRs.*

Samples	$M_w$ [g/mol]	$C_{\text{NP}}$ [nM]	$C_{\text{Au}}$ [ $\mu\text{g/mL}$ ]
5 nm AuNPs	$6.3 \times 10^5$	31.76	20
25 nm AuNPs	$8.9 \times 10^7$	0.22	20
50 nm AuNPs	$7.5 \times 10^8$	0.027	20
100 nm AuNPs	$6.3 \times 10^9$	0.0032	20
40 nm AuNRs	$8.8 \times 10^7$	0.23	20
100 nm AuNRs	$5.8 \times 10^8$	0.035	20

### **2.6.1.3 Concentration of Au NP/NRs measured by Inductively Coupled Plasma Mass Spectrometer (ICP-MS) compared to the calculated mass concentration converted from molar concentration of NPs/NRs**

Further confirmation of the mass concentration of Au element in the Au NP/NRs was conducted with ICP-MS (Agilent 7700, Germany). Firstly, initial condensed Au NP/NRs, whose molar concentration of NP/NRs in nM has been calculated from UVvis, were diluted 10 times with Milli-Q water and then 20  $\mu\text{L}$  of this diluted Au NP/NRs was transferred to an Eppendorf tube with three parallel tubes prepared at the same time and then 200  $\mu\text{L}$  Aqua Regia was added to each tube and incubated overnight. After that, the 220  $\mu\text{L}$  sample in each tube was transferred to an ICP-MS tube and 2 mL 2% V/V HCl was added to dilute the samples for ICP-MS measurement. Then the concentration of Au element in initial condensed Au NP/NRs was 1110 times the concentration directly detected by ICP-MS. The mass concentration of Au ( $C_{\text{Au}}$ ) element in initial condensed Au NP/NRs solution according to the ICP-MS measurement of 1110 times dilution sample and the corresponding mass concentration of Au

element (CAu) calculated from the molar mass of Au NP/NRs as shown in Table 2-3 combined with the molar concentration of Au NP/NRs according to UVvis measurement were presented in Table 2-5.

*Table 2-5 Comparison of mass concentration of Au element calculated from the number concentration of NPs and those measured from ICP-MS.*

Samples	C <sub>NP</sub> [nM]	M <sub>w</sub> [g/mol]	C <sub>Au</sub> [μg/L] calculated	C <sub>Au</sub> [μg/L] by ICP-MS
5 nm AuNPs	2787.21	6.3×10 <sup>5</sup>	1.8×10 <sup>6</sup>	1.1×10 <sup>6</sup>
25 nm AuNPs	25.22	8.9×10 <sup>7</sup>	2.2×10 <sup>6</sup>	1.4×10 <sup>6</sup>
50 nm AuNPs	2.08	7.5×10 <sup>8</sup>	1.6×10 <sup>6</sup>	1.2×10 <sup>6</sup>
100 nm AuNPs	0.11	6.3×10 <sup>9</sup>	7.0×10 <sup>5</sup>	7.5×10 <sup>5</sup>
40 nm AuNRs	7.88	8.8×10 <sup>7</sup>	7.0×10 <sup>5</sup>	4.6×10 <sup>5</sup>
100 nm AuNRs	0.95	5.8×10 <sup>8</sup>	5.4×10 <sup>5</sup>	2.8×10 <sup>5</sup>

According to Table 2-5, the mass concentration of Au (CAu) based on ICP-MS measurement is always much lower than the value converted from molar concentration of NP/NRs except for the 100 nm Au NPs. This is because of the error in the solid sphere model used for the calculation of molar mass of Au NP/NRs. It can be predicted that the actual Au mass concentration used in the cell viability test and also the uptake experiment is not exact 10 μg/mL and 20 μg/mL for all the Au NPs/NRs except the 100 nm Au NPs. And the corresponding actual concentration was shown in Table 2-6, which indicates that the actual exposed mass concentration of 100 nm Au NPs is much higher than all the other Au NPs/NRs and even about twice the concentration of 5 nm and 25 nm Au NPs.

*Table 2-6 Calculated concentration and the corresponding actual concentration used in later uptake experiments*

Samples	5 nm AuNPs	25 nm Au NPs	50 nm AuNPs	100 nm Au NPs	40 nm Au NRs	100 nm Au NRs
Calculated concentration, [μg/mL]	10	10	10	10	10	10
Actual concentration, [μg/mL]	6.3	6.1	7.5	10.6	6.5	5.1
Calculated concentration, [μg/mL]	20	20	20	20	20	20
Actual concentration, [μg/mL]	12.6	12.2	15.0	21.3	13.1	10.3

#### **2.6.1.4 DLS and UVvis measurement for the Au NP/NRs**

##### **Dynamic light scattering and zeta-potential**

To determine the hydrodynamic diameters  $d_H$  of all AuNPs, dynamic light scattering (DLS) was used as seen in Figure 2-4. The zeta-potentials  $\zeta$  of each particle was measured with laser Doppler anemometry and evaluated using a Malvern Zetasizer Nanoparticle analyzer ZEN 3600 instrument. Data are presented in Figure 2-5.

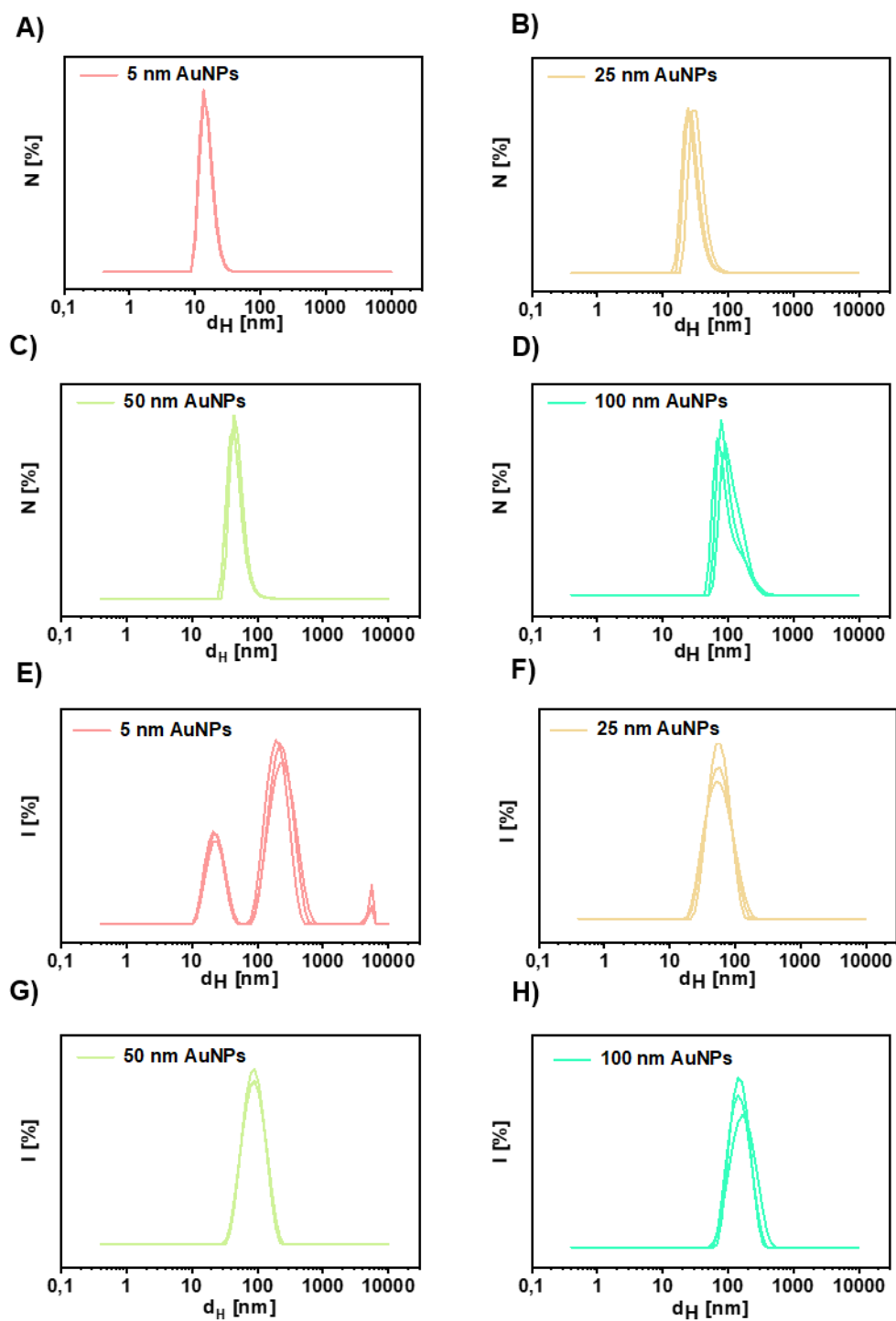


Figure 2-4 hydrodynamic diameter  $d_H$  of 5, 25, 50, 100 nm AuNPs as recorded by DLS. (A, B, C, D) are number distribution and (E, F, G, H) are intensity distribution. Detailed information was shown in Table 2-3.

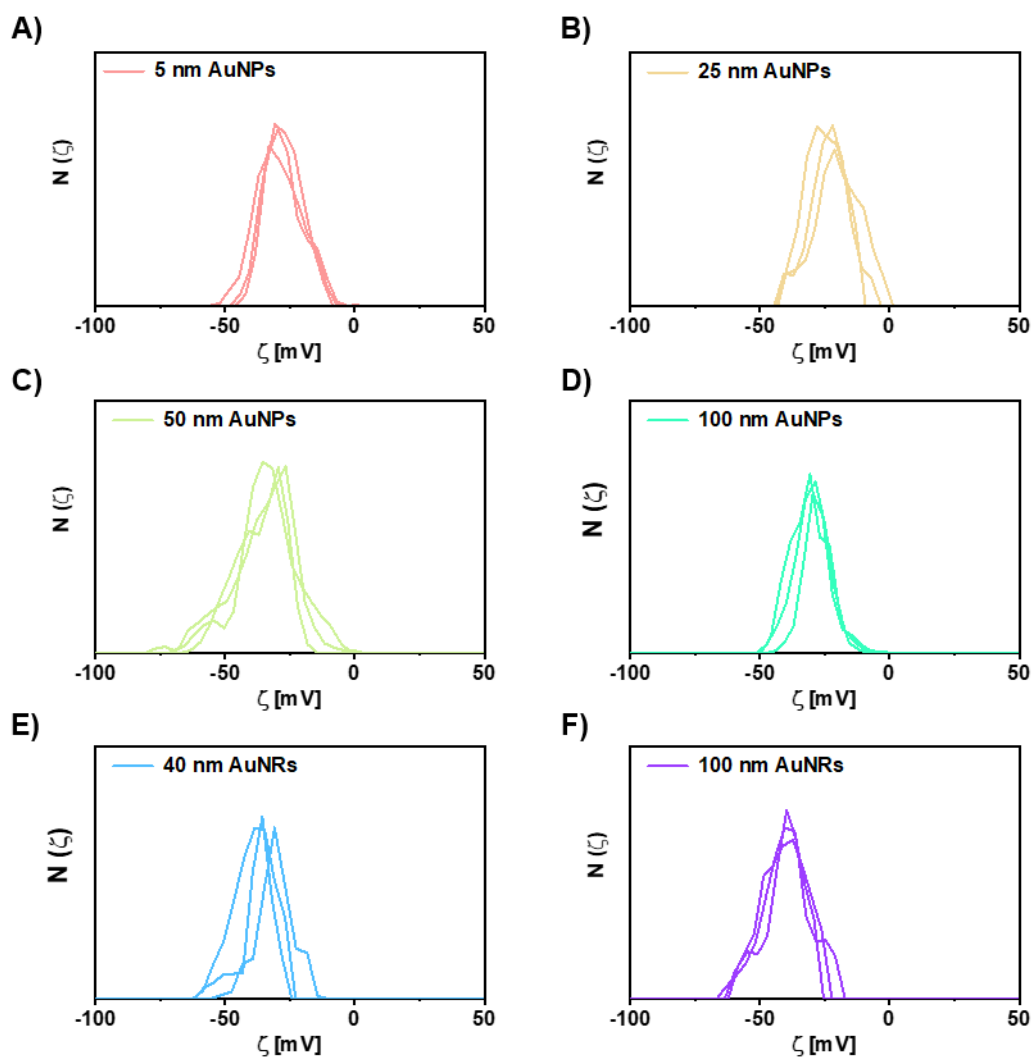


Figure 2-5 Zeta potentials  $\zeta$ , of A) 5, B) 25, C) 50, D) 100 nm AuNPs, E) 40, and F) 100 nm AuNRs respectively. Detailed information is shown in Table 2-3.

### UV/vis absorption spectroscopy

The UV/vis absorption spectra of AuNPs and AuNRs were evaluated with an Agilent 8453 spectrometer as previously reported. NPs/NRs were dispersed in water, see Figure 2-6.

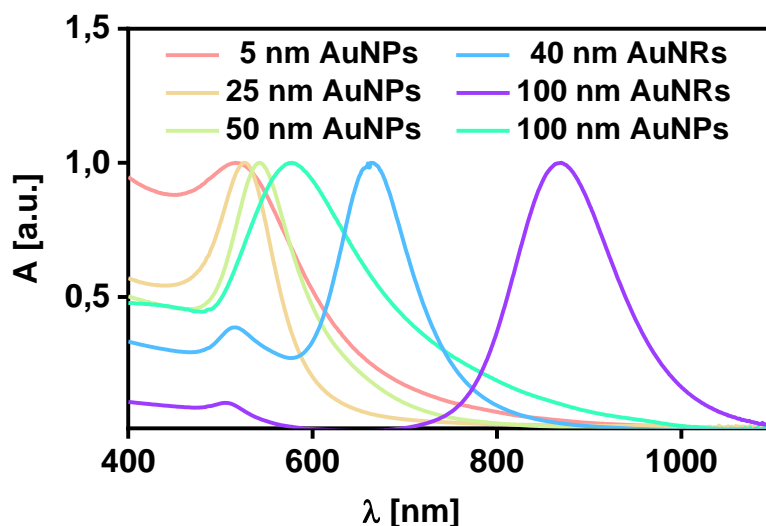


Figure 2-6 UV-Vis absorption spectra of 5, 25, 50, 100 nm AuNPs and 40, 100 nm AuNRs. This graph was done by Xing Sun. Detailed information of the NPs is shown in Table 2-3.

### 2.6.2 IFT at the Au NP/NRs colloid-toluene interface

The concentration of Au NP/NRs used in the interfacial tension measurement was the Au NP/NRs molar concentration based on the UVvis measurement and listed in Table 2-7. And the molar mass of Au NP/NRs listed in Table 2-3 was used to calculate the corresponding Au element mass concentration and also listed in Table 2-7, which might exist an error compared to the actual Au mass concentration measured with ICP-MS and this error has been discussed in chapter 2.6.1.3 referring to the Table 2-5. Figure 2-7 showed the dynamic IFT measurement results representative of more than three parallel measurements and according to this figure, the IFT at the Au NP/NRs colloid—toluene interface was stable during the 30 min measurement and was completely same as the water-toluene IFT 35 mN/m and the IFT showed no variation between different sizes and shapes of Au NP/NRs. The IFT 2-3 mN/m fluctuation was within our instrument measurement precision because this fluctuation also occurred when we many times measure the same sample, which can not be completely avoided in our measurements.

Table 2-7 The Au NP/NRs molar concentration used in the IFT measurement and the corresponding calculated mass concentration in terms of Au element.

Samples	$M_w$ [g/mol]	$C_{Au}$ [ $\mu\text{g/mL}$ ]	$C_{NP}$ [nM]
5 nm AuNPs	$6.3 \times 10^5$	112	177.86
25 nm AuNPs	$8.9 \times 10^7$	112	1.26
50 nm AuNPs	$7.5 \times 10^8$	112	0.15
100 nm AuNPs	$6.3 \times 10^9$	112	0.018
40 nm AuNRs	$8.8 \times 10^7$	112	1.27
100 nm AuNRs	$5.8 \times 10^8$	112	0.19

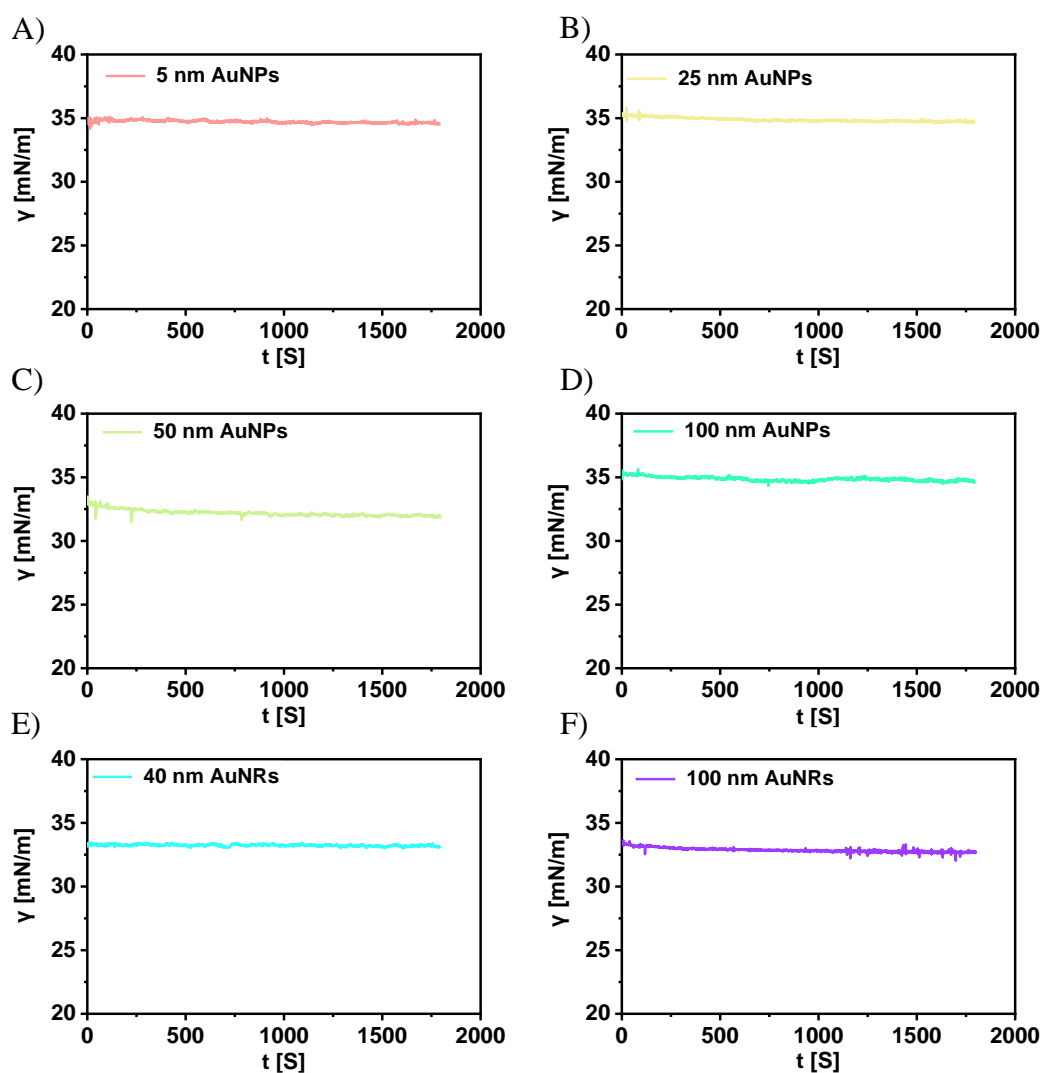


Figure 2-7 Dynamic IFT at the Au NPs/AuNRs colloid-toluene interface during 30 mins measurement. The graphs are representative of three parallel measurements.

## 2.6.3 Cell viability

### 2.6.3.1 Cell viability of HeLa cells incubated with different concentrations of Au NP/NRs in Static system

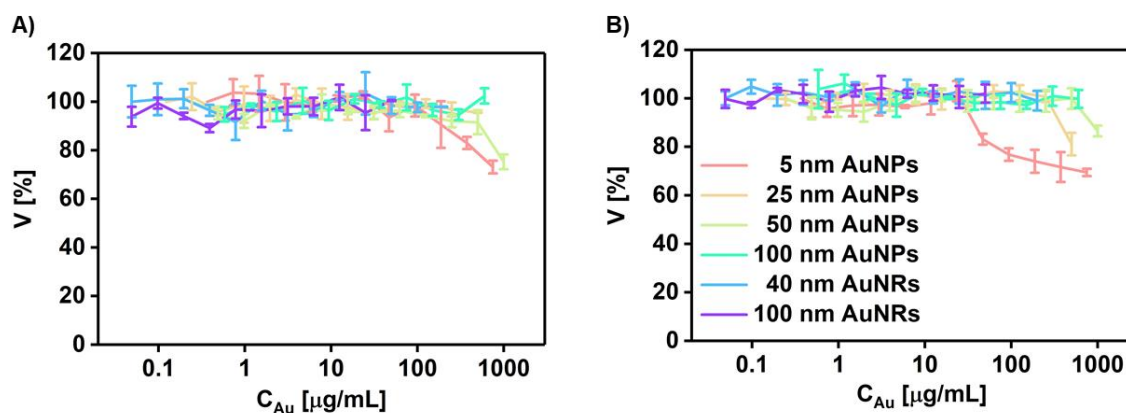


Figure 2-8 Cell viability of HeLa cells exposed to 5, 25, 50, and 100 nm AuNPs and 40 and 100 nm AuNRs for A) 24h, B) 48h in static conditions. The data in the figure corresponds to mean values  $\pm$  standard deviations (SD) from three independent experiments. This graph was done by Xing Sun.

Good biocompatibility is the basis for the biomedical applications of NPs. Generally, the toxicity of Au NPs is concentration-dependent and the cytotoxicity often increased with the increase of Au NPs concentration. When the cell viability is higher than 90%, we think that this nanoparticle showed no toxicity. Here from Figure 2-8, we can conclude that all the six different sizes of Au NP/NRs showed no toxicity to HeLa cells at low concentration exposure (less than 10  $\mu\text{g/mL}$ ) no matter after 24 h incubation or 48 h incubation. When the concentration in terms of Au element increased to some extent, some of the Au NP/NRs showed moderate toxicity. For the 5 nm Au NPs, when the concentration was lower than 187.5  $\mu\text{g/mL}$ , the cell viability after 24 h incubation was higher than 90%, and when the concentration increased further, the cell viability decreased evidently to lower than 90% level. We can describe this 187.5  $\mu\text{g/mL}$  as a ‘24 h highest tolerance concentration’, which is the highest concentration that can keep the cell viability higher than 90% after 24 h incubation. Table 2-8 listed the ‘24 h highest tolerance concentration’ and ‘48 h highest tolerance concentration’ for all these six sizes of Au NPs. According to Table 2-8, we can predict that 5 nm Au NPs showed the highest cytotoxicity to HeLa cells when compared to 25 nm, 50 nm, and 100 nm Au NPs and 40 nm and 100 nm Au NRs at the same mass concentration of Au element and after same time incubation. What is more, considering the Au element mass concentration calculation error as presented in Table 2-5, the actual Au mass concentration was only about 60% of the designed



concentration for 5 nm Au NPs, thus the highest tolerance concentration of Hela cell to 5 nm Au NPs should be 60% of the value presented in Table 2-8.

*Table 2-8 highest tolerance concentration of Hela cells to 6 sizes of Au NPs in static incubation<sup>a</sup>*

Au NPs	Highest exposure concentration, [ug/mL]	24 h highest tolerance concentration, [μg/mL]	48 h highest tolerance concentration, [μg/mL]
5 nm AuNPs	750	187.5	23.4
25 nm AuNPs	500	---	250
50 nm AuNPs	1000	500	500
100 nm AuNPs	600	---	---
40 nm AuNRs	200	---	---
100 nm AuNRs	50	---	---

<sup>a</sup>---means the cell viability was still higher than 90 % even incubated in the highest concentration of Au element, so the highest tolerance concentration was not found in the experiment currently and this highest tolerance concentration should be equal to or higher than the highest exposure concentration listed in Table 2-8.

### **2.6.3.2 Cell viability of Hela cells incubated with Au NPs/NRs in Static, Dynamic, and Fluid system**

From Figure 2-9, it can be concluded that the 6 sizes of Au NP/NRs did not show toxicity to Hela cells at the designed 20 μg/mL in terms of Au element mass concentration, no matter in Static, Dynamic, or Fluid incubation system supported by the higher than 90 % cell viability. Besides, the cells can have already internalized the same amount of Au NP/NRs as listed in Table 2-12, Table 2-13, and Table 2-14 since the incubation procedures in this cell viability test were completely the same as those conducted in the uptake experiments and also based on the assumption of neglectable exocytosis of Au NP/NRs during the 6 h incubation in complete cell culture media and 4 h incubation with Resazurin. Thus the actual Au concentration inside Hela cells is much higher than the initially exposed 20 μg/mL and should be the value listed in Table 2-9, Table 2-10, and Table 2-11 assuming that all the Au detected by ICPMS was the Au NPs internalized in Hela cells instead of attachment to the outside surface of Hela cells. Thus, the Hela cells can stand such a high concentration of Au without showing evident cell death. This much higher Au concentration inside cells compared to the initial Au concentration in the Au NP/NRs exposure has already been reported by Neus Feliu et al..[112] But actually the fact can be that a large fraction of the internalized Au NPs has already been exocytosed during the 6 h attachment in complete cell media and also the 4 h incubation with Resazurin, so the

internalized Au concentration inside HeLa cells listed in Table 2-9, Table 2-10 and Table 2-11 is the value immediately after the 24 h incubation in the corresponding conditions before the 6 h incubation in complete media and also 4 h incubation with Resazurin. According to Chithrani B. D., the endocytosis and exocytosis of Au NPs in vesicle intact would not cause any cytotoxicity,[37] thus, we can guess our Au NP/NRs enter and leave the HeLa cells in vesicles intact.

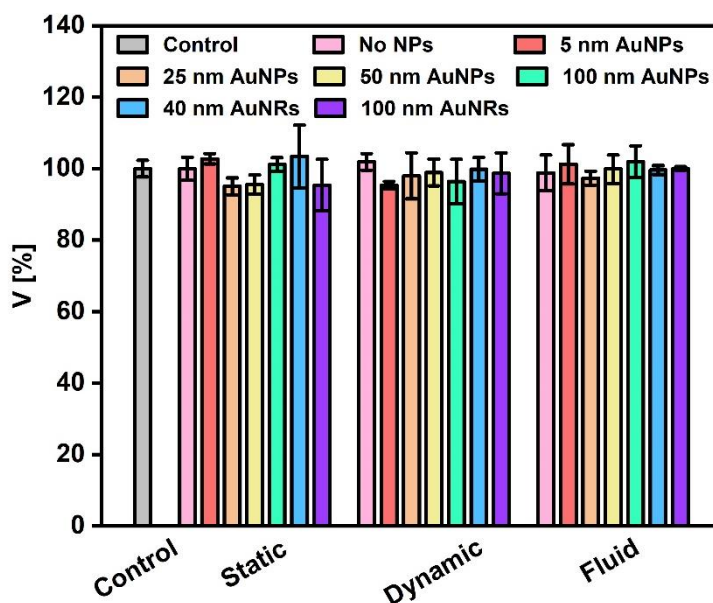


Figure 2-9 Cell viability of HeLa cells exposed to 5, 25, 50, and 100 nm AuNPs and 40 and 100 nm AuNRs at  $C_{Au}=20 \mu\text{g/mL}$  for 24h in Static, Dynamic, and Fluid systems respectively. The data were mean values  $\pm$  standard deviations (SD) from three independent experiments. This graph was done by Xing Sun.

Table 2-9 Concentration of Au inside HeLa cells after incubation for 24 h at Au concentration of  $20 \mu\text{g/mL}$  in Static incubation

Au NPs	$M_w$ [g/mol]	$m_{(Au \text{ per cell})}$ , [pg/cell]	$V_{cell}$ , [mL]	$C_{(Au)}$ inside per cell, [ $\mu\text{g/mL}$ ]	$C_{NP}$ inside per cell, [ $10^9/\text{mL}$ ]
5 nm AuNPs	$6.3 \times 10^5$	$0.51 \pm 0.07$	$5 \cdot 10^{-9}$	$102 \pm 14$	$91647 \pm 12579$
25 nm AuNPs	$8.9 \times 10^7$	$0.87 \pm 0.01$	$5 \cdot 10^{-9}$	$174 \pm 2$	$1007 \pm 12$
50 nm AuNPs	$7.5 \times 10^8$	$9.99 \pm 1.80$	$5 \cdot 10^{-9}$	$1998 \pm 360$	$1546 \pm 278$
100 nm AuNPs	$6.3 \times 10^9$	$11.54 \pm 2.16$	$5 \cdot 10^{-9}$	$2308 \pm 432$	$223 \pm 42$
40 nm AuNRs	$8.8 \times 10^7$	$0.78 \pm 0.19$	$5 \cdot 10^{-9}$	$156 \pm 38$	$1067 \pm 260$
100 nm AuNRs	$5.8 \times 10^8$	$3.30 \pm 0.24$	$5 \cdot 10^{-9}$	$660 \pm 48$	$685 \pm 50$

Avogadro's constant  $N_A = 6.02 \times 10^{23} \text{ mol}^{-1}$ .  $V_{cell (HeLa)} \approx 5000 \mu\text{m}^3 = 5 \cdot 10^{-9} \text{ mL}$  [127].

Table 2-10 Concentration of Au inside Hela cells after incubation for 24 h at Au concentration 20  $\mu\text{g/mL}$   
in Dynamic incubation

Au NPs	$M_w$ [g/mol]	$m_{\text{Au}}$ per cell, [pg/cell]	$V_{\text{cell}}$ , [mL]	$C_{\text{Au}}$ inside cell, [ $\mu\text{g/mL}$ ]	$C_{\text{NP}}$ inside cell, [ $10^9/\text{mL}$ ]
5 nm AuNPs	$6.3 \times 10^5$	$0.61 \pm 0.08$	$5 * 10^{-9}$	$122 \pm 16$	$109618 \pm 14376$
25 nm AuNPs	$8.9 \times 10^7$	$0.63 \pm 0.10$	$5 * 10^{-9}$	$126 \pm 20$	$729 \pm 115$
50 nm AuNPs	$7.5 \times 10^8$	$3.09 \pm 0.89$	$5 * 10^{-9}$	$618 \pm 178$	$478 \pm 138$
100 nm AuNPs	$6.3 \times 10^9$	$4.81 \pm 0.84$	$5 * 10^{-9}$	$962 \pm 168$	$93 \pm 16$
40 nm AuNRs	$8.8 \times 10^7$	$0.36 \pm 0.01$	$5 * 10^{-9}$	$72 \pm 2$	$493 \pm 14$
100 nm AuNRs	$5.8 \times 10^8$	$2.58 \pm 0.37$	$5 * 10^{-9}$	$516 \pm 74$	$536 \pm 77$

Avogadro's constant  $N_A = 6.02 \times 10^{23} \text{ mol}^{-1}$ .  $V_{\text{cell (Hela)}} \approx 5000 \mu\text{m}^3 = 5 * 10^{-9} \text{ mL}$ [127].

Table 2-11 Concentration of Au inside Hela cells after incubation for 24 h at Au concentration 20  $\mu\text{g/mL}$   
in Fluid incubation

Au NPs	$M_w$ [g/mol]	$m_{\text{Au}}$ per cell, [pg/cell]	$V_{\text{cell}}$ , [mL]	$C_{\text{Au}}$ inside cell, [ $\mu\text{g/mL}$ ]	$C_{\text{NP}}$ inside cell, [ $10^9/\text{mL}$ ]
5 nm AuNPs	$6.3 \times 10^5$	$0.41 \pm 0.03$	$5 * 10^{-9}$	$82 \pm 6$	$73677 \pm 5391$
25 nm AuNPs	$8.9 \times 10^7$	$0.42 \pm 0.03$	$5 * 10^{-9}$	$84 \pm 6$	$486 \pm 35$
50 nm AuNPs	$7.5 \times 10^8$	$1.63 \pm 0.16$	$5 * 10^{-9}$	$326 \pm 32$	$252 \pm 25$
100 nm AuNPs	$6.3 \times 10^9$	$1.97 \pm 0.14$	$5 * 10^{-9}$	$394 \pm 28$	$38 \pm 3$
40 nm AuNRs	$8.8 \times 10^7$	$0.66 \pm 0.06$	$5 * 10^{-9}$	$132 \pm 12$	$903 \pm 82$
100 nm AuNRs	$5.8 \times 10^8$	$0.83 \pm 0.06$	$5 * 10^{-9}$	$166 \pm 12$	$172 \pm 12$

Avogadro's constant  $N_A = 6.02 \times 10^{23} \text{ mol}^{-1}$ .  $V_{\text{cell (Hela)}} \approx 5000 \mu\text{m}^3 = 5 * 10^{-9} \text{ mL}$ [127].

### 2.6.3.3 Cell viability based on Dead/Live staining in Static, Dynamic, and Suspension systems

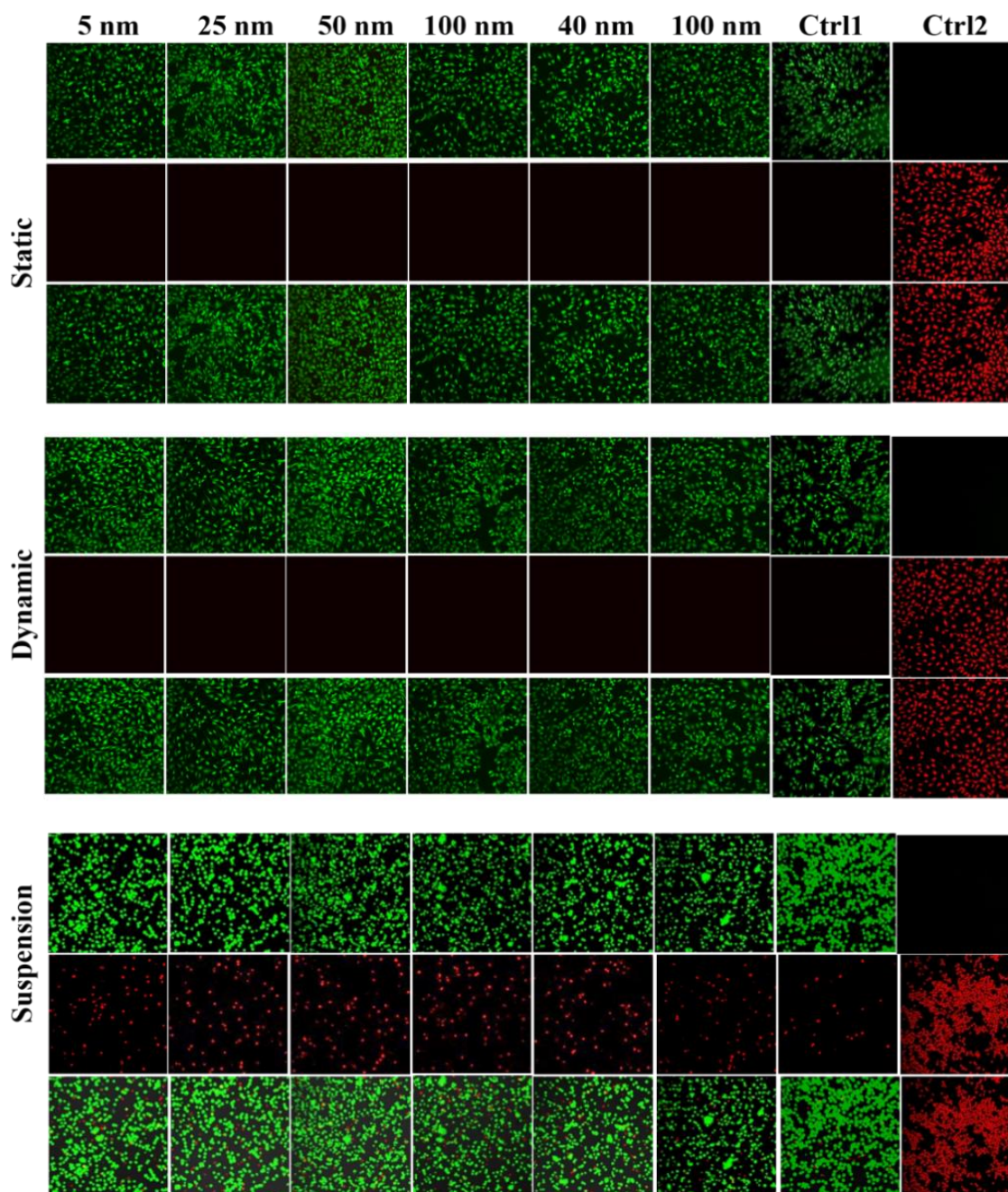


Figure 2-10 Cell Dead/Live staining images for cells incubated with 5, 25, 50, and 100 nm AuNPs and 40, 100 nm AuNRs at  $C_{Au}$  20  $\mu\text{g}/\text{mL}$  for 24h. Ctrl1 was for cells with no NPs added, and Ctrl2 was for cells with no NPs added but ethanol added to kill the cells. The pictures are representative of three individual measurements.

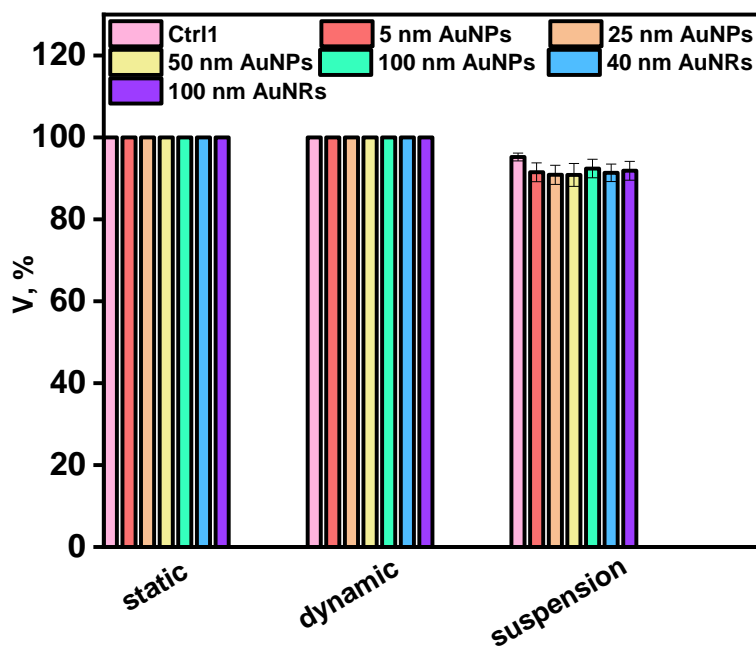


Figure 2-11 Cell Viability calculated from Dead/Live images for cells incubated with 5, 25, 50, and 100 nm AuNPs and 40, 100 nm AuNRs at  $C_{Au}$  20  $\mu$ g/mL for 24h, Ctrl1 was a sample with no AuNPs added, as in Figure 2-10. The data shown corresponds to mean values  $\pm$  standard deviations (SD) from three independent experiments

## 2.6.4 Growth curve of cells in different systems

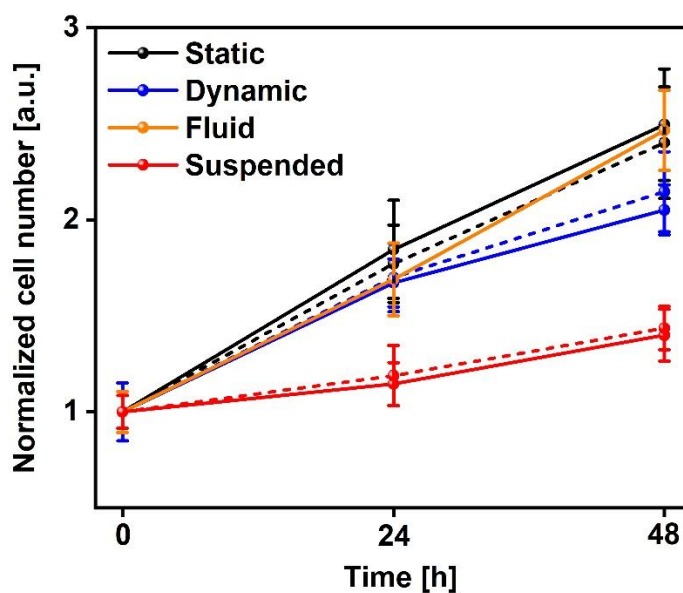


Figure 2-12 HeLa cell growth curves from the static, dynamic, fluid, and suspended conditions over time. Solid lines represent the systems in  $V=6$  mL cell media, while dash lines represent systems in  $V=3$  mL cell media. The data shown correspond to mean values  $\pm$  standard deviations (SD) from three independent experiments. This graph was done by Xing Sun.

## 2.6.5 Uptake of Au NP/NR into adhered Hela cells incubated in Static system

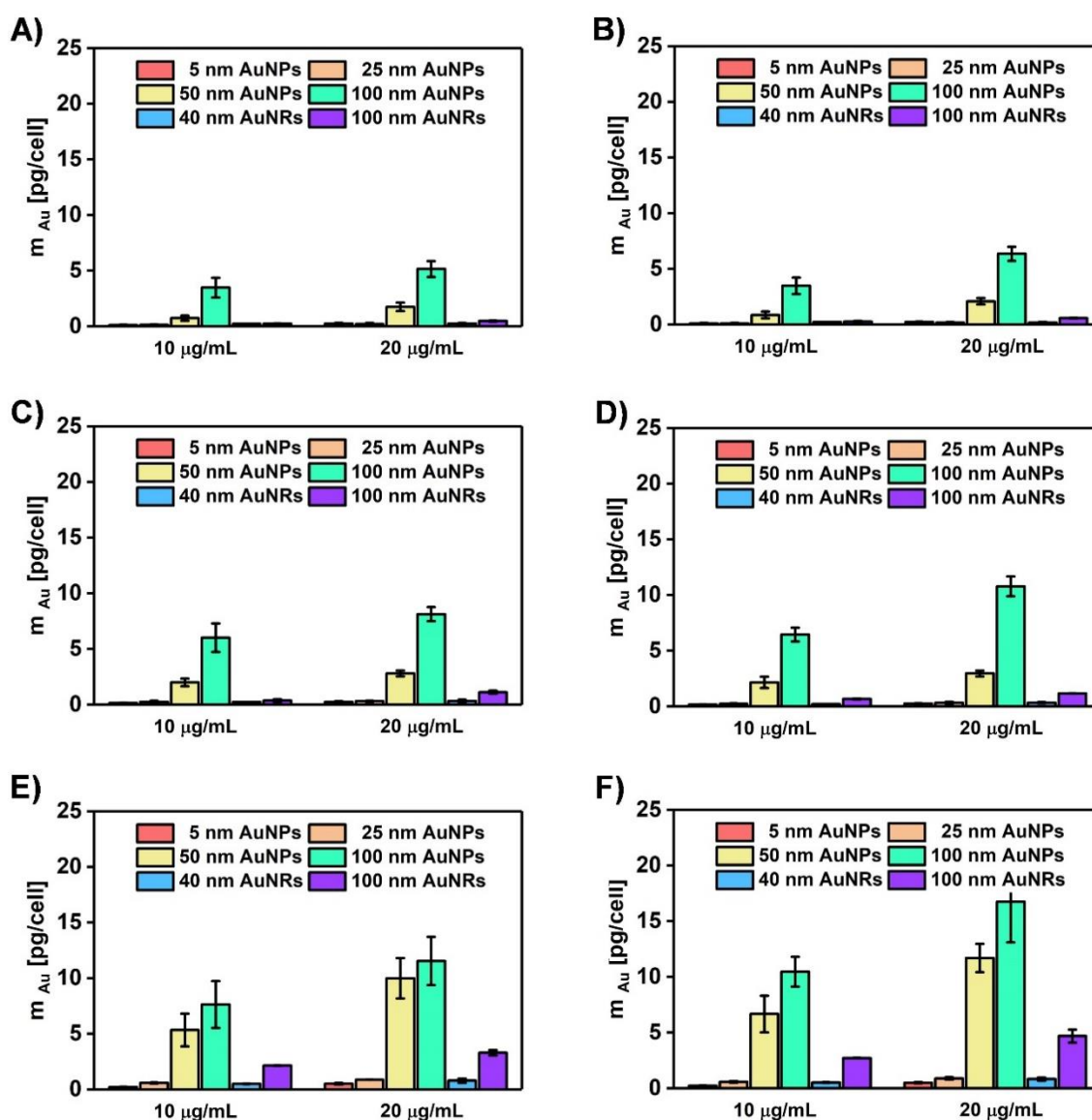


Figure 2-13 Internalized Au mass per cell for Hela cells incubated with 5, 25, 50, and 100 nm AuNPs and 40 and 100 nm AuNRs in static conditions after different time incubation. The concentrations of NPs/NRs were 10 and 20  $\mu\text{g/mL}$ . The experiments can be separated into two groups, group 1 (A, C, E) was with 3 mL of Au NP/NRs, A) is for 4h, C) is for 8h, and E) is for 24h; group 2 (B, D, F) was with 6 mL of Au NP/NRs, B) is for 4h, D) is for 8h and F) is for 24h. The data shown correspond to mean values  $\pm$  standard deviations (SD) from three independent experiments. This graph was done by Xing

Sun.

To see the effect of incubation time on the uptake amount, the uptake data were presented in a different style in Figure 2-14.

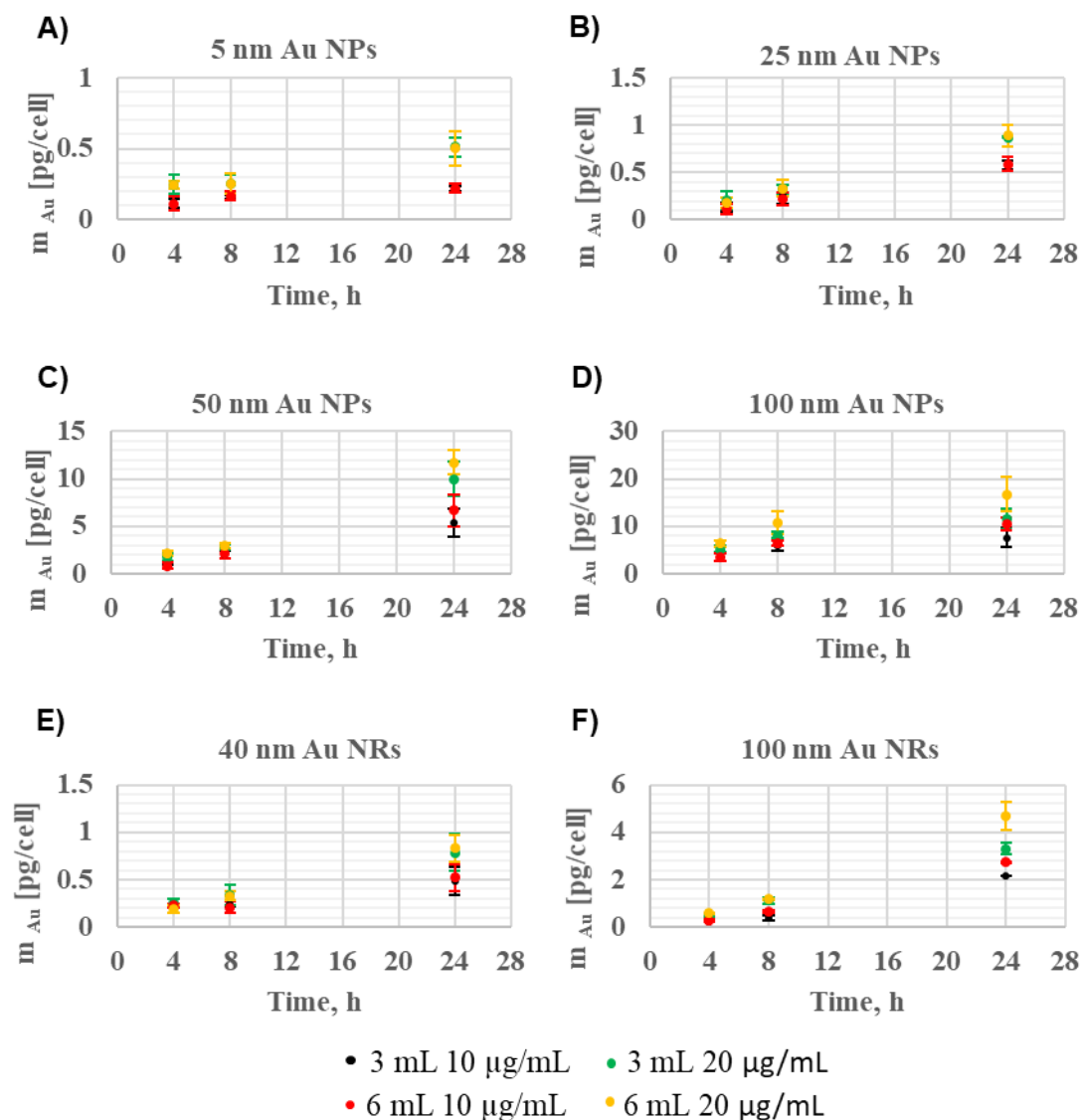


Figure 2-14 Internalized Au mass per cell for HeLa cells incubated with 5, 25, 50, and 100 nm AuNPs and 40 and 100 nm AuNRs in static conditions for different time incubation. (A), (B), (C), (D), (E), and (F) were for HeLa cells incubated with 5, 25, 50, and 100 nm AuNPs and 40 and 100 nm AuNRs respectively, while the different color represents the volume and concentration of the Au NP/NRs. If in the graphs, these four colors were not completely presented, the fact is that the black dot is completely covered up by the red dots and the green dots are completely covered up by the yellow dots.

*Table 2-12 Internalized Au mass per cell for HeLa cells incubated with 5, 25, 50, and 100 nm AuNPs and 40 and 100 nm AuNRs in static condition.*

NPs		5 nm AuNPs	25 nm AuNPs	50 nm AuNPs	100 nm AuNPs	40 nm AuNRs	100nm AuNRs
10 μg/mL 3 mL	4 h	0.12±0.03	0.13±0.04	0.75±0.23	3.48±0.88	0.22±0.00	0.23±0.04
	8 h	0.16±0.01	0.27±0.10	2.00±0.34	6.02±1.28	0.24±0.03	0.38±0.12
	24 h	0.22±0.02	0.58±0.05	5.35±1.47	7.63±2.10	0.49±0.14	2.15±0.01
10 μg/mL 6 mL	4 h	0.11±0.05	0.11±0.05	0.87±0.30	3.48±0.73	0.23±0.02	0.27±0.06
	8 h	0.17±0.03	0.22±0.07	2.16±0.51	6.46±0.63	0.21±0.06	0.67±0.06
	24 h	0.22±0.03	0.59±0.07	6.67±1.65	10.47±1.33	0.52±0.14	2.73±0.02
20 μg/mL 3 mL	4 h	0.25±0.07	0.21±0.09	1.75±0.38	5.16±0.72	0.26±0.05	0.48±0.04
	8 h	0.25±0.07	0.32±0.05	2.81±0.23	8.13±0.63	0.34±0.11	1.13±0.14
	24 h	0.51±0.07	0.87±0.01	9.99±1.80	11.54±2.16	0.78±0.19	3.30±0.24
20 μg/mL 6 mL	4 h	0.24±0.03	0.18±0.05	2.10±0.28	6.36±0.64	0.19±0.04	0.58±0.03
	8 h	0.25±0.07	0.33±0.09	2.97±0.26	10.78±2.38	0.33±0.05	1.17±0.01
	24 h	0.50±0.12	0.89±0.11	11.70±1.26	16.7±3.65	0.83±0.14	4.69±0.59



## 2.6.6 Uptake of Au NP/NR into adhered Hela cells incubated in Dynamic system

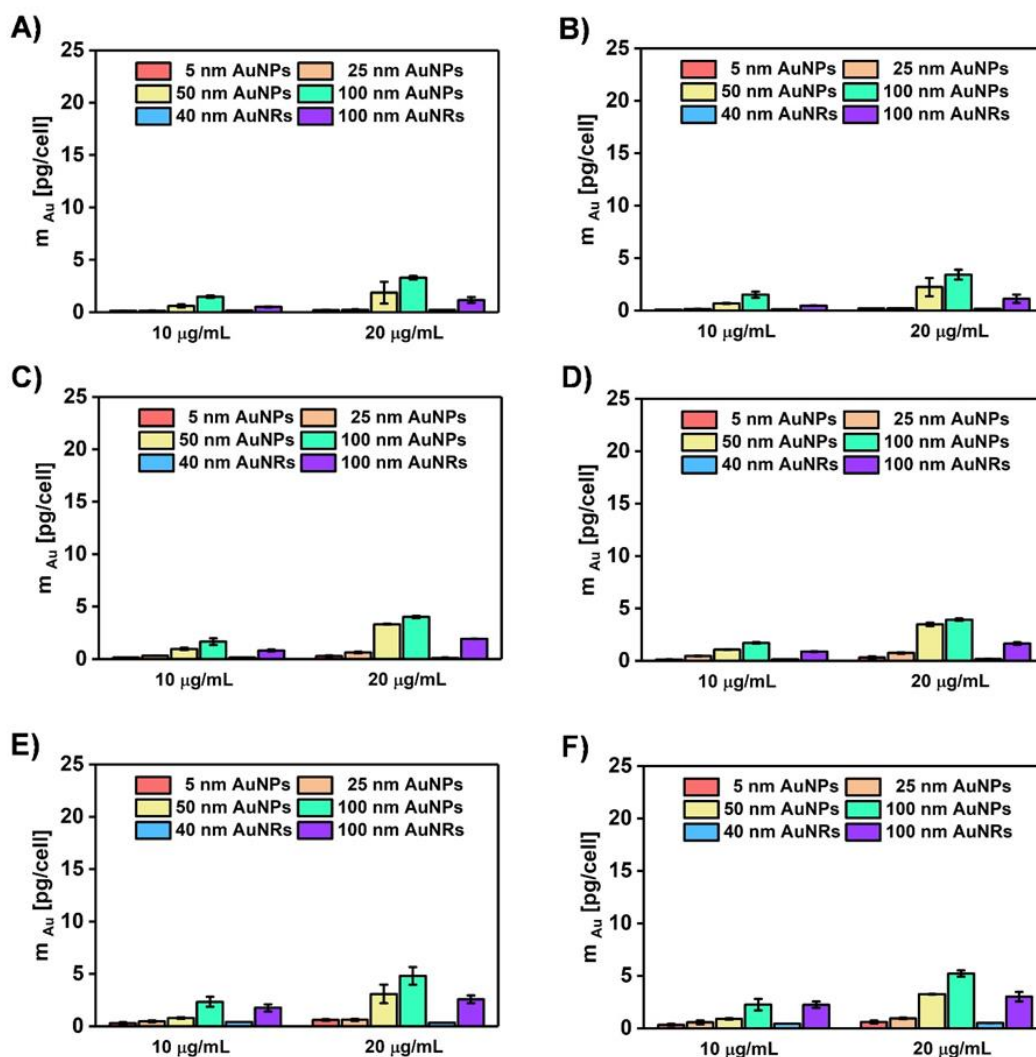


Figure 2-15 Internalized Au mass per cell for Hela cells incubated with 5, 25, 50, and 100 nm AuNPs and 40 and 100 nm AuNRs in dynamic conditions after different time incubation. The concentrations of NPs were 10 and 20  $\mu\text{g/mL}$ . The experiments can be separated into two groups, group 1 (A, C, E) was with 3 mL of cell media, A) is for 4h, C) is for 8h, and E) is for 24h; group 2 (B, D, F) was with 6 mL of cell media, B) is for 4h, D) is for 8h and F) is for 24h. The data shown correspond to mean values  $\pm$  standard deviations (SD) from three independent experiments. This graph was done by Xing Sun.

To see the effect of incubation time on the uptake amount, the uptake data were presented in a different style in Figure 2-16.

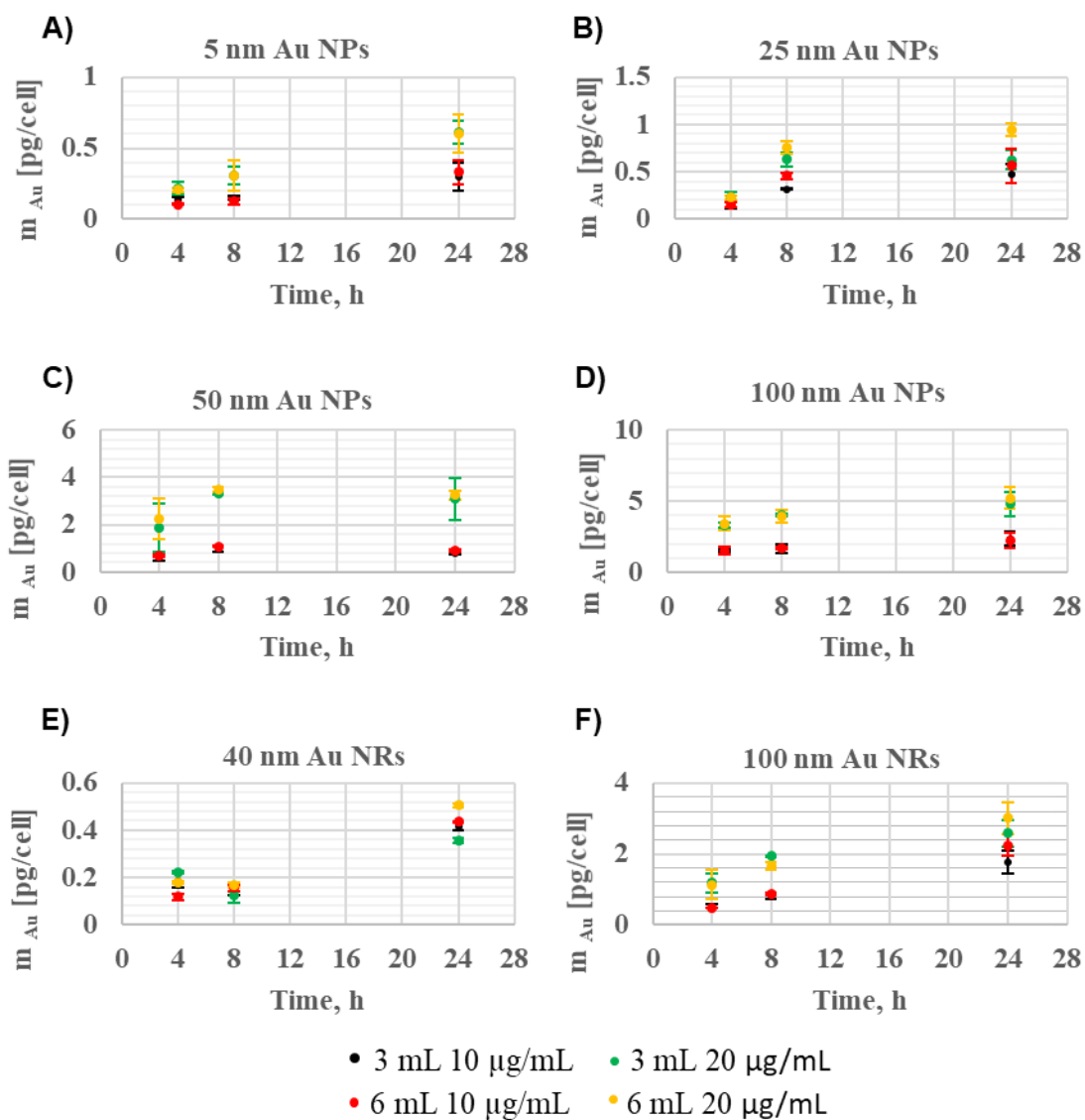


Figure 2-16 Internalized Au mass per cell for HeLa cells incubated with 5, 25, 50, and 100 nm AuNPs and 40 and 100 nm AuNRs in dynamic conditions after different time incubation. (A), (B), (C), (D), (E), and (F) were for HeLa cells incubated with 5, 25, 50, and 100 nm AuNPs and 40 and 100 nm AuNRs respectively, while the different color represents the volume and concentration of the Au NP/NRs. If in the graphs, these four colors were not completely presented, the fact is that the black dot is completely covered up by the red dots and the green dots are completely covered up by the yellow dots.

Table 2-13 Internalized Au mass per cell for HeLa cells incubated with 5, 25, 50, and 100 nm AuNPs and 40 and 100 nm AuNRs in dynamic conditions.

NPs		5 nm AuNPs	25 nm AuNPs	50 nm AuNPs	100 nm AuNPs	40 nm AuNRs	100nm AuNRs
10 μg/mL 3 mL	4 h	0.13±0.02	0.14±0.03	0.62±0.16	1.49±0.11	0.19±0.03	0.52±0.05
	8 h	0.15±0.01	0.32±0.00	0.98±0.11	1.67±0.32	0.15±0.02	0.83±0.09
	24 h	0.30±0.10	0.48±0.10	0.80±0.07	2.35±0.47	0.42±0.02	1.77±0.33
10 μg/mL 6 mL	4 h	0.11±0.00	0.15±0.03	0.69±0.03	1.53±0.29	0.12±0.02	0.48±0.01
	8 h	0.12±0.02	0.46±0.03	1.07±0.02	1.71±0.07	0.16±0.01	0.88±0.03
	24 h	0.33±0.08	0.56±0.18	0.89±0.06	2.26±0.55	0.44±0.00	2.24±0.30
20 μg/mL 3 mL	4 h	0.21±0.05	0.24±0.05	1.88±1.04	3.31±0.16	0.22±0.01	1.18±0.28
	8 h	0.30±0.06	0.63±0.07	3.33±0.05	4.02±0.10	0.12±0.03	1.94±0.01
	24 h	0.61±0.08	0.63±0.10	3.09±0.89	4.81±0.84	0.36±0.01	2.58±0.37
20 μg/mL 6 mL	4 h	0.21±0.01	0.23±0.02	2.25±0.87	3.43±0.47	0.18±0.01	1.14±0.40
	8 h	0.31±0.10	0.76±0.07	3.48±0.09	3.92±0.42	0.17±0.01	1.66±0.11
	24 h	0.60±0.13	0.95±0.06	3.26±0.19	5.22±0.79	0.50±0.01	3.00±0.45

## 2.6.7 Uptake of Au NP/NR into adhered HeLa cells incubated in Fluid system

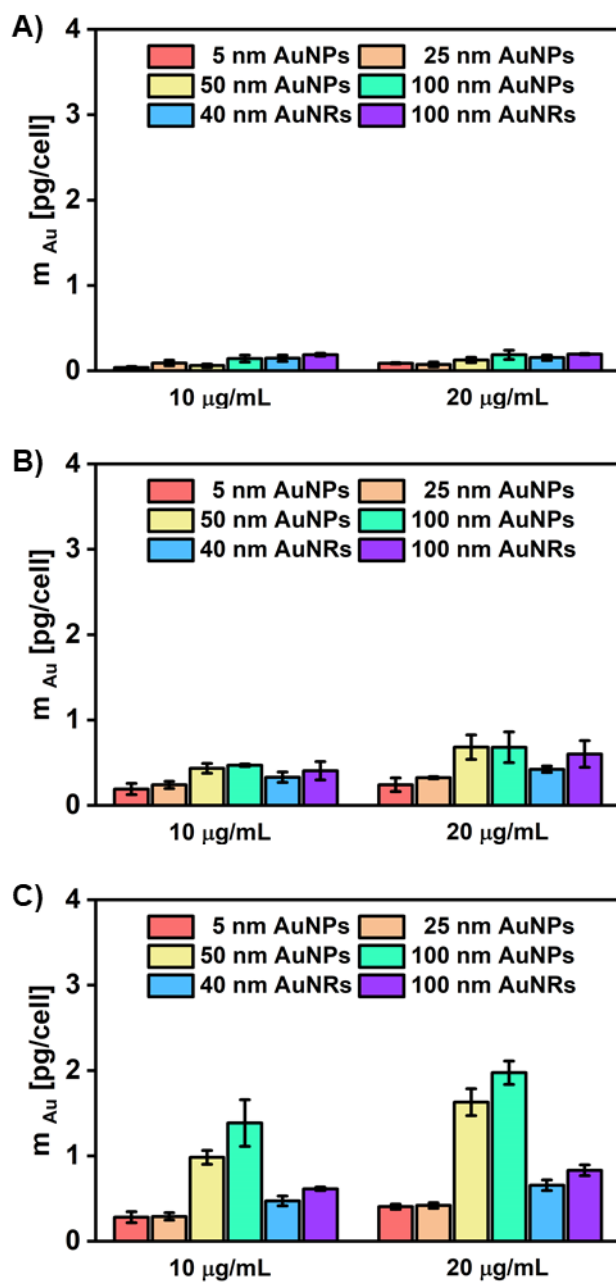


Figure 2-17 Internalized Au mass per cell for HeLa cells incubated with 5, 25, 50, and 100 nm AuNPs and 40 and 100 nm AuNRs in fluid condition after different time incubation. The concentrations of NPs were 10 and 20  $\mu\text{g/mL}$ . And the volume of cell media was always 6 mL. A) is for 4h, B) is for 8h, and C) is for 24h. The data shown correspond to mean values  $\pm$  standard deviations (SD) from three independent experiments ( $n=3$ )

To see the effect of incubation time on the uptake amount, the uptake data were presented in a different style in Figure 2-18.

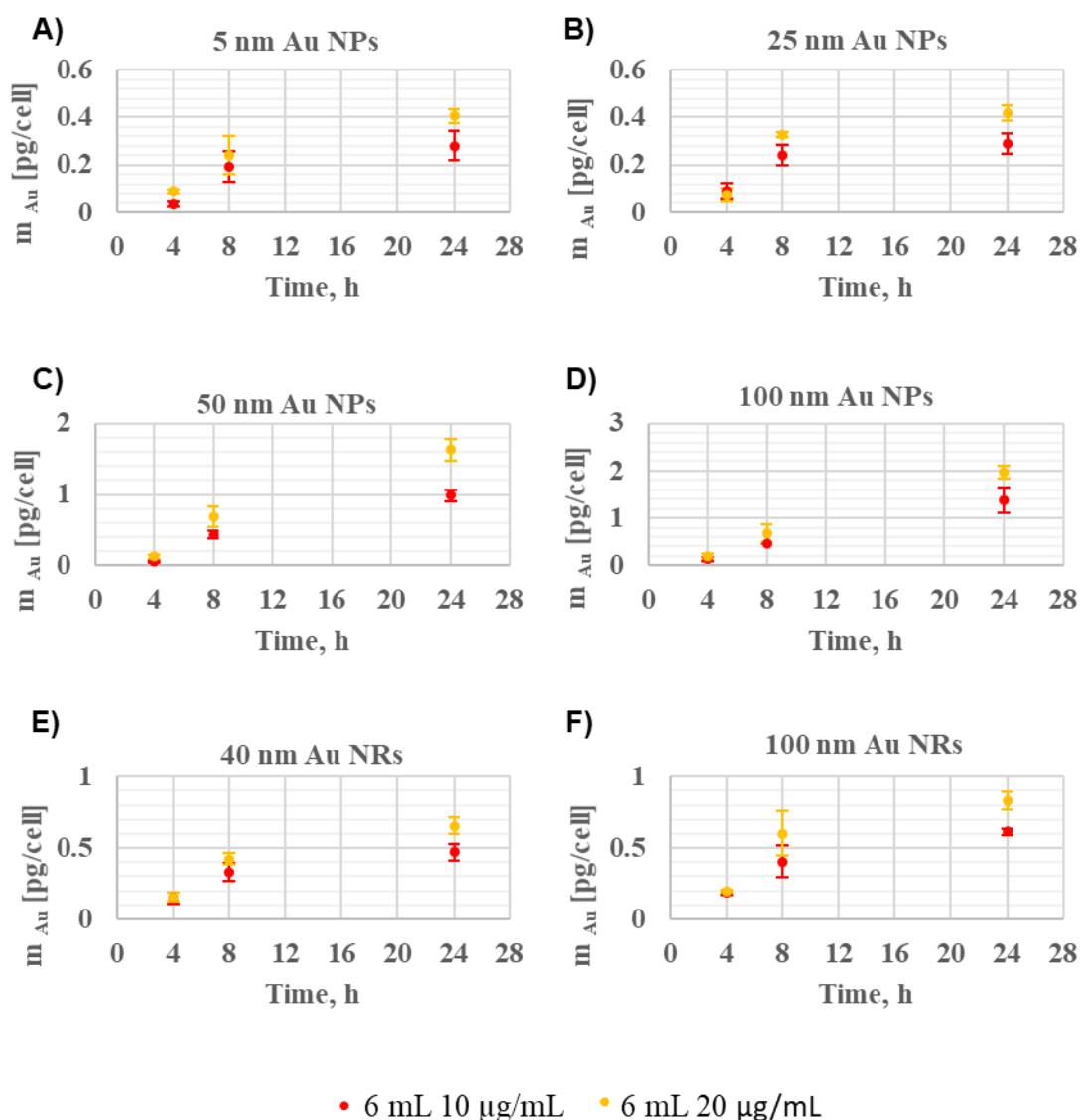


Figure 2-18 Internalized Au mass per cell for HeLa cells incubated with 5, 25, 50, and 100 nm AuNPs and 40 and 100 nm AuNRs in fluid condition after different time incubation. (A), (B), (C), (D), (E), and (F) were for HeLa cells incubated with 5, 25, 50, and 100 nm AuNPs and 40 and 100 nm AuNRs respectively, while the different color represents the concentration of the Au NP/NRs.

Table 2-14 Internalized Au mass per cell for HeLa cells incubated with 5, 25, 50, and 100 nm AuNPs and 40 and 100 nm AuNRs in Fluid condition

NPs			5 nm AuNPs	25 nm AuNPs	50 nm AuNPs	100 nm AuNPs	40 nm AuNRs	100nm AuNRs
10 μg/mL	6 mL	4 h	0.04±0.01	0.09±0.03	0.06±0.02	0.14±0.04	0.15±0.04	0.19±0.02
		8 h	0.19±0.06	0.24±0.04	0.43±0.06	0.47±0.01	0.33±0.06	0.41±0.11
		24 h	0.28±0.06	0.29±0.04	0.98±0.08	1.38±0.27	0.47±0.06	0.61±0.02
20 μg/mL	6 mL	4 h	0.09±0.01	0.07±0.03	0.13±0.03	0.19±0.05	0.15±0.03	0.20±0.01
		8 h	0.24±0.08	0.33±0.01	0.68±0.14	0.68±0.18	0.42±0.04	0.60±0.16
		24 h	0.41±0.03	0.42±0.03	1.63±0.16	1.97±0.14	0.66±0.06	0.83±0.06

## 2.6.8 Separation of suspended HeLa cells with free Au NPs/NRs

For the supernatant samples, the concentration of Au directly detected by the ICP-MS machine was shown in Figure 2-19 and the total amount of Au existing in the supernatant after each time washing was calculated based on the value in Figure 2-19 connected with the corresponding dilution times and presented in Figure 2-20. And the Au sticking to the cell membrane or settling down to the bottom of the tube was collected together with the cell pellet and the amount of this part Au NP was shown in Figure 2-21 based on the ICP-MS measurement of the cell pellet. We can see that in the case of 25 and 50 nm AuNPs, three times of washing was enough for NP-cell separation, while for 100 nm AuNPs a fourth time was needed for the separation. Another thing that needs attention is that the total Au mass existing in the supernatant after 1st wash time for 100 nm Au NPs is higher than the other three sizes of Au NPs and Au NRs, which seems to be opposite to our expectation considering the 100 nm Au NPs are much heavier and tend to settle down to the bottom of the tube after the centrifugation. But the truth is that the exposed concentration of Au NPs 20 μg/mL was based on our calculation from the molar concentration transferred from UVvis absorbance intensity rather than directly detected by ICP-MS. And from Table 2-6, for this calculated 20 μg/mL Au NPs, the actual concentration measured from ICP-MS should be much lower than 20 μg/mL for 5 nm, 25 nm, 50 nm Au NP and 40 nm, 100 nm Au NRs. Only for 100 nm Au NPs, the actual concentration can be a little higher than 20 μg/mL. This is why the Au mass existing in the supernatant is the highest for 100 nm Au NPs. As was shown in Figure 2-21, the amounts

of gold sticking to each cell after the fourth washing were lower than 0.1 pg, which almost reached the minimal detection limit of the ICP-MS.

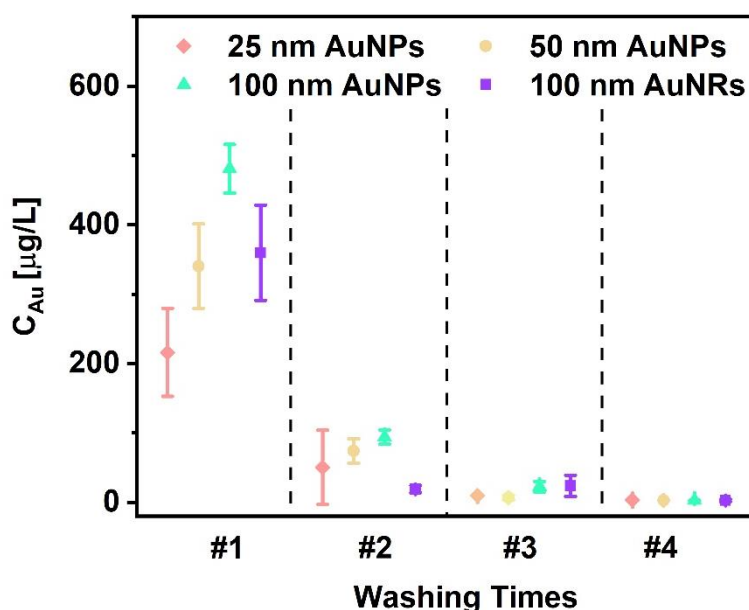


Figure 2-19 The Au concentration directly got from ICP-MS measurement for the digested and diluted supernatant samples after different washing times. The data shown correspond to mean values  $\pm$  standard deviations (SD) from three independent experiments. This graph was done by Xing Sun.

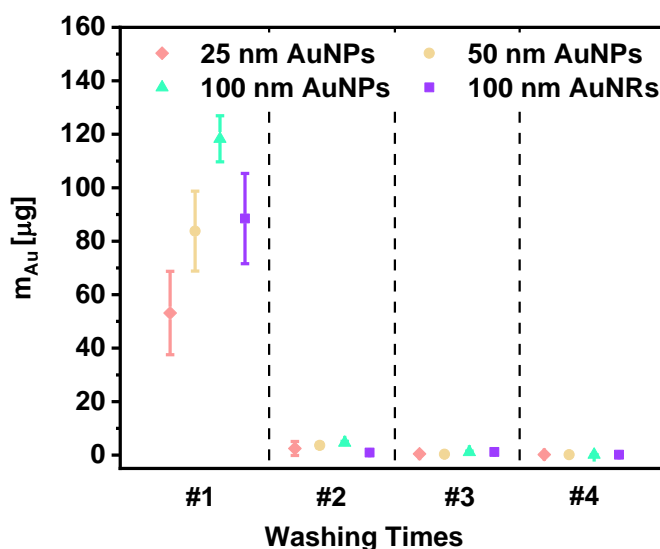


Figure 2-20 Total Au mass in supernatant from different washing steps when doing the NP-cell separation test. The data shown correspond to mean values  $\pm$  standard deviations (SD) from three independent experiments. This graph was done by Xing Sun.

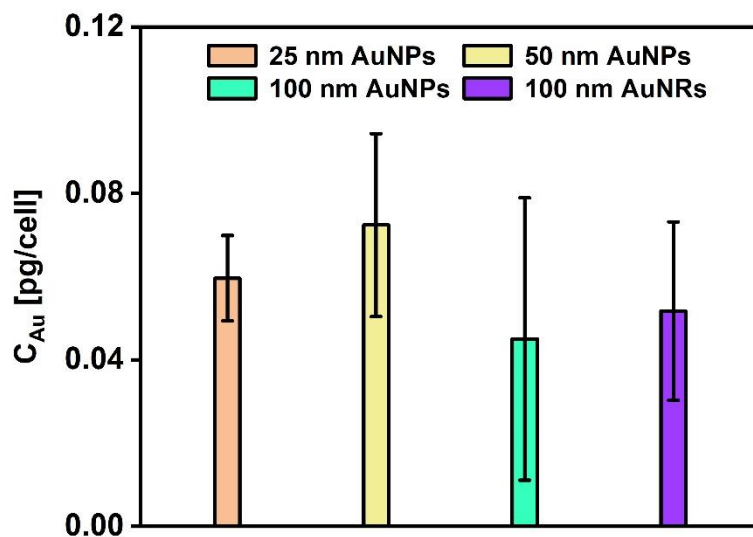


Figure 2-21  $C_{Au}$  sticking to cells after 4 times washing in the NP-cell separation test. This graph was done by Xing Sun.



## 2.6.9 Uptake of Au NP/NR into suspended Hela cells incubated in Suspension system

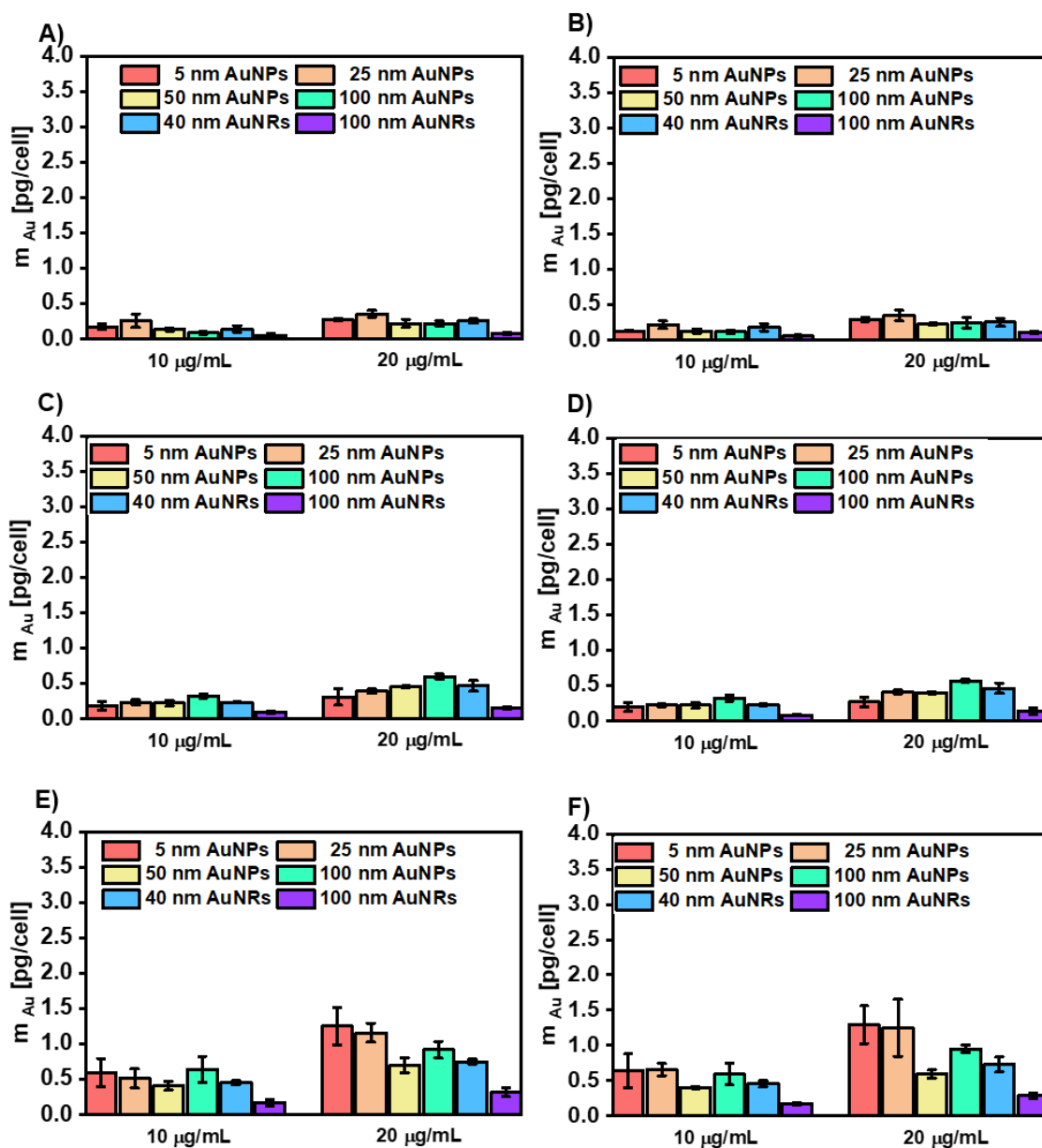


Figure 2-22 Internalized Au mass per cell for Suspended Hela cells incubated with 5, 25, 50 and 100 nm AuNPs and 40 and 100 nm AuNRs in Suspension system after different time incubation. The concentrations of NPs/NRs were 10 and 20  $\mu\text{g/mL}$ . The experiments can be separated into two group, group 1 (A, C, E) was with 3 mL of cell media, A) is for 4h, C) is for 8h and E) is for 24h; group 2 (B, D, F) was with 6 mL of cell media, B) is for 4h, D) is for 8h and F) is for 24h. The data shown correspond to mean values  $\pm$  standard deviations (SD) from three independent experiments.

To see the effect of incubation time on the uptake amount, the uptake data were presented in a different style in Figure 2-23.

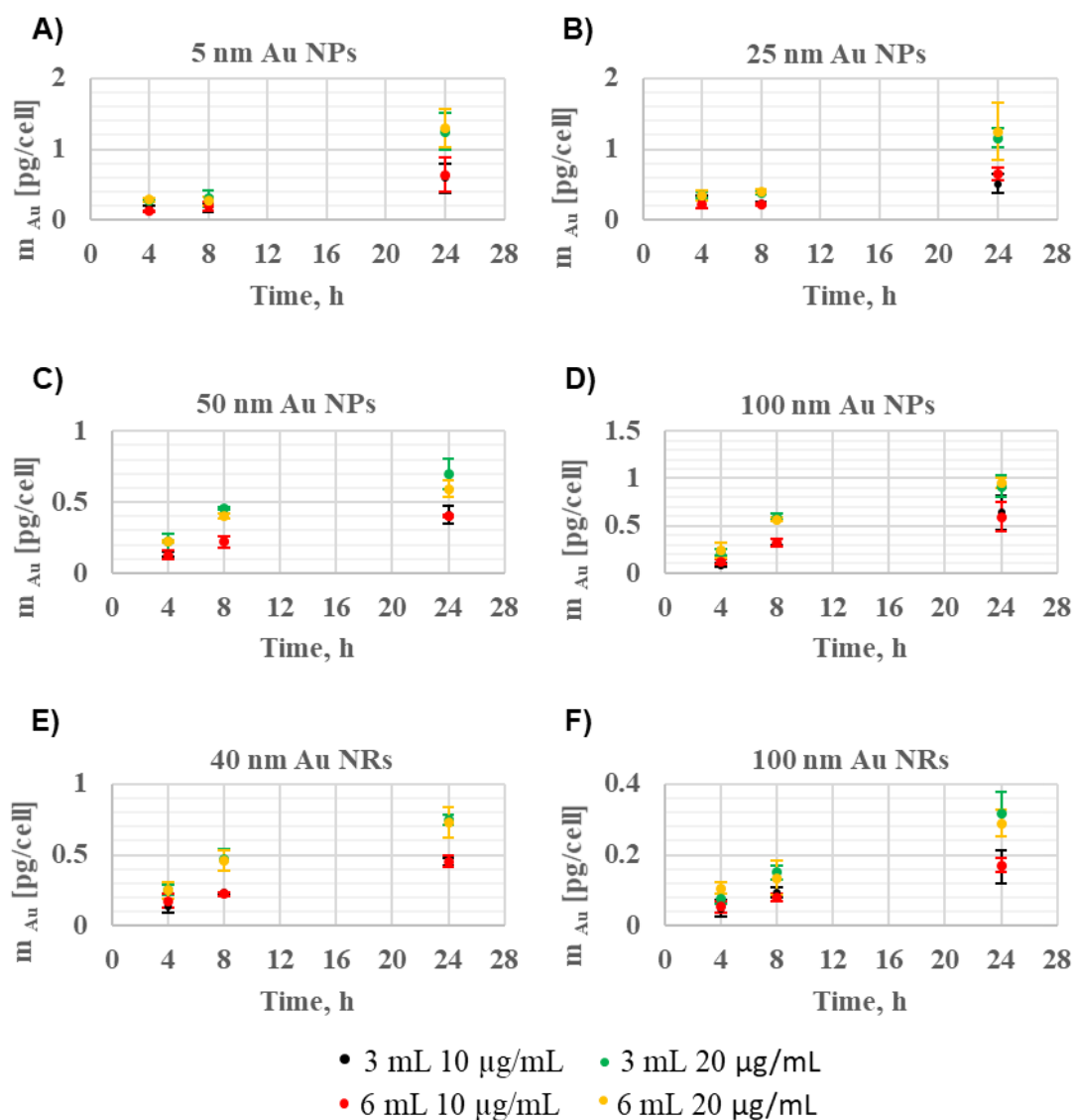


Figure 2-23 Internalized Au mass per cell for suspended HeLa cells incubated with 5, 25, 50, and 100 nm AuNPs and 40 and 100 nm AuNRs in Suspension system after different time incubation. (A), (B), (C), (D), (E), and (F) were for HeLa cells incubated with 5, 25, 50, and 100 nm AuNPs and 40 and 100 nm AuNRs respectively, while the different color represents the volume and concentration of the Au NP/NRs. If in the graphs, these four colors were not completely presented, the fact is that the black dot is completely covered up by the red dots and the green dots are completely covered up by the yellow dots.

Table 2-15 Internalized Au mass per cell for suspended HeLa cells incubated with 5, 25, 50, and 100 nm AuNPs and 40 and 100 nm AuNRs in the Suspension system.

NPs		5 nm AuNPs	25 nm AuNPs	50 nm AuNPs	100 nm AuNPs	40 nm AuNRs	100nm AuNRs
10 μg/mL 3 mL	4 h	0.17±0.04	0.26±0.09	0.13±0.02	0.08±0.02	0.14±0.05	0.05±0.02
	8 h	0.18±0.06	0.23±0.03	0.22±0.04	0.32±0.03	0.23±0.01	0.09±0.01
	24 h	0.59±0.20	0.51±0.13	0.41±0.06	0.64±0.18	0.45±0.03	0.17±0.05
10 μg/mL 6 mL	4 h	0.12±0.01	0.22±0.05	0.13±0.03	0.11±0.03	0.18±0.05	0.05±0.02
	8 h	0.20±0.06	0.22±0.02	0.22±0.04	0.32±0.04	0.23±0.01	0.08±0.01
	24 h	0.64±0.24	0.66±0.09	0.40±0.01	0.59±0.15	0.46±0.04	0.17±0.02
20 μg/mL 3 mL	4 h	0.27±0.01	0.35±0.05	0.22±0.06	0.22±0.04	0.25±0.03	0.08±0.02
	8 h	0.31±0.12	0.39±0.03	0.45±0.01	0.59±0.03	0.47±0.08	0.15±0.02
	24 h	1.25±0.26	1.16±0.13	0.70±0.11	0.92±0.12	0.75±0.03	0.31±0.06
20 μg/mL 6 mL	4 h	0.29±0.03	0.35±0.08	0.22±0.01	0.24±0.08	0.25±0.06	0.11±0.02
	8 h	0.27±0.07	0.41±0.03	0.40±0.02	0.57±0.02	0.46±0.07	0.13±0.05
	24 h	1.29±0.27	1.25±0.40	0.59±0.06	0.95±0.05	0.73±0.11	0.29±0.04

## 2.6.10 Uptake results discussion

### 2.6.10.1 The effect of Au NP/NR size on the uptake amount

According to Figure 2-13, Figure 2-15, and Figure 2-17, the significantly higher internalized Au mass per cell of (‘bigger Au NP/NRs’) 50 nm, 100 nm Au NP and 100 nm Au NR compared to (‘smaller Au NP/NRs’) 5 nm, 25 nm Au NP, and 40 nm Au NR are presented in both Static, Dynamic and Fluid systems, while disappeared in Suspension system as shown in Figure 2-22.

According to Table 2-5 and Table 2-6, the initial actual exposure Au mass concentration of 5 nm, 25 nm Au NP and 40 nm, 100 nm Au NRs is lower than the exposure Au mass concentration of 50 nm and 100 nm Au NPs. However, this exposure concentration difference is too small to explain the much larger difference in internalized Au mass per cell between ‘bigger Au NP/NRs’ and ‘smaller Au NP/NRs’ in the Static and Dynamic systems as shown in Table 2-12 and Table 2-13.

Generally, the uptake of Au NP/NRs by cells can be separated into two steps, the 1st step is the adhesion of Au NP/NRs to cells and the 2nd step is the wrapping of Au NP/NRs into cells. After being mixed with media, the Au NP/NRs will immediately be covered with large quantities of proteins forming protein corona. And, the adhesion possibility of Au NP/NR-protein compound to cell membrane can be controlled by the concentration of Au NP/NRs surrounding a single cell and also the receptor density on the cell membrane, besides whether the Au NP/NR-protein compound can be successfully attached to the cell membrane can also be influenced by the flow shear and the relative motion between Au NP/NRs and cells such as in Dynamic, Fluid and Suspension systems. The wrapping of Au NP/NRs into cells might be controlled by the energy required for cell membrane curvature and also the density of involved proteins inside the cell such as the clathrin, actin, and scaffold proteins. Devika C. B. has reported 50 nm as the optimized endocytosis size compared to other larger or smaller sizes [20] and attributed to both the energy consumption and also the receptor density required, but 50 nm was not the optimized endocytosis size in our results, on the contrary, the 100 nm Au NPs has the highest uptake and except the actual highest concentration initially added, there must be other reasons that caused the highest uptake of 100 nm Au NPs compared to other Au NP/NRs.

In the Static system, the higher uptake of 'bigger Au NP/NRs' can be partly explained by the higher Au element mass concentration surrounding the cells at the bottom of the flask which was caused by Gravity-inducing-sedimentation of 'bigger Au NP/NRs'. As reported, the movement of Au NP/NRs in the Static system is controlled by the balance between Brownian motion and the sedimentation induced by Gravity and also the fluctuation induced by interparticle forces, for example, van der Waals forces [128-130]. It has been reported by Feliu N [112] and Cho, E. C [111] that the sedimentation velocity of Au NPs induced by Gravity is proportional to  $r^2$ , and the Brownian motion velocity is in inverse proportion to  $r^{3/2}$ , and thus theoretically the 5 nm, 25 nm Au NP, and 40 nm Au NR will disperse homogeneously in Static system and the concentration of Au element in 5 nm, 25 nm Au NP, and 40 nm Au NR exposure will always be the same as the initially designed. And this theoretical calculation has also been in accordance with X. Sun's practical measurement that no sedimentation of 5 nm, 25 nm Au NP, and 40 nm Au NR has been observed. [126] But there is also a mismatch between the theory and the practical measurement. For the 50 nm, and 100 nm Au NP, the theoretical velocity induced by Gravity is  $30 \times 10^{-8}$  m/S,  $8 \times 10^{-8}$  m/S respectively and the 100 nm Au NR should be in the same order of magnitude as 50 nm Au NPs. [111, 112] But the calculated sedimentation

speed of 50 nm, 100 nm Au NP and 100 nm Au NR in Felio N's work[112] and Cho, E. C[111] was higher than practically measured in X. Sun's work[126], where only 12 %, 58 % and 10 % of 50 nm, 100 nm Au NP and 100 nm Au NR was collected in the bottom 200 uL on the condition that the distance was only less than 1 cm from the top layer of Au NP/NRs to the bottom of the tube. Whereas, according to the theoretical sedimentation velocity calculated by Felio N's work[112] and Cho, E. C[111], it takes less than 24 h for the 100 nm Au NPs to complete this less than 1cm path sedimentation, thus 100 % of the 100 nm Au NP can arrive at the bottom of tube theoretically. The possible factors that caused this mismatch can come from two major factors. The 1st factor is the operation error in X. Sun's experiment[126], sucking out the upper 200 uL layer of Au NP will inevitably disturb the Au NP in the lower layer and thus the Au NP measured in the upper 200 layer might also include some Au NPs which come from the lower layer because of this pipette disturbance. 2nd factor is that the actual sedimentation velocity of Au NP is affected by many other factors which have been ignored in the calculation reported by Felio N 's work[112]and Cho, E. C[111], such as the interparticle forces and also the important role of cells and the interaction between Au NP and protein and the other compositions in the media. Whatever the actual sedimentation speed of the 'bigger Au NP/NRs' is, it can be predicted that the 'bigger Au NP/NRs' 50 nm, 100 nm Au NP and 100 nm Au NR in our Static incubation will also sediment during the 24 incubation, which result in the higher concentration of Au element at the bottom of the flask than initially added and the higher contact possibility between 'bigger Au NP/NRs' and cell membrane and consequently contribute to the higher internalized Au element mass per cell for 'bigger Au NP/NRs' (50 nm, 100 nm Au NP and 100 nm Au NR) compared to 'smaller Au NP/NRs' 5 nm, 25 nm Au NP, and 40 nm Au NR.

While, in the Dynamic and Fluid system, the higher internalized Au mass per cell of 'bigger Au NP/NRs' still exists even though the Gravity-inducing sedimentation has been disturbed, which can be because Au mass of per 50 nm, 100 nm Au NP and 100 nm Au NR is about thousands of times the Au mass of per 5 nm Au NP and even 'eat' only one 100 nm Au NPs can bring in a large amount of internalized Au mass. And when the uptake amount was compared in terms of NP/NR number per cell, the uptake for 50 nm, 100 nm Au NP and 100 nm Au NR is still lower than 5 nm, 25 nm Au NP, and 40 nm Au NR. This can be calculated using the internalized Au mass per cell listed in Table 2-12, Table 2-13, Table 2-14, and Table 2-15, and the molar mass listed in Table 2-3. This lower internalized NP/NR number per cell for 'bigger Au NPs/NRs' (50 nm, 100 nm Au NP and 100 nm Au NR) has been reported

regardless of the exocytosis of Au NPs [37, 38]. However, we must know that this lower amount uptake in terms of internalized NP/NR number per cell of 50 nm, 100 nm Au NP and 100 nm Au NR than 5 nm, 25 nm Au NP, and 40 nm Au NR is not only caused by the lower number concentration of Au NP initially designed in these bigger Au NPs/NRs colloids but also caused by the longer wrapping time required by ‘bigger Au NP/NRs’ endocytosis.[37] It has been reported[37, 131-134], that the endocytosis of Au NPs is an ATP-consuming process. After Au NP/NRs mixed in the media, the proteins in the media would immediately cover the Au NPs and Au NRs and thus form protein corona. Then this Au NP-protein complex adhered to the cells and bind the cells through receptor-ligand binding and then enter cells mainly through endocytosis. The endocytosis speed is controlled by the thermodynamic driving force for wrapping and also the receptor diffusion kinetics, which caused the different endocytosis speeds between different sizes of Au NP/NRs. It can be predicted that it takes a longer time and consumes more energy for bigger Au NPs to enter cells than small Au NPs, which is also in accordance with the reported progress for the uptake of different sizes SeNPs [135] and also the permeability Coefficient of different sizes Silica NPs into blood-brain barrier [136].

#### **2.6.10.2 The effect of Au concentration and Au NP/NRs volume on the uptake amount**

Another trend is that the uptake amount of all 6 sizes of Au NPs/NRs has been increased when the Au element concentration was increased from 10  $\mu\text{g/mL}$  to 20  $\mu\text{g/mL}$  regardless of the incubation time, NP/NR size, and the NP/NR movement or cell status, which was shown in Figure 2-14, Figure 2-16, Figure 2-18, and Figure 2-23 and this positive concentration-dependent uptake behavior has also been reported in X. Sun’s work [126] for the uptake of Au NPs in the human, horse, dog stem cells and also murine alveolar macrophages. This is because the adhesion of Au NP/NRs to the cell membrane is the basis for the later uptake and the higher concentration of Au NP directly increased the contact possibility between cells and Au NP/NRs in all of these 4 systems for any size of the Au NPs/NRs. But the volume of Au NP/NR exposure increased from 3 mL to 6 mL did not cause any effect on the Au NP/NRs uptake amount regardless of the incubation time, NP/NR size, and the NP/NR movement or cell status, which was also shown in Figure 2-14, Figure 2-16, Figure 2-18, and Figure 2-23.

More than enough Au NP/NRs in the 3 mL colloid might be one reason that explains the no effect of increased Au NP/NRs colloid volume to 6 mL. For 5 nm, 25 nm Au NP, and 40 nm Au NR, no matter in Static, Dynamic, or Suspension system, the highest uptake in terms of Au element is less than 1 pg/cell, thus the total uptake amount is less than 0.6  $\mu\text{g}$  assuming the cell number of  $60 \times 10^4$ , which is lower than 2% of the total Au element initially added (3 mL).

Thus, the initial added 3 mL Au NP/NR exposure is excess and the increasing of Au NP/NR volume without increasing in concentration will not cause any effect on the cell uptake amount. And for the 50 nm, 100 nm Au NP and 100 nm Au NR, the highest uptake in terms of Au element is about 10 pg/cell, a totally of 6  $\mu\text{g}$  assuming  $60 \times 10^4$  cells, which is lower than 1/5 of the total Au element in the initially added 3 mL Au NP/NR exposure. Thus the 3 mL Au NP/NRs was more than excess too.

In the Dynamic and Suspension system, the increasing of Au NP/NR volume did not increase the number of Au NP/NRs closely surrounding a single cell considering the fact that the actual region where Au NP/NRs can interact with one cell is constant and also very narrow and thus the contact possibility between Au NPs/NRs and Hela cells did not change and thus the uptake amount was not affected by the increase of Au NP/NRs volume in the Dynamic, Fluid and Suspension system. But in the Static system, where 'bigger Au NP/NRs' 50 nm, 100 nm Au NP and 100 nm Au NR can sediment because of gravity and the higher total amount of Au element possibly results in higher Au concentration in the bottom of the flask and thus affects the contact possibility between cells and these 'bigger Au NP/NRs'. Actually, from our results, the increase of Au NP exposure volume from 3 mL to 6 mL did not cause any effect on the uptake amount of 50 nm, 100 nm Au NP and 100 nm Au NRs, which is opposite to our former expectation. One reason can be that the actual sedimentation speed of Au NPs is much lower than the theoretical value, so the Au NP/NRs which is more than 0.24 cm distance away from the bottom of the flask cannot reach the attached cells in the limited 24 h incubation, and thus even though the Au NP/NR exposure volume was increased to 6 mL, the actual concentration of Au element at the bottom of the flask was not largely different from the concentration when the Au NP/NR exposure was 3 mL. Another possible reason is that even though the Au NP/NRs which are more than 0.24 cm distance from the bottom of the flask have reached the adhered cells at the bottom of the flask in the limited 24 h incubation, the uptake amount of 50 nm, 100 nm Au NP and 100 nm Au NRs has reached its maximum amount which is limited by the receptor density on the cell membrane and also the ATP consuming endocytosis process.

### **2.6.10.3 The effect of Au NP/NRs movement on the uptake amount**

The difference between the internalized Au mass per cell of 'bigger Au NP/NRs' (50 nm, 100 nm Au NP, 100 nm Au NR) and the internalized Au mass per cell of 'smaller Au NPs/NRs' (5 nm, 25 nm Au NP, 40 nm Au NR) has become smaller when the incubation system changed from Static, Dynamic to Fluid. There are two possible reasons. 1st possible reason has been mentioned above and it is that the sedimentation of 50 nm, 100 nm Au NP, and 100 nm Au NR

has been disturbed in the Dynamic and Fluid system by periodical mixing and continuous unidirectional flow respectively. Thus, the Au element concentration in 50 nm, 100 nm Au NP, and 100 nm Au NR exposure in the Dynamic and Fluid system will always be homogeneous and always be the same as initially added. The 2nd possible reason is that Au NPs and Au NRs have been moved away by scouring in the Dynamic system and unidirectional flow in the Fluid system before they can adhere to cells or enter the cells through endocytosis. It has been reported[37, 131-134], that the endocytosis of Au NPs is an ATP-consuming process. And the wrapping time and wrapping energy required for ‘bigger Au NP/NRs’ is higher than ‘smaller Au NP/NRs’ [135, 136]. Thus, the scour in the Dynamic system and unidirectional flow in the Fluid system has a larger adverse influence on the uptake of ‘bigger Au NPs’ by moving away the Au NPs before they can be ‘eaten’ by the cells compared to ‘smaller Au NPs’. In another word, the tolerance of scouring and flow shear in the Dynamic and Flow system for ‘bigger Au NPs’ endocytosis is much lower than ‘smaller Au NPs’.

Besides, the 4 h uptake of 50 nm and 100 nm Au NP in Fluid system is even less than 10% of the 4 h uptake in the dynamic system, which was partly due to the 1.7 times cell density in Fluid system compared to the Dynamic system, but the main reason is that it is much harder for Au NPs/NRs to adhere to cells in the unidirectional flow in the Fluid system compared to the Dynamic system which can also be supported by the uptake amount difference of 6 sizes of Au NPs/NRs in these two systems as presented in Table 2-13 and *Table 2-14*. In the Dynamic system, in about 2/3 of the incubation time, cells were only exposed to a thin film of Au NPs/NRs and CO<sub>2</sub>, and in only 1/3 of the incubation time, cells were exposed to scour of Au NPs/NRs and the Au NPs/NRs scour over the cells was so gentle that it might not take the Au NPs/NRs away when the Au NPs/NRs tried to attach to the cell membrane. While, in the Fluid system, all the incubation time, cells were exposed to flow shear of Au NPs/NRs. Assuming that this scour or shear of the flow of Au NPs/NRs plays a negative effect on the adhesion between Au NPs/NRs and cells, then the contact possibility in the Fluid system is lower than in the Dynamic system, which matches the much lower uptake amount of 50 nm, 100 nm Au NP, 100 nm Au NR in Fluid system compared to Dynamic system as shown in Table 2-13 and Table 2-14.

#### **2.6.10.4 The special uptake behavior in the Suspension system**

It is a special phenomenon that in a Suspension system, the internalized Au mass per cell of ‘bigger Au NP/NRs’ (50 nm, 100 nm Au NP, 100 nm Au NR) is no longer higher than the internalized Au mass per cell of ‘smaller Au NP/NRs’ (5 nm, 25 nm Au NP, 40 nm Au NR)



and in some cases, the uptake of the 5 nm Au NP can be even higher than the uptake of 100 nm Au NR in terms of Au element mass per cell, which is completely different from the common trend presented in Static, Dynamic and Fluid system. It has also been reported by Xiangsheng Liu et al[137] that the uptake of 16 nm Au NPs (two types, one modified with 10-mercaptopdecyl tetraethylene glycol and another modified with PEG2000) was higher when Au NPs were added to suspended RAW264.7 than added to adherent RAW 264.7. And Xiangsheng Liu et al.[137] also analyzed this higher uptake amount in suspension RAW264.7 to be caused by the higher contact possibility between Au NP and suspended cells based on the Brownian mobility of both Au NPs and cells, and also the higher contact area of suspended RAW264.7 to Au NP compared to the only upward contact surface of adherent RAW264.7 to Au NPs.

In Static, Dynamic, and Fluid systems, Hela cells were always adhered to the flask surface and in a healthy status. While in the Suspension system, all the Hela cells were suspended in the media, and after suspension for 8 hours, the Hela cells formed accumulation spheres according to the observation under an optical microscope and when the suspension was kept longer, the Hela cells would form macroscopic spheres which can easily settle to the bottom of the falcon tube after 2 mins natural sedimentation according to our observation. The occurrence of this macroscopic sphere hindered the Au NP/NRs from adhesion to the Hela cells inside the macroscopic sphere, which decreased the uptake of 'bigger Au NP/NRs' to a larger extent than the 'smaller Au NP/NR' (5 nm, 25 nm Au NP, 40 nm Au NR) since the macroscopic sphere is not that compact and the 'smaller Au NP/NR' can still permeate it through intensive Brownian motion. Besides, the status of Hela cells is not as healthy as they were in adhered status, thus the density of receptors and proteins for NP/NRs endocytosis and also the receptor diffusion kinetics might also be weakened in the Suspension system which also contributes to the lower amount of cell uptake, but this effect on the uptake of 'bigger Au NP/NRs' can be much more serious than on the uptake of 'smaller Au NP/NR'. Besides, for incubation less than 8 h, the Hela cells have not formed macroscopic tumor spheres yet, but owing to the higher Brownian motion speed, the smaller Au NP/NRs has a higher possibility to contact Hela cells compared to the bigger Au NPs, which also contribute to the uptake of smaller Au NPs in suspended Hela cells.

#### **2.6.10.5 Time-dependent uptake behavior in all the four systems**

Besides, in all the four systems, time-dependent uptake behavior all exists and the uptake amount of the 6 sizes Au NP/NRs all followed the same trend that the uptake amount increased

with the incubation time increased from 4 h to 8 h and then 24 h, which is in accordance with many reports about the time-dependent uptake of Au NPs[37], carbon nanodots[138] and also polymer NPs[139]. Because of the limited timepoints, we cannot see whether the uptake amount has arrived at a platform or has already decreased within this 24 h incubation as has been presented also in Xing's work[126]. But it is also meaningful to discuss that the uptake amount in the Suspension system also followed the same time-dependent behavior as in the other 3 systems even though the cells in the suspension system formed bigger macroscopic spheres after a longer incubation time. One possible reason can be the limited timepoints measured covered up the fact which might be that the cells in Static, Dynamic, and Fluid status were divided into two daughter cells after about 18 h incubation thus the Au inside per cell can be diluted at this timepoint, but this diluted uptake amount per cell is still higher than the uptake amount at 8 h timepoint. And in Suspension system even though the cells were not divided into daughter cells during 24 hours, the cells formed macroscopic spheres and the uptake amount per cell might have already reached a platform before 24 h but have not presented in our results because of the only three timepoints measured. Another possible reason is that the exocytosis and endocytosis always coexist so that the formation of macroscopic cell spheres not only hindered the contact between Au NP/NR but also prevent the Au NP/NP exocytosis, and the balance between these two effects result in the total uptake amount increased with prolonging time.

## 3. Uptake of different sizes Au NPs in Red blood cells

### 3.1 Introduction

Erythrocytes (Red Blood Cells, RBCs) are currently intensively investigated as cell-based drug carriers because of their easy accessibility, longevity, large surface and good biocompatibility, and safe elimination.[140] Thus many works were studying the interaction between RBCs and NPs[54, 141], and also camouflaging the NPs with erythrocyte membrane to enhance the therapeutic efficiency[142-144]. For Au NPs application in vivo, there must be an interaction between Au NPs and Red Blood Cells if the Au NPs are injected through an intravascular route. Thus, in this chapter, we use the ex vivo RBCs to detect the uptake of Au NP into RBCs, which can be a basis for ex vivo manipulation of Au NPs cargo into RBCs and also provide a reference for in vivo interaction between Au NPs and RBCs. And according to some publications [21, 54], the uptake of NPs into RBCs might highly rely on a non-endocytic path and avoid location in the lysosome, which is largely different from the common endocytosis route. Besides, compared to the Hela cells used in Chapter 2, RBCs are nature suspension cells, thus the contact possibility between RBCs and different sizes of Au NPs will be different from the contact possibility between adhered Hela cells and different sizes of Au NPs. Thus, in this chapter, we study the uptake behavior of different sizes of Au NPs into RBCs to see whether it follows a time-dependent, dose-dependent, and also size-dependent rule as shown in adherent Hela cells.

### 3.2 Major reagents

Name	Purity	Company	Function
Gold(III) chloride trihydrate	≥99.9%	Sigma Aldrich	Au NPs synthesis
Tetraoctylammonium bromide	98%	Sigma Aldrich	Au NPs synthesis
Toluene	100.0 %	VWR	Au NPs synthesis and also Interfacial tension measurement
Sodium borohydride	≥98.0%	Sigma Aldrich	Au NPs synthesis
Hydrochloric Acid			Au NPs synthesis and ICP-MS sample digestion

Sodium Hydroxide	≥99%	Carl Roth	Au NPs synthesis
1-dodecanethiol			Au NPs synthesis
Methanol	100.0 %	VWR	Au NPs synthesis
Chloroform	100%	VWR	Au NPs synthesis
poly(isobutylene-alt-maleic anhydride)			PMA-g-dodecyl synthesis
1-dodecylamine	97%	Alfa Aesar	Au NPs synthesis
Sodium citrate dihydrate	99%	Sigma Aldrich	Au NPs synthesis
CH <sub>3</sub> O-PEG-SH, 2000 Dalton		PAPP POLYMERE	Au NPs synthesis
Tetrahydrofuran	≥99.5%	Carl Roth	PMA-g-dodecyl synthesis
RPMI 1640		Thermofisher, Gibco	Cell culture
Phosphate buffered saline		Thermofisher, Invitrogen	Cell culture
Albumax		Sigma Aldrich	Cell culture

### 3.3 Abbreviations

HAuCl <sub>4</sub>	tetrachloroauric acid
TOAB	Tetraoctylammonium bromide
NaBH <sub>4</sub>	Sodium borohydride
HCl	Hydrochloric Acid
NaOH	Sodium Hydroxide
DDT	1-dodecanethiol
DDA	dodecylamine
PMA-g-dodecyl	an amphiphilic polymer which is based on a backbone of poly(isobutylene-alt-maleic anhydride), functionalized with dodecylamine[116].
EP	eppendorf
Au	Gold

NP	nanoparticle
SPR	surface plasmon resonance
RT	Room temperature
RBCs	Red Blood Cells
Au NP@PMA	Au NPs capped with PMA-g-dodecyl

### 3.4 Key instruments

Name	Model	Company	Function
Inductively coupled plasma mass spectrometry (ICP-MS)	7700 series	Agilent	Element concentration measurement
Transmission electron microscopy (TEM)	JEM-1400PLUS	JEOL	Au NPs core size measurement
Dynamic light scattering (DLS)	NANO ZS	Malvern	Au NP hydrodynamic diameter measurement and zeta potential measurement
UV-Vis Spectrophotometer	Cary 60	Agilent	UV-vis absorbance spectra measurement
Countess 3FL Automated Cell Counter		Thermofisher	RBCs counting

### 3.5 Materials and Methods

#### 3.5.1 Au NPs synthesis and characterization

All the Au NPs used in Chapter 3 were synthesized and characterized following completely the same protocols written in Chapter 2. And all the Au NPs used in this chapter are the Au NPs coated with PMA-g-dodecyl polymer, which is also the same as in Chapter 2.

#### 3.5.2 RBCs uptake experiment

The uptake of Au NPs into human erythrocytes (RBCs) was measured by inductively coupled plasma mass spectrometry (ICP-MS, Agilent 7700 Series). Firstly, AuNPs colloids were diluted with a certain volume of the cell medium (the volume of media used was much higher

than 9 times the volume of the initial Au NPs colloid) to double the desired gold elemental mass concentrations  $C(\text{Au})$ , meaning that the  $C(\text{Au})$  after this dilution step is 40 and 80  $\mu\text{g}/\text{mL}$ , which has been confirmed by ICP-MS measurement. Then RBCs were counted using a Neubauer chamber and diluted with media to double the desired cell densities of  $N_{\text{cell}} = 10^7$  and  $2 \times 10^7$  RBCs/mL, meaning that the cell density after this dilution step is  $2 \times 10^7$  and  $4 \times 10^7$  RBCs/mL respectively. Then 1 mL diluted cell suspension and 1 mL diluted Au NPs were added together to 6-well plates (surface area/well = 887 mm<sup>2</sup>) and mixed by slightly shaking the plate (orbital, double orbital, manually). This resulted in  $V_{\text{total}} = 2$  mL/well,  $m_{\text{Au}} = 40$  and 80  $\mu\text{g}/\text{well}$ , and  $N_{\text{cell}} = 2 \times 10^7$  and  $4 \times 10^7$  RBCs/well. Plates were incubated for different times for up to 24 hours and incubated at 37 °C under a standard Plasmodium atmosphere (5% CO<sub>2</sub>, 5% O<sub>2</sub>, 90% N<sub>2</sub>). After exposure, the content of the wells was transferred to 2 mL reaction tubes and centrifuged at 70-100 rcf for 5 minutes (reduced deceleration) to pellet cells while NPs stay in the supernatant. Cells were washed three times with a medium without supplements ( $V=1$  mL) to remove NPs attached to the outer cell membrane and stored at room temperature (RT) afterward until further processed for ICP-MS measurement. The final cell number was calculated by automatic counting using the Countless 3FL Automated Cell Counter (ThermoFisher®) after the addition of medium in the third washing step. Preliminary experiments showed washing with PBS caused cells to lyse and saline promoted clumping of RBCs which led us to wash with medium (results not shown). To guarantee that three washing steps are sufficient, the supernatant after the washing steps were collected and the amount of gold was analyzed. The data suggests that three washing steps are adequate. To quantify the internalized AuNPs, cells were pelleted via centrifugation and digested with 125  $\mu\text{L}$  of nitric acid (HNO<sub>3</sub>; (67 wt%, Fisher Chemical) overnight at RT. After that, 375  $\mu\text{L}$  of hydrochloric acid (HCl; (35 wt%, Fisher Chemical) were added inside to form aqua regia (3:1 HCl: HNO<sub>3</sub> ratio) and left for digestion for 24 h. Ultimately, the samples were further diluted 10 times with 2% (V/V) HCl (prepared by mixing 2 mL 35 wt% HCl aq. With 98 mL Milli-Q water) and then measured by ICP-MS to determine elemental Au concentration. From each sample, after digestion with nitric acid and hydrochloric acid, every 200  $\mu\text{L}$  liquid was transferred to an ICP tube with 1.8 mL 2% (V/V) HCl for measurement with ICP-MS and thus technical duplicates for each sample. And for every result at least 3 individual uptake experiments were conducted which means at least 6 ICP samples were measured. Because of the quantities of experiments conducted, Different Au NP@PMA batches and RBC donors were used. The cell culture and the uptake experiments were conducted by Arne krüger and the Au NP@PMA synthesis,

characterization, and ICP-MS sample preparation and measurement were conducted by Yalan Huang.

### 3.6 Results and discussions

#### 3.6.1 Characterization of Au NPs

##### Transmission electron microscopy

Transmission electron microscopy (TEM) images were used to investigate the shape and size distribution of all Au NPs. To determine the size distribution of the core diameter  $d_c$  of the different batches of Au NPs,  $d_c$  was calculated by counting more than 100 NPs in each TEM image for all the Au NPs except the 4 nm Au NPs and more than 200 NPs were counted in each TEM image for the 4 nm Au NP using the ImageJ software. Illustrative TEM images of the AuNPs are displayed in Figure 3-1 and the obtained size distribution histograms and further characterizations can be seen in Figure 3-2 and Table 3-1.

*Table 3-1 characterization table of different batches of Au NPs*

NPs size	Batch ID	$\lambda_{SPR}$ [nm]	$d_{c-TEM}$ [nm]	Hydrodynamic diameter from DLS			$\zeta$ [mV]
				$d_{h(N)}$ [nm]	$d_{h(V)}$ [nm]	$d_{h(I)}$ [nm]	
4 nm	401	518	4.4±0.9	13.6 ± 0.9			-48.3 ± 0.7
4 nm	402	517	3.9±0.9	11.4± 1.4			-48.6 ± 2.5
4 nm	403	521	4.2±0.9	10.6 ± 2.5			-28.4 ± 0.9
4 nm	404	520	4.8 ±1.2	12.4 ± 1.1			- 41.7 ± 0.6
4 nm	405	521	4.6±1.0	12.7 ± 1.4			- 47 ± 0.5
25 nm	252	525	31.7±2.2	30.1 ± 1.0	36.7 ± 0.7	52.5 ± 0.2	-30.1 ± 0.5
50 nm	502	542	54.2±7.1	44.7 ± 0.3	57.0 ± 0.5	82.3 ± 0.8	-38.7 ± 0.4
100 nm	1003	584	105.2±16.3	104.4 ± 6.7	138.4 ± 2.9	134.1 ± 1.9	-31.5 ± 0.6

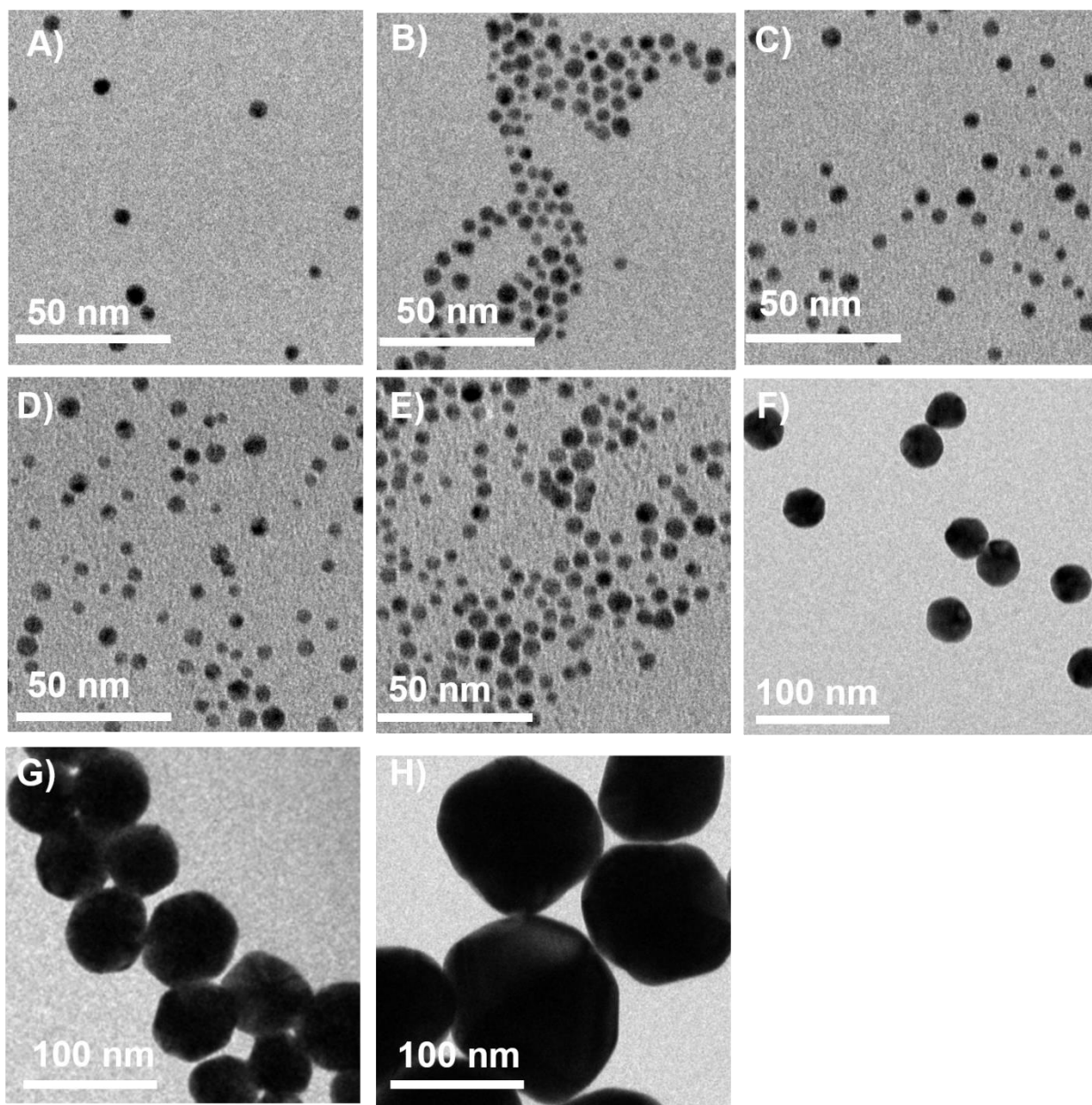


Figure 3-1 Representative TEM images of the Au NPs including A) ID401, B) ID402, C) ID403, D) ID404, E) ID405, F) ID252, G) ID502, H) ID1003 respectively.



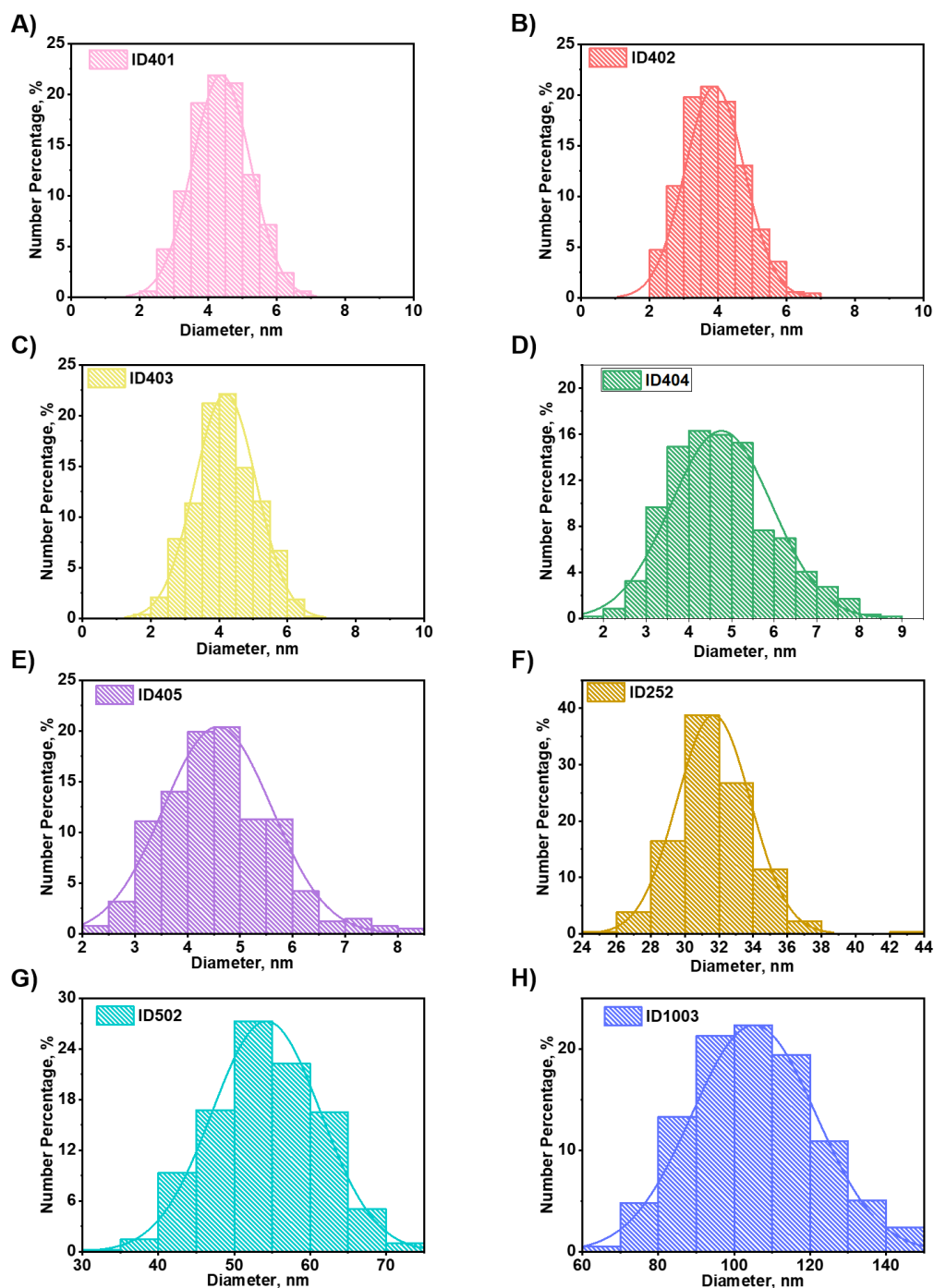


Figure 3-2 Size distribution histogram and size distribution Gaussian fitting of the Au NPs including A) ID401, B) ID402, C) ID403, D) ID404, E) ID405, F) ID252, G) ID502, H) ID1003 respectively based on the analysis of TEM images. Mean values of Au NPs for each batch were presented in Table 3-1.

### Dynamic light scattering and zeta-potential

Dynamic light scattering (DLS) was used to determine the hydrodynamic diameters  $d_H$  of all Au NPs, as seen in Figure 3-3, Figure 3-4, and Figure 3-5. The zeta-potentials  $\zeta$  was measured

with laser Doppler anemometry, and evaluated using a Malvern ZetasizerNano particle analyzer ZEN 3600 instrument. Data are presented in Figure 3-6 and Table 3-1.

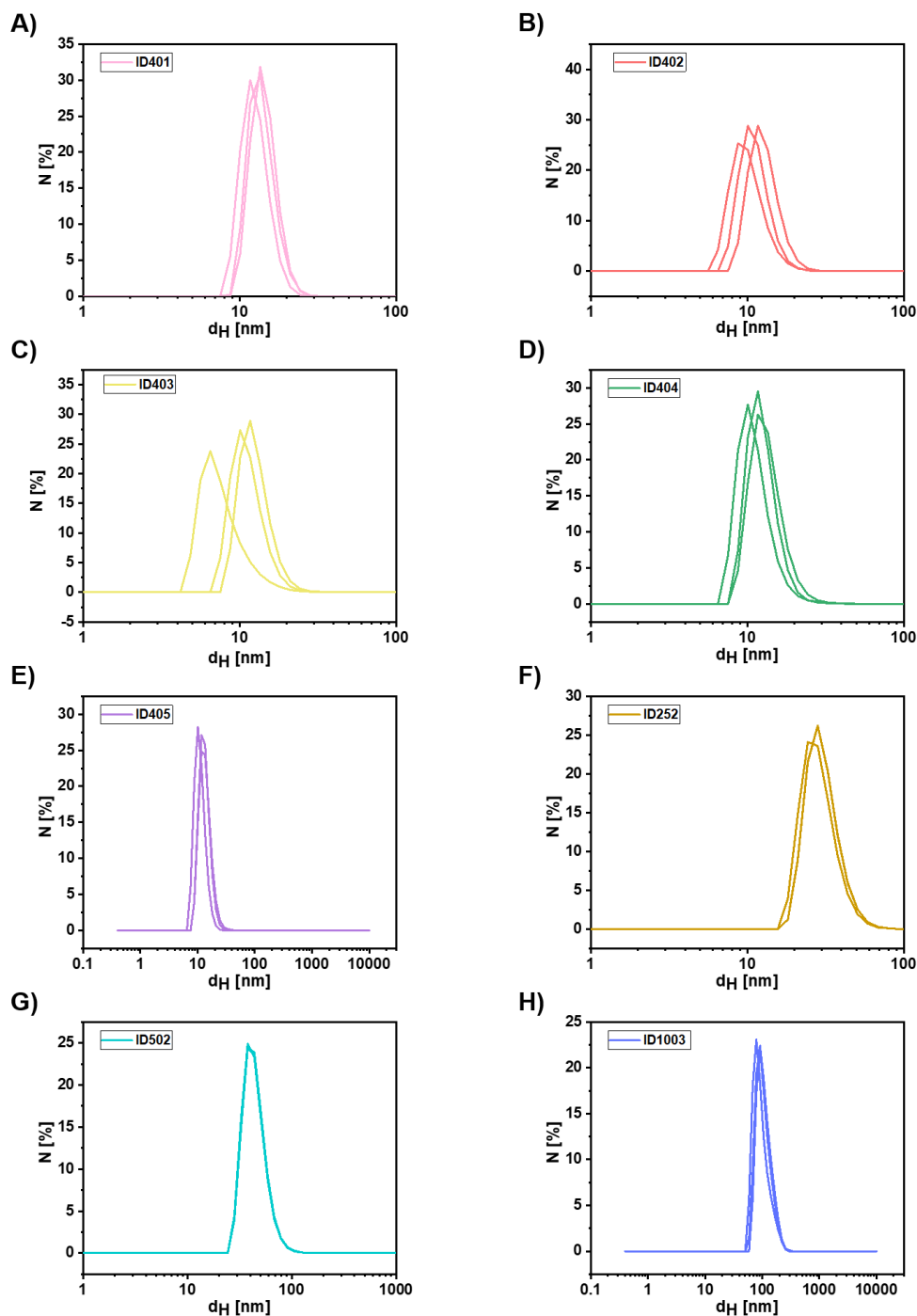


Figure 3-3 Hydrodynamic diameter  $d_H$  of Au NPs A) ID401, B) ID402, C) ID403, D) ID404, E) ID405, F) ID252, G) ID502, H) ID1003 as recorded by DLS based on number distribution. Detailed information was shown in Table 3-1.

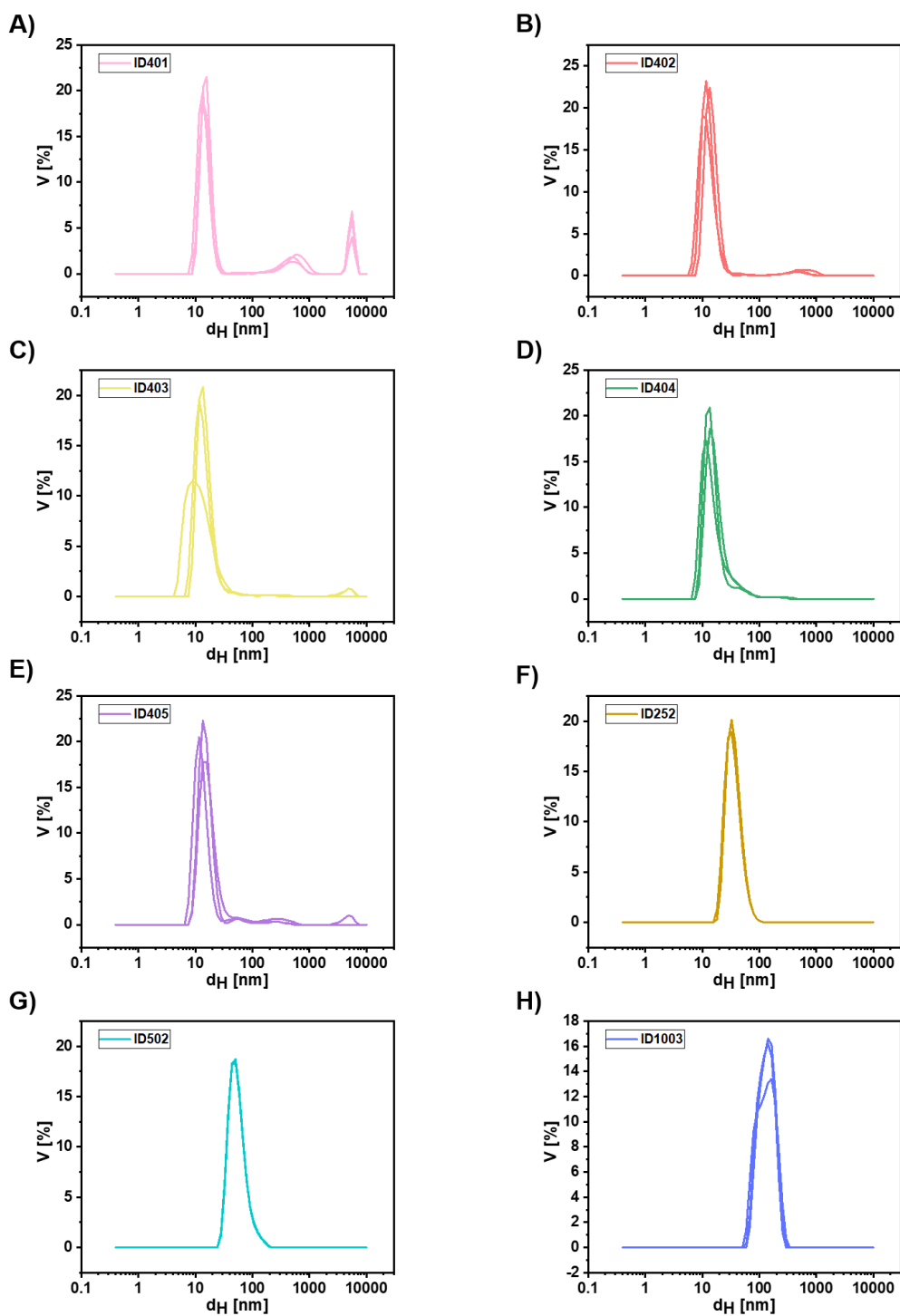


Figure 3-4 Hydrodynamic diameter  $d_H$  of Au NPs A) ID401, B) ID402, C) ID403, D) ID404, E) ID405, F) ID252, G) ID502, H) ID1003 as recorded by DLS based on volume distribution. Detailed information was shown in Table 3-1.

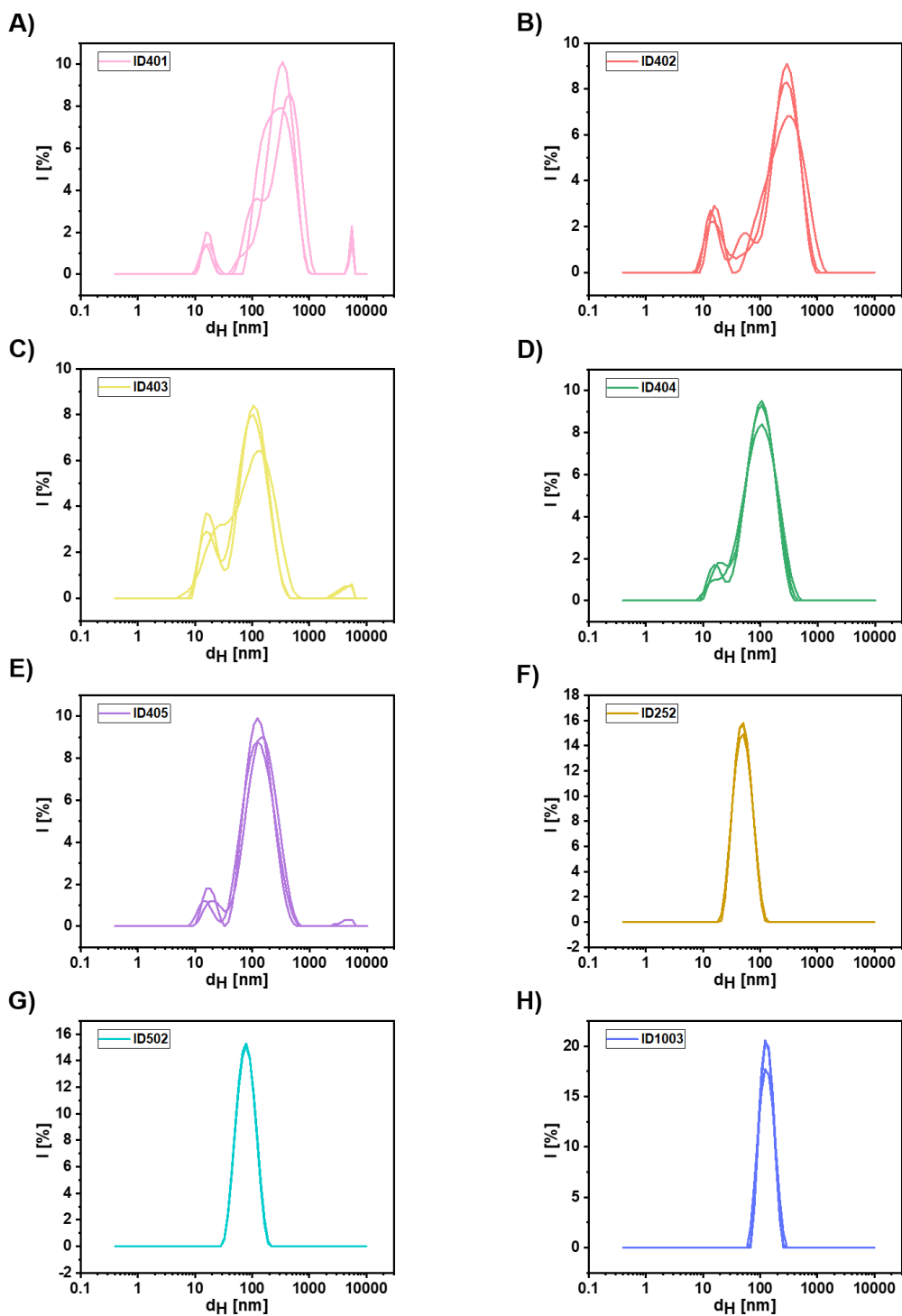


Figure 3-5 Hydrodynamic diameter  $d_H$  of Au NPs A) ID401, B) ID402, C) ID403, D) ID404, E) ID405, F) ID252, G) ID502, H) ID1003 as recorded by DLS based on intensity distribution. Detailed information was shown in Table 3-1.

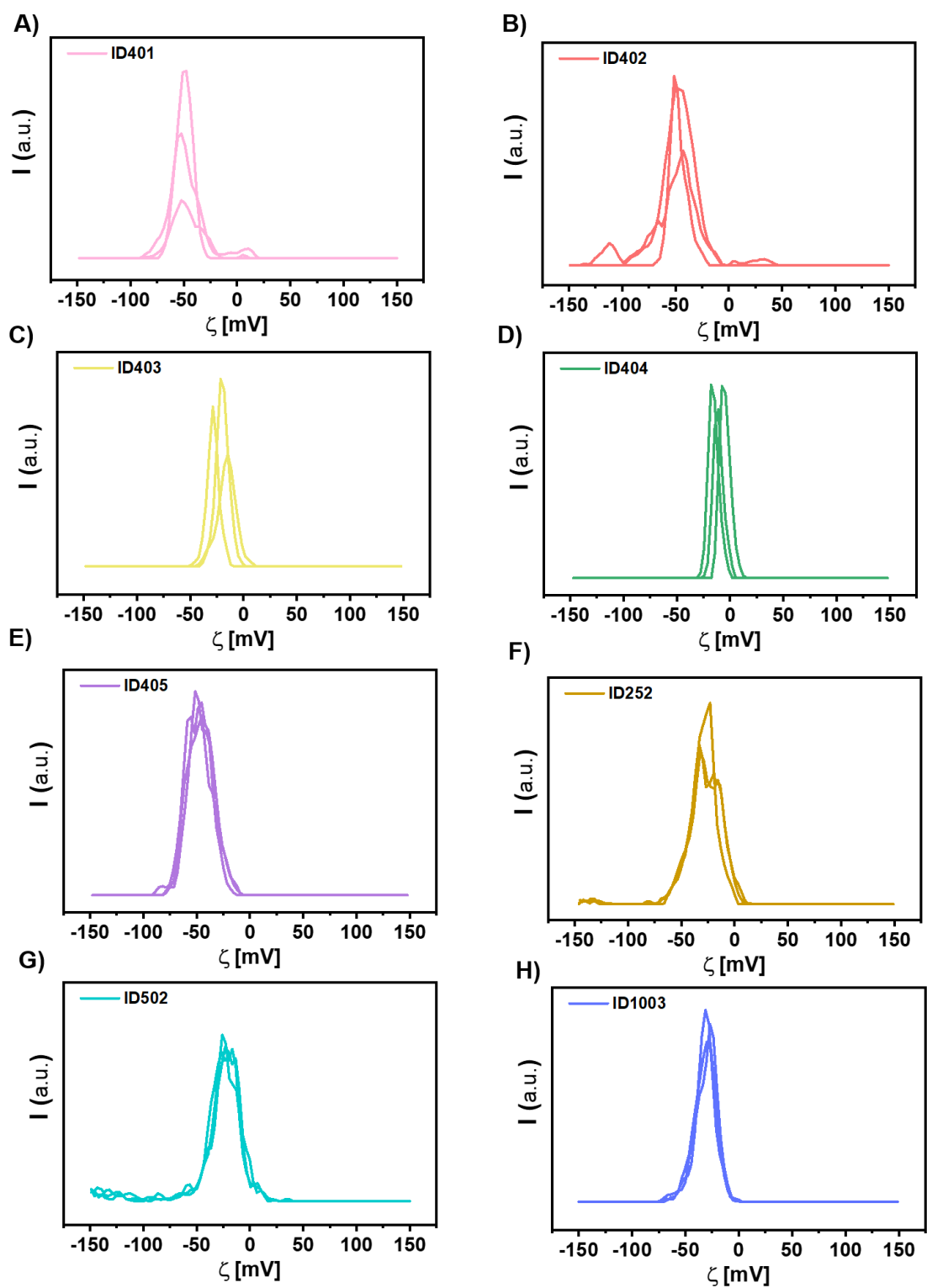


Figure 3-6 Zeta potential of Au NPs A) ID401, B) ID402, C) ID403, D) ID404, E) ID405, F) ID252, G) ID502, H) ID1003 as recorded by DLS. Detailed information was shown in Table 3-1.

## UV/vis absorption spectroscopy

The UV/vis absorption spectra of Au NPs were evaluated with an Agilent 8453 spectrometer as previously reported, as presented in Figure 3-7.

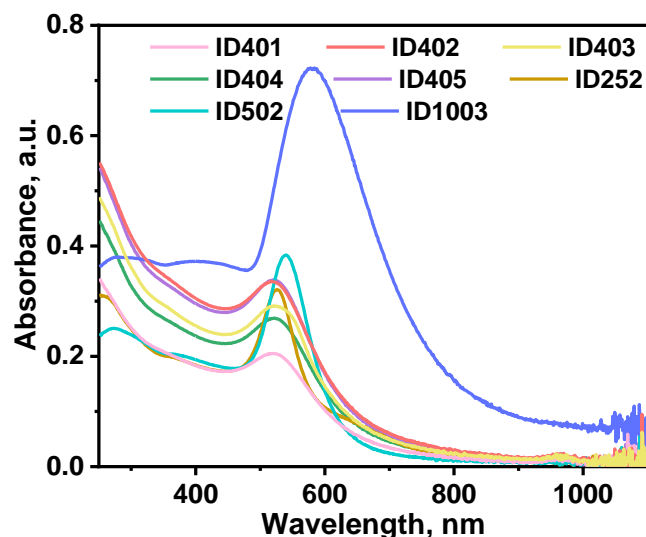


Figure 3-7 UV-vis absorbance spectra of all batches Au NPs.

### 3.6.2 The effect of cell density on the uptake of 4 nm Au NP into RBCs

Just to find the most suitable cell density used for the uptake experiment design. Cell density of  $N_{(\text{cell})} = 10^7$  and  $2 \times 10^7$  RBCs/mL were chosen to conduct the uptake experiment. Because the RBCs will not divide during the experiment, thus the cell number in every well was always the same as initially seeded  $2 \times 10^7$  and  $4 \times 10^7$  RBCs/well. And the total amount of Au element will be 40 and 80  $\mu\text{g}$  per well according to ICP-MS measurement. It was assumed that the contact possibility between Au NPs and RBCs will decrease with the increase in cell density. However, according to the results presented in Figure 3-8 and also the T-test with excel, the P value is always much higher than 0.05, indicating that there was no significant difference between the uptake amount under cell density  $N_{(\text{cell})} = 10^7$  RBCs/mL and under cell density  $2 \times 10^7$  RBCs/mL. One possible reason is the excess amount of Au, and the total Au internalized into RBCs only counted less than 5 % of the initially added Au NPs according to Table 3-2. Another important reason is that the increased cell density did not decrease the number of Au NPs which can truly interact with the cells because the space occupied per RBC presented in Table 3-2 is about 1000 and 500 times the actual Mean corpuscular volume of the Red Blood cells in these two cell density conditions assuming that the Mean corpuscular volume of the RBCs in our incubation is always not larger than 96 femtoliters per cell. Thus, the large amount

of Au NPs in the space occupied per RBC is more than excess and they can continuously diffuse to the cells through Brownian motion after the depletion of the nearby Au NPs. The space occupied per RBC is calculated as the total volume divided by the total cell number. The uptake amount per cell might be still the same even though the cell density was increased to  $4 \times 10^7$  RBCs/mL,  $8 \times 10^7$  RBCs/mL, or even higher if the cell nutrient can be secured.

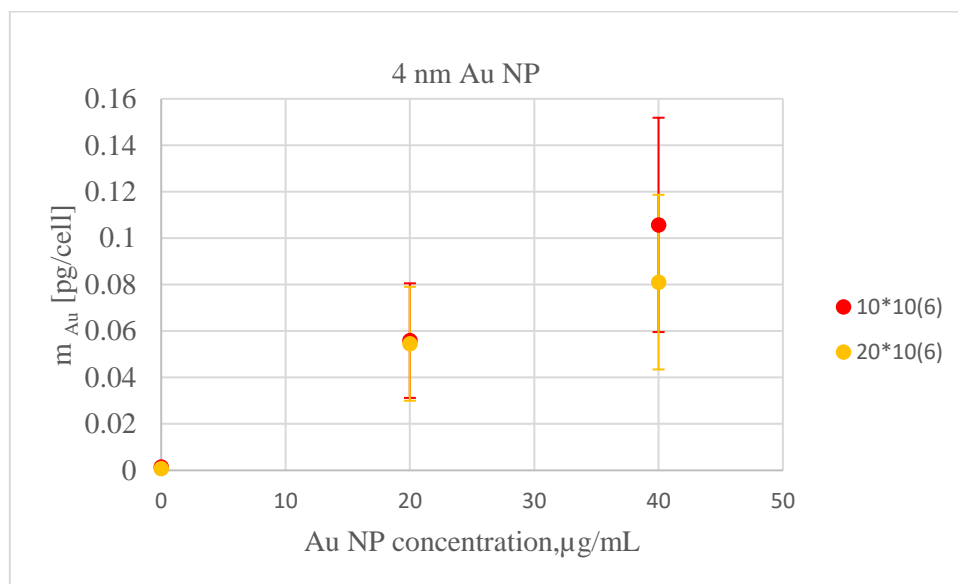


Figure 3-8 Uptake of 4 nm Au NPs into RBCs under different cell densities and also different Au element concentrations. The red dots record the uptake under cell density  $10^7$  RBCs/mL, and the yellow dots record the uptake under cell density  $2 \times 10^7$  RBCs/mL.

Table 3-2 Comparison between the internalized Au into RBCs and the initially added Au mass

Cell density, RBCs/mL	Concentration of Au added initially, μg/mL	Total mass of Au internalized into RBCs, μg	Total mass of Au added initially, μg	Total volume of Au NPs exposure, mL	Space occupied per BRCs, μL
$10^7$	20	$1.11 \pm 0.49$	40	2	0.1
$2 \times 10^7$	20	$2.18 \pm 0.98$	40	2	0.05
$10^7$	40	$2.44 \pm 0.92$	80	2	0.1
$2 \times 10^7$	40	$3.24 \pm 1.50$	80	2	0.05

### 3.6.3 The effect of Au NP concentration on the uptake of Au NP into RBCs

The concentration-dependent uptake behavior has been reported for the uptake of Au NPs into different cell lines including mesenchymal stem cells and macrophages[126], human epithelial colorectal adenocarcinoma (Caco-2 cells), mouse peritoneal macrophages (MPM)[145], and human adenocarcinoma alveolar basal epithelia (A549 cells)[146], and which is mainly because of the higher contact possibility between NPs and cells under the higher concentration

of NPs. This same concentration-dependent uptake behavior is also presented in the uptake of 4 nm Au NPs into RBCs as shown in Figure 3-9. It can be seen that the uptake of Au under a concentration of 40  $\mu\text{g/mL}$  is much higher than the uptake of Au under a concentration of 20  $\mu\text{g/mL}$  and it was amazing that after 12 h and 24 h incubation, the uptake of Au under the concentration of 40  $\mu\text{g/mL}$  exceeds 2 times the uptake of Au under the concentration of 20  $\mu\text{g/mL}$ . But the time-dependent uptake behavior was not shown under the concentration of 20  $\mu\text{g/mL}$  when the incubation changes from 6, 12 to 24 h as presented in Figure 3-9. According to Figure 3-10, the concentration-dependent uptake behavior also occurred in the uptake of 4 nm, 25 nm, and 50 nm Au NP even in a lower concentration range.

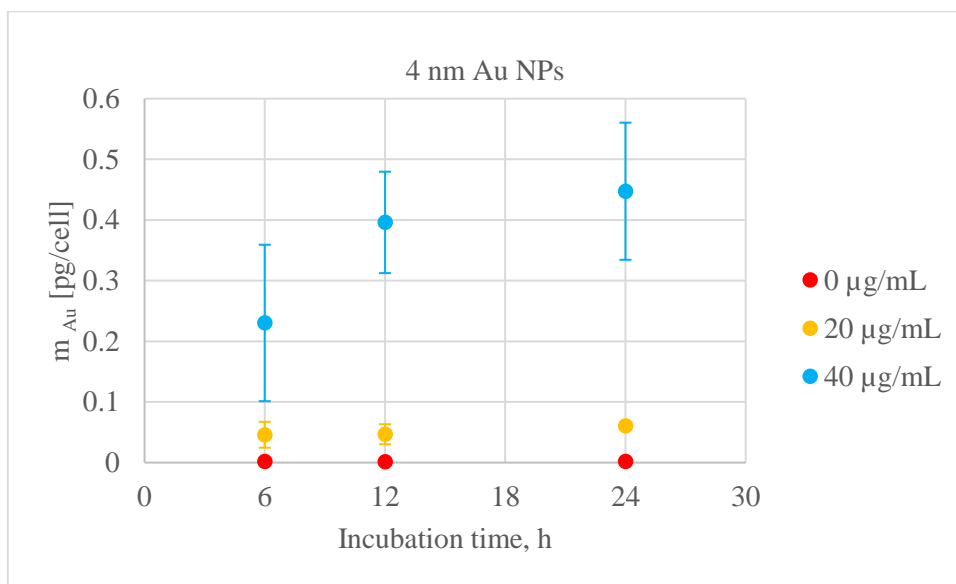


Figure 3-9 Uptake of Au into RBCs after different incubation times and under different concentrations of Au.



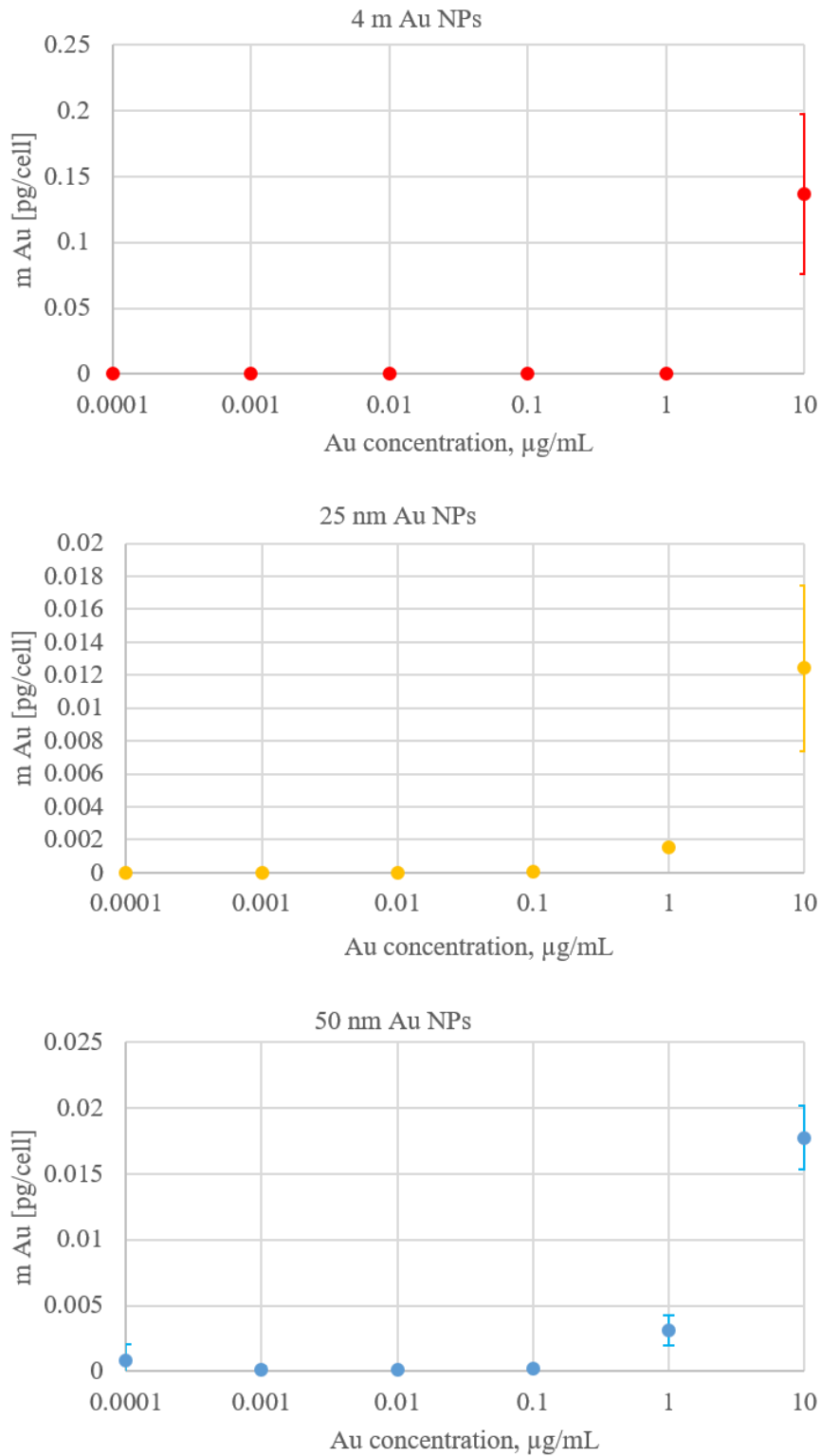


Figure 3-10 Uptake of Au into RBCs 24 h incubation time under different concentrations of Au.

### 3.6.4 The effect of Au NP size on the uptake of Au NP into RBCs

It has been intensively reported that the uptake of inorganic NPs is largely affected by the size, surface charge, and also shapes. According to Figure 3-11, the uptake of 4 nm Au NPs into

RBCs is much higher than 25 nm and 50 nm, which means this size-dependent uptake difference can be even enlarged if the uptake amount is in terms of Au NP number per cell. The low uptake of 50 nm Au NPs into RBCs can be caused by the 50 nm Au NP sedimentation to the bottom of the plate instead of contacting the RBCs suspended in the media[111, 112, 126]. 50 nm Au NP can sediment to the bottom of the plate because of gravity, thus the actual Au mass concentration at the bottom exceeded the saturation of the cell, while the actual Au mass concentration at the distance far from the bottom was much lower than the initial concentration, which results in the low uptake. Besides, the 5 nm has a higher Brownian motion speed [112] compared to 25 and 50 nm, which also provides more opportunity for 5 nm Au NPs to touch the RBCs, which results in the highest uptake compared to 25 and 50 nm.

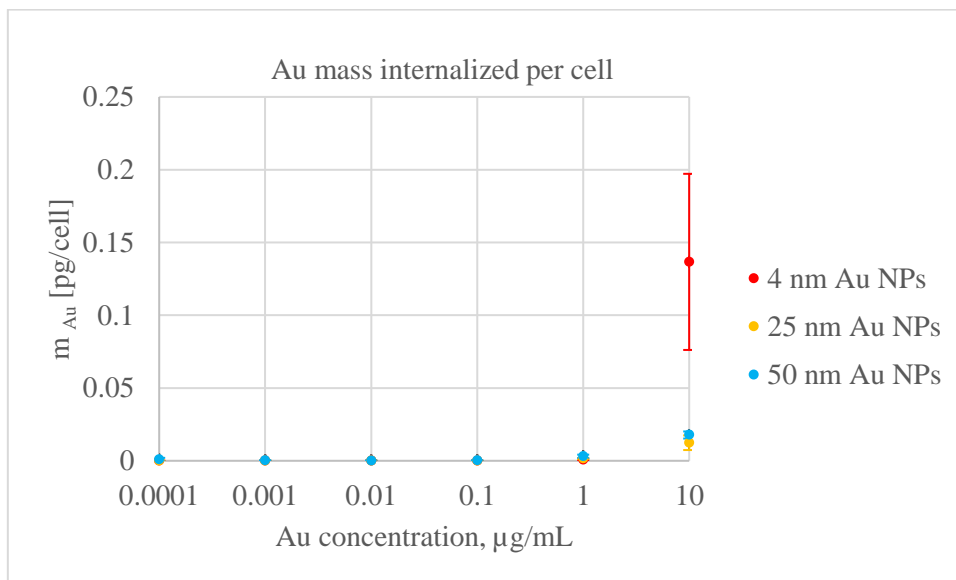


Figure 3-11 Uptake of different sizes Au NPs into RBCs.

## 4. The intake and metabolism of Au NP and BSA-Eu in mosquitoes

### 4.1 Introduction

Mosquito, a kind of arthropod vector, is of enormous importance to human health. The mosquito can transfer the virus to humans through one tiny bite for blood. Considering the increasing resistance of mosquitoes to traditional chemical insecticides and also the concomitant environmental challenge caused by traditional chemical insecticides [147-149], Currently, there are many investigations on NPs working as insecticides to kill Larva, pupa, and adult mosquitoes and also weaken mosquito productivity of eggs [150-155]. However, there was no investigation on the biodistribution and trafficking of NPs in mosquitoes. Following ingestion by adult mosquitoes, NPs would have to traffic in the alimentary tract, penetrate diverticula, cardia, foregut, or midgut barriers, disseminate into the hemocoel, and then be internalized by target tissues and cells [156]. The physicochemical properties of NPs including size, shape, and surface ligand would also affect the distribution of NPs in the mosquito since there are also many barriers in mosquitoes similar to a mouse, rabbits, and humans [157, 158]. Thus, in this chapter, we quantitatively investigate the intake and metabolism of Au NPs and BSA-Eu in mosquitoes using ICP-MS.

### 4.2 Major reagents

Name	Purity	Company	Function
Bovine Serum Albumin	96%	Sigma Aldrich	Labelling BSA
DOTA-NHS ester	$\geq 90\%$	Macrocyclic	Labelling BSA
PBS buffer (pH 8)		Thermofisher	Labelling BSA
MES buffer (pH 6)	$\geq 99.5\%$	Sigma Aldrich	Labelling BSA
EuCl <sub>3</sub>	99.99%	Sigma Aldrich	Labelling BSA
Coomassie (Bradford) Protein Assay Kit		Thermofisher	Detect the concentration of BSA
Potassium iodide	$\geq 99.0\%$	Sigma Aldrich	Feed mosquitoes
Sodium Bromide	$\geq 99.0\%$	Sigma Aldrich	Feed mosquitoes
Fructose			Feed mosquitoes

FlyNap® Anesthetic Kit		Carolina	Kill mosquitoes
Gold(III) chloride trihydrate	≥99.9%	Sigma Aldrich	Au NPs and NRs synthesis
Tetraoctylammonium bromide	98%	Sigma Aldrich	Au NPs synthesis
Toluene	100.0 %	VWR	Au NPs synthesis and also Interfacial tension measurement
Sodium borohydride	≥98.0%	Sigma Aldrich	Au NPs and NRs synthesis
Hydrochloric Acid			
Sodium Hydroxide	≥99%	Carl Roth	Au NPs and NRs synthesis
1-dodecanethiol			
Methanol	100.0 %	VWR	Au NPs synthesis
Chloroform	100%	VWR	Au NPs and NRs synthesis
poly(isobutylene-alt-maleic anhydride)			
1-dodecylamine	97%	Alfa Aesar	Au NPs and NRs synthesis
Sodium citrate dihydrate	99%	Sigma Aldrich	Au NPs synthesis
CH <sub>3</sub> O-PEG-SH, 2000 Dalton		PAPP POLYMERE	Au NPs and NRs synthesis

### 4.3 Abbreviations

HAuCl <sub>4</sub>	tetrachloroauric acid
TOAB	Tetraoctylammonium bromide
NaBH <sub>4</sub>	Sodium borohydride
HCl	Hydrochloric Acid
NaOH	Sodium Hydroxide
DDT	1-dodecanethiol

DDA	dodecylamine
PMA	an amphiphilic polymer which is based on a backbone of poly(isobutylene-alt-maleic anhydride), functionalized with dodecylamine, yielding dodecylamine hydrophobic side chains through formation of amide bonds upon reaction with the maleic anhydride rings (PMA).
PMA-g-dodecyl	an amphiphilic polymer which is based on a backbone of poly(isobutylene-alt-maleic anhydride), functionalized with dodecylamine, yielding dodecylamine hydrophobic side chains through the formation of amide bonds upon reaction with the maleic anhydride rings (PMA).
EP	Eppendorf
Au	Gold
NP	nanoparticle
SPR	surface plasmon resonance
RT	Room temperature
BSA-Eu	Europium labelled BSA
ICP-MS	Inductively Coupled Plasma Mass Spectrometry

## 4.4 Key instruments

Name	Model	Company	Function
Inductively coupled plasma mass spectrometry (ICP-MS)	7700 series	Agilent	Element concentration measurement
Transmission electron microscopy (TEM)	JEM-1400PLUS	JEOL	Au NPs core size measurement
Dynamic light scattering (DLS)	NANO ZS	Malvern	Au NP hydrodynamic diameter measurement and zeta potential measurement
UV-Vis Spectrophotometer	Cary 60	Agilent	UV-Vis absorbance spectra Measurement

## 4.5 Materials and Methods

### 4.5.1 synthesis of 4 nm Au NP

The 4 nm Au NP@PMA used in Chapter 4 was the same batch ID 404 and ID 405 used in Chapter 3. Thus, the synthesis just refers to Chapter 2 and the characterization data is the same as in Chapter 3 and thus not written in this Chapter 4.

### 4.5.2 labeling of BSA with Eu

#### Reactions parameters of the labeling of BSA with Eu element.

A general protocol for BSA labeling with Eu is used in this chapter [159, 160].

Step1 was the conjugation of BSA with DOTA-NHS ester. The detailed operation is: BSA powder was dissolved in PBS (pH8) solution and mixed with fresh DOTA-NHS ester solution prepared by the dissolution of DOTA-NHS ester in PBS (pH8) solution, with a molar ratio of  $n(\text{BSA}): n(\text{DOTA-NHS ester}) = 1:50$  and then this mixture was gently stirred at room temperature overnight. In this work, the BSA concentration in this mixture was kept at about 3-8 mg/mL.

Step2 was to change the buffer from PBS (pH8) solution to MES (pH6). The operation was: the liquid after step1 was centrifuged at 9000 rpm for 30 min in an ultrafiltration tube (MWCO:3kD) and afterward redissolved in enough volume of MES (pH6) buffer and then this centrifugation and redissolution operation was repeated.

After the buffer exchange to MES (pH6), the conjugation of Eu is step3. Detailed operation is: EuCl<sub>3</sub> powder is dissolved in MES (pH6) and then added to the BSA-DOTA conjugation with a molar ratio n(BSA-Dota conjugate):n(EuCl<sub>3</sub>)=1:50. Then this mixture was incubated in 43 °C water bath for 1 h.

Step4 was to separate the insoluble BSA occurring after step 3 from those soluble BSA-Eu by using a 0.22 μm PES filter membrane. Then the soluble BSA-Eu was collected and the insoluble BSA was discarded.

Step5 was to remove the excess Eu<sup>3+</sup> and DOTA. The detailed operation was: the soluble BSA-Eu in MES (pH6) together with excess Eu<sup>3+</sup> and DOTA was centrifuged at 9000 rpm for 30 min in an ultrafiltration tube (MWCO:3kD) and afterward dissolved in enough volume of Milli-Q water and then this centrifugation and dissolution operation was repeated for several times until there was almost no Eu<sup>3+</sup> in the supernatant. In our work, the Eu will work as a signal to indirectly present the amount of BSA-Eu, thus the excess Eu<sup>3+</sup> must be completely washed away from the BSA-Eu.

About this general protocol above, there were two problems to be solved. One problem is the yield percentage of BSA-Eu compared to the initial amount of BSA. Another problem is deciding the wash times during the step5 to completely remove the excess Eu<sup>3+</sup>. To solve these two problems, Coomassie assay combined with UV-vis spectroscopy was used to detect the concentration of BSA, and ICP-MS was applied to measure the Eu in the supernatant.

### **Coomassie (Bradford) Protein Assay Kit standard curve measurement and accuracy check**

Firstly, Coomassie dye was used to detect the concentration of BSA after each step during the labeling just to find the yield of BSA after each step. When Coomassie dye binds a protein in an acidic medium, an immediate shift in absorption maximum from 465nm to 595nm occurs with a concomitant color change from brown to blue. However, the absorbance intensity at 595nm (ABS595) is non-linear with increased BSA concentration, thus the standard curve must be measured. Here the standard curve listed as Equation 4-1, and Equation 4-2 were measured

by our groupmate Bing Qi. In Equation 4-1 and Equation 4-2,  $y = \text{ABS}_{595}(\text{BSA sample}) - \text{ABS}_{595}(\text{blank sample})$  meaning subtract absorbance intensity at 595 nm of blank from absorbance intensity at 595 nm of BSA samples. Here, the blank is a 1.5 mL Coomassie assay mixed with 30  $\mu\text{L}$  Milli-Q water, while the BSA sample is a 1.5 mL Coomassie assay mixed with 30  $\mu\text{L}$  BSA.  $x$  is the BSA concentration in  $\mu\text{g}/\text{mL}$ . for blank,  $x=0$ ,  $y=0.01295$  instead of  $y=0$  caused by the fitting error of the standard curve. Equation 4-1 is applicable for BSA sample concentration between 100-1500  $\mu\text{g}/\text{mL}$  and the correlation coefficient  $R^2 = 0.997$ . Equation 4-2 is for BSA sample concentration between 0-25  $\mu\text{g}/\text{mL}$  and the correlation coefficient  $R^2 = 0.99314$ . Then self-prepared BSA solution of known concentration was used to check the operation error and accuracy of the standard curves, and the calculated concentration based on the Coomassie assay was presented in Figure 4-1. All the operations followed the Coomassie (Bradford) Protein Assay Kit standard manual instructions offered by Thermofisher, which has emphasized several points including 1. Coomassie assay must be equilibrated to room temperature before use. 2. Mix is essential before pipette or measurement just to make sure the dye-BSA-dye aggregates disappear. 3. Remove or dilute the Strong alkaline buffer and surfactant existing in the matrix of the BSA sample.

$$y = -3.18321 * 10^{-7}x^2 + 0.00133x + 0.01295 \quad \text{Equation 4-1}$$

$$y = -3.09058 * 10^{-4}x^2 + 0.03927x - 0.02198 \quad \text{Equation 4-2}$$



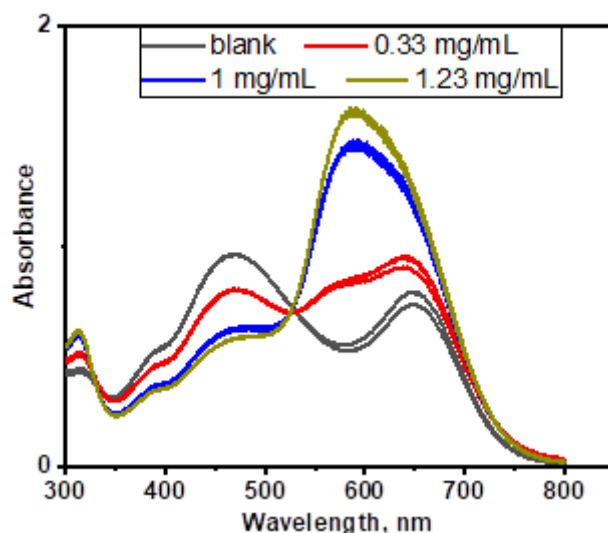


Figure 4-1 UV-vis absorbance spectra of Coomassie dye linked with blank and self-prepared BSA solution of known concentrations. Different colors represent different concentration samples, and the black line was for 1.5 mL Coomassie assay mixed with 30  $\mu$ L Milli-Q water. And other lines were for 1.5 mL Coomassie assay mixed with 30  $\mu$ L BSA solution of corresponding concentrations with replicate parallel samples.

Table 4-1 Difference between known concentration and concentration calculated from the standard curve

BSA solution	Prepared known concentration, $\mu$ g/mL	Sample preparation	Concentration calculated from the standard curve, $\mu$ g/mL	An error of calculated concentration to a known concentration
1	330	30 $\mu$ L BSA solution mix with 1.5 mL Coomassie assay	228	30.9 %
2	1000	30 $\mu$ L BSA solution mix with 1.5 mL Coomassie assay	820	18%
3	1230	30 $\mu$ L BSA solution mix with 1.5 mL Coomassie assay	1037	15.7%

### Measurement of Eu element in BSA-Eu by ICP-MS

To identify excess free Eu has been completely removed during step5 in the labeling protocol and also calculate how many Eu molecules have been successfully labeled per BSA molecule, the measurement of Eu in supernatant collected in step5 and Eu in BSA-Eu samples must be conducted with ICP-MS. The sample preparation was almost the same as Au NPs mentioned in chapter 2. Firstly, 20  $\mu$ L supernatant or 10  $\mu$ L BSA-Eu was pipette to EP tube and then 200

$\mu\text{L}$  fresh Aqua Regia ( $\text{V}(\text{HNO}_3 \text{ (aq, 67 wt\%)}): \text{V}(\text{HCl} \text{ (aq, 35 wt\%)}=1:3$ ) was added to the supernatant or BSA-Eu sample in the EP tube and the mixture was kept overnight at RT for digestion. After that, the digested sample was diluted with 1.8 mL of 2% V/V HCl (prepared by mixing 2 mL 35 wt% HCl aq. With 98 mL Milli-Q water) and then measured by ICP-MS.

### **The yield of BSA after different steps during the labeling reaction**

To know the yield of BSA after different steps during the labeling reaction, BSA samples were collected after step2, step4, and step5 separately and then linked with Coomassie dye and measured with UV-vis absorbance spectroscopy. Based on the absorbance intensity at 595 nm and the standard curves Equation 4-1 and Equation 4-2, the concentration and mass of BSA after different steps were calculated and listed in Table 4-2.

*Table 4-2 Concentration and mass of BSA after each labeling step based on Coomassie assay<sup>a</sup>*

After each step	Concentration of BSA, mg/mL	Mass of BSA, Mg	Yield percentage
After step2	0.6	10.8	100%
After step4	0.6	3.6	33.3%
After step5	0.645	3.225	29.8%

<sup>a</sup> *The initial BSA concentration and mass were not presented in Table 4-2, just assuming the yield percentage after step2 was 100%.*

From Table 4-2, we can know that about 67% of BSA has been lost between step2 and step4, because of the removal of large quantities of insoluble BSA aggregate after adding  $\text{EuCl}_3$  during the step3. And all the centrifugation and wash-in step5 did not cause much loss of BSA as listed in Figure 4-2. To conclude, the very low yield percentage of BSA-Eu was just caused by the formation of insoluble BSA after the adding of  $\text{Eu}^{3+}$  instead of any other wash problem.

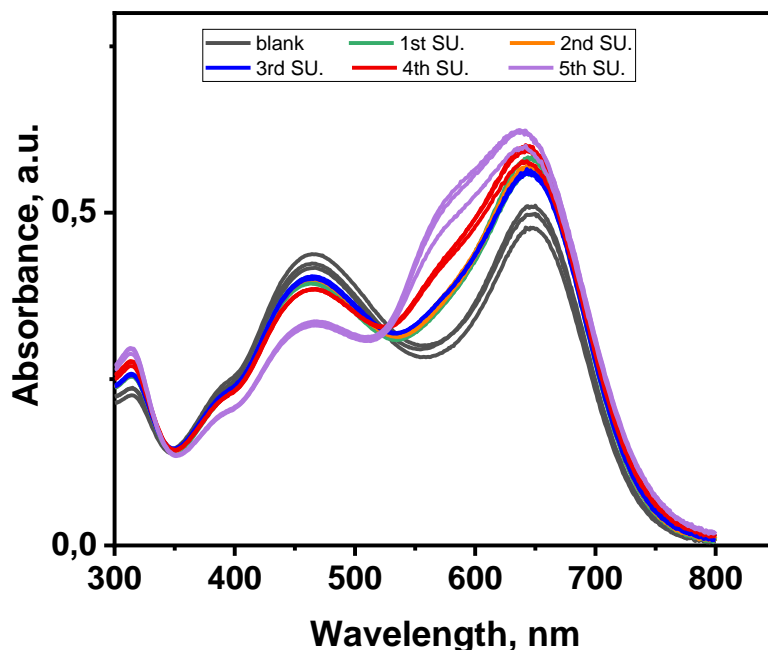


Figure 4-2 UV-vis absorbance of Coomassie dye linked with blank and supernatant collected after each time ultrafiltration during step5.

About the complete wash of excess  $\text{Eu}^{3+}$  during step5, the very low concentration of Eu element in the supernatant after 5th ultrafiltration compared to the Eu concentration in the BSA-Eu solution indicates that the  $\text{Eu}^{3+}$  has almost been completely washed away after ultrafiltration for 5 times. The Eu element concentration measured by ICP-MS was listed in Table 4-3. And the strange molar ratio of Eu to BSA in the supernatant after 5th ultrafiltration was because of the not precise measurement of BSA concentration in this low concentration range. Consequently, each BSA molecule was labeled with 2.7 Eu molecules.

Table 4-3 Concentration and the total amount of BSA and Eu existing in BSA- Eu and the 5th supernatant<sup>a</sup>

Sample	BSA concentration, mg/mL	Total BSA mass, mg	Eu concentration, $\mu\text{g/mL}$	Total Eu mass, $\mu\text{g}$	The molar ratio of Eu to BSA $n_{(\text{Eu})}/n_{(\text{BSA})}$
BSA-Eu	0.645	3.225	20	20	2.7
Supernatant after 5th ultrafiltration	0.023	0.138	0.029	0.17	0.5

Two assumptions were made. 1st assumption was that Equation 4-1 and Equation 4-2 are still available to BSA-dota conjugation and also BSA-Eu. 2nd assumption was that the molar mass of BSA-DOTA conjugation and also BSA-Eu was almost the same as pure BSA.

## **Optimize the labeling protocol**

Just as mentioned above, a large quantity of insoluble BSA came out after the addition of  $\text{EuCl}_3$ . But then it was found that adding  $\text{EuCl}_3$  to pure BSA solution without Dota-NHS ester will not induce any insoluble BSA after 1 h incubation at 43 °C even though the molar ratio of  $\text{EuCl}_3$  to BSA changed from 10:1 to 50 :1. Thus we doubt that the occurrence of insoluble BSA was related to the existing of Dota-NHS ester conjugated to BSA or the excess Dota-NHS ester. And Dota-NHS ester conjugated to BSA was the basis for the successful labeling of Eu to BSA, thus the only attempt was to completely remove the excess dota-NHS ester by 5 times ultrafiltration during step2 and after this 5 times ultrafiltration, BSA-dota conjugation concentration was calculated based on the standard curves Equation 4-1 and Equation 4-2.  $\text{EuCl}_3$  was added to BSA-dota conjugation at molar ratio range from 10:1 to 50:1. Our observation indicated that no insoluble BSA occurred and proved that the wash of excess dota-NHS ester worked. Coomassie assay combined with UVvis absorbance measurement proved a high yield of BSA-Eu as shown in Table 4-4. Finally, the yield percentage of BSA-Eu was about 50% and the loss of BSA-Eu was only during the 5 times ultrafiltration during step5. The labeling efficiency is also higher than the old protocol, for the 5 batches of BSA-Eu listed in Table 4-4, which is about 6 molecules of Eu were labeled per molecule of BSA, while the labeling efficiency for the old protocol is about 3 molecules of Eu labeled to per molecule of BSA. Besides, according to Table 4-4, 4 times ultrafiltration was already enough to almost washing away all the excess  $\text{Eu}^{3+}$  because more times ultrafiltration will not get more excess  $\text{Eu}^{3+}$  in the supernatant. Consequently, this optimized protocol was applied for the preparation of BSA-Eu, which was used to feed mosquitoes.

Table 4-4 important data for batches of BSA-Eu labeled with modified protocol<sup>a</sup>

Batches number	1	2	3	4	5
Mass of BSA-dota conjugation after 5th ultrafiltration in step2, mg	4	4	4	4	2
The molar ratio of EuCl <sub>3</sub> to BSA-dota conjugation in step3	10:1	20:1	30:1	40:1	50:1
Mass of BSA-Eu after step4, mg	4	4	4	4	2
Mass of BSA-Eu after step5 (5 times ultrafiltration in step5), mg	1.78	2.05	1.94	2.04	1.08
Yield percentage of BSA-Eu	37 %	51.25 %	48.5 %	51 %	54%
Mass of Eu labeled to BSA by ICP-MS, µg	28.06	20.99	25.69	30.40	13.41
Molecules of Eu labeled per molecule BSA	6.84	4.44	5.73	6.47	5.36
Mass of Eu in the supernatant after 1st ultrafiltration in step5, µg	20	23	43	75	45
Mass of Eu in the supernatant after 2nd ultrafiltration in step5, µg	6.1	0.66	13.78	20.35	23.79
Mass of Eu in the supernatant after 3rd ultrafiltration in step5, µg	0.55	0.08	1.62	2.51	3.25
Mass of Eu in the supernatant after 4th ultrafiltration in step5, µg	0.05	0.21	0.77	0.79	0.53

<sup>a</sup>Two assumptions were made. 1st assumption was that Equation 4-1 and Equation 4-2 are still available to BSA-dota conjugation and also BSA-Eu. 2nd assumption was that the molar mass of BSA-DOTA conjugation and also BSA-Eu was almost the same as pure BSA.

### 4.5.3 mosquito feeding, anesthetizing, and digestion for ICP-MS measurement

Feeding and anesthesia: mosquitos were starved 12 hours in advance, then they were fed with two drops of food mixture and the drop volume was 30 µL. The feeding time is 30 mins. After these 30 mins feeding, those mosquitoes, which have intake the food mixture judged from the 'black' color of their abdomen, were anesthetized with a flow of CO<sub>2</sub> and then chilled at -20 °C

for one hour until the mosquitoes were killed completely. Or the mosquitoes were killed by FlyNap® Anesthetic Kit (Carolina TM, Germany). The feeding and anesthesia of the mosquitoes were under the help of Stephanie Jansen and Anna Heitmann.

Digestion for ICP-MS measurement: Then already killed mosquitoes were transferred to EP tubes and firstly immersed and incubated in enough volume of HNO<sub>3</sub> (aq, 67 wt%) overnight, and later twice the volume of HCl (aq, 35 wt%) was added to form Aqua Regia to further dissolve the Au NPs and protein and other parts inside the mosquito. After 48 h incubation, the digested liquid was diluted with some volume of 2% V/V HCl (prepared by mixing 2 mL 35 wt% HCl aq. With 98 mL Milli-Q water). Then this liquid containing some undissolved parts of the mosquitoes, for example, the wings, legs, etc.. was separated into two EP tubes and marked as parallel samples. Then these parallel samples were filtered by a 0.22 μm PVDF Membrane Filter separately and measured by ICP-MS. The neglectable difference in the Au and Eu concentration between these parallel samples detected by ICP-MS indicated the sufficient digestion of Au NPs and Eu-BSA and Eu-transferrin. Thus, this digestion method was applied to all the mosquitoes.

## **4.6 Results and discussion**

### **4.6.1 The optimized food mixture for mosquitoes**

According to many publications, blood intake is necessary for female mosquitoes to lay eggs [161-164]. Thus, blood mixed with self-synthesized Au NPs and BSA-Eu together to form a food mixture was used to feed mosquitoes. The best food mixture should achieve two goals: 1. There is enough amount of Au NPs and Eu-BSA in the food so that the element in the mosquitoes after feeding can show enough strong signal detected by ICP-MS. 2. The mosquitoes are not reluctant to this food mixture and are willing to intake such food mixture during the 30 mins feeding time. Thus, different compositions of food mixture were investigated and presented in Table 4-5. The total volume of the food mixture was 40 μL or 50 μL, which is just the food volume for one vial and if more than one vial of mosquitoes was fed, then every vial of mosquitoes was fed with the same volume of food mixture. After being fed 30 min with the food mixture presented in Table 4-5, those fully engorged mosquitoes, whose abdomen was filled with food mixture judged from the color of the abdomen as showed were collected and the number of mosquitoes collected for corresponding food mixture condition was also presented in Table 4-5 and these fully engorged mosquitoes were digested and measured by ICP-MS as shown in Table 4-6. From the Table 4-5, it can be calculated that for

every food mixture condition, more than 10 mosquitoes were collected per vial (20 mosquitoes were fed in each vial), which meant that all these 8 food mixtures presented in Table 4-5 were acceptable to these female mosquitoes. For some food mixture conditions, the number of mosquitoes collected per vial can be lower than in other conditions, but this did not mean that these food mixtures were ‘awful’ to mosquitoes considering the limited number of parallel vials tested and the difference between individual mosquitoes.

*Table 4-5 Compositions of the food mixture for mosquitoes<sup>a</sup>*

Food mixture condition	composition of food mixture, $\mu\text{L}$				Designed Concentration of elements in food mixture, mg/mL			Number of vials fed	Number of mosquitoes collected per vial
	V (NPs)	V(Eu-transferrin)	V(blood)	V(water)	C(Au, food)	C(Eu, food)	C(transferrin, food)		
C0	5	15	20	0	0.9	0.056	11.25	1	18
C1	5	15	30	0	0.72	0.045	9	1	17
C2	5	25	10	0	0.9	0.09	18.75	1	18
C3	6.25	18.75	25	0	0.9	0.056	11.25	4	17
C4	6.25	0	25	18.75	0.9	0	0	6	14
C5	0	0	25	25				4	13
C6	25	0	25	0	3.6			2	15
C7	0	0	20	20				1	19

<sup>a</sup> In Table 4-5,  $C_{(\text{Au, food})}$ ,  $C_{(\text{Eu, food})}$ , and  $C_{(\text{transferrin, food})}$  only refer to the Au in the Au NPs, Eu and transferrin in the Eu-transferrin ignoring the Au, Eu element, and the transferrin already existing in the blood. C0, C1, C2, etc. were used to mark the different food mixture conditions and are the abbreviation for condition 0, condition 1, condition 2, etc.

Table 4-6 Au and Eu elements detected in mosquitoes fed with the food mixture presented in Table 4-5<sup>a</sup>

Food mixture conditions	$C_{(Eu, food)}$ / $C_{(Au, food)}$	$m_{(Au, int)}$ , [ $\mu$ g]	$m_{(Eu, int)}$ , [ $\mu$ g]	$m_{(Eu, int)}$ / $m_{(Au, int)}$	$V_{(Au, int)}$ , [ $\mu$ L]	$V_{(Eu, int)}$ , [ $\mu$ L]
Condition 0	0.0625	$1.37 \pm 0.12$	$0.07 \pm 0.00$	$0.05 \pm 0.00$	$1.52 \pm 0.14$	$1.23 \pm 0.01$
Condition 1	0.0625	$0.78 \pm 0.29$	$0.05 \pm 0.01$	$0.07 \pm 0.04$	$1.08 \pm 0.40$	$1.07 \pm 0.13$
Condition 2	0.1042	$0.04 \pm 0.01$	$0.39 \pm 0.26$	$10.33 \pm 7.98$	$0.05 \pm 0.02$	$4.11 \pm 2.73$
Condition 3	0.0625	$1.46 \pm 0.31$	$0.08 \pm 0.03$	$0.06 \pm 0.02$	$1.62 \pm 0.34$	$1.48 \pm 0.49$
Condition 4	0	$1.49 \pm 0.47$	$4.58 * 10^{(-7)} \pm 1.55 * 10^{(-7)}$	$3.19 * 10^{(-7)} \pm 8.00 * 10^{(-8)}$	$1.66 \pm 0.52$	---
Condition 5	---	$0.00 \pm 0.00$	$1.07 * 10^{(-6)} \pm 5.96 * 10^{(-7)}$	---	---	---
Condition 6	0	$6.63 \pm 2.41$	$6.62 * 10^{(-7)} \pm 2.52 * 10^{(-7)}$	$1.44 * 10^{(-7)} \pm 1.55 * 10^{(-7)}$	$1.84 \pm 0.67$	---

<sup>a</sup> In Table 4-6,  $m_{(Au, int)}$  and  $m_{(Eu, int)}$  refer to the detected Au and Eu mass per mosquito assuming that all Au NPs and Eu-transferrin which were drunk by mosquito were detected.  $V_{(Au, int)}$  and  $V_{(Eu, int)}$  were calculated as  $V_{(Au, int)} = m_{(Au, int)}/C_{(Au, food)}$ ,  $V_{(Eu, int)} = m_{(Eu, int)}/C_{(Eu, food)}$ . This calculation was based on the assumption that the mosquito did not choose which food component it likes and just suck the whole food as its initial composition was.

As presented in Table 4-6,  $m_{(Au)}$  and  $m_{(Eu)}$  detected in mosquitoes fed with food mixture condition 5 were close to zero indicating that mosquitoes' intake of pre-existing Au and Eu elements in blood and Milli-Q water can be ignored. Based on this information and also considering that the only difference between food mixture condition 7 and condition 5 is the total volume, we infer that the Au and Eu in the mosquitoes fed with food mixture condition 7 were also close to zero, thus these mosquitoes fed with food condition 7 were not measured. For mosquitoes fed with every food mixture condition presented in Table 4-6 except condition 2 and condition 5, there were two common trends. 1. the  $m_{(Eu, int)}/m_{(Au, int)}$  was close to  $C_{(Eu, food)}/C_{(Au, food)}$  indicating that the mosquitoes just drunk this food mixture as its original composition and mosquitoes did not trash the Au NPs or chose which compound is more delicious to them. 2. The  $V_{(Au, int)}$  and  $V_{(Eu, int)}$  were always 1-2  $\mu$ L. Thus, any food mixture in Conditions 0, 1, 3, 4, and 6 worked well for mosquitoes.

For Condition 5,  $m_{(Eu, int)}/m_{(Au, int)}$  cannot be calculated because neither Au NPs nor Eu-transferrin was added to this food mixture, and the  $C_{(Au, food)}$  and  $m_{(Au, int)}$  were close to zero. But what caused the abnormal intake in condition 2 is the lowest volume ratio of blood in the food mixture compared to other food conditions. The food mixture changed from condition 0



to condition 1 to increase the total volume of the food mixture so that the drop can be large enough for all 20 mosquitoes living in one vial to eat and also the drop will not evaporate or attach to the vial surface completely during this 30 min feeding time. At the same time, with the food mixture composition changed from condition 1 to condition 3, condition 0, the  $C_{(\text{Au, food})}$  and  $C_{(\text{Eu, food})}$  were increased and the volume of blood was decreased, resulting in the increased  $m_{(\text{Eu, int})}$ ,  $m_{(\text{Au, int})}$  and every slight increase in  $V_{(\text{Au, int})}$  and  $V_{(\text{Eu, int})}$ , meaning the decreased extent of blood in the food mixture is still acceptable to mosquitoes. The food mixture changed from condition 3 to condition 4 and condition 6 was to replace Eu-transferrin with Milli-Q water or Au NPs resulting in a similar  $V_{(\text{Au, int})}$  indicating that the change of Eu-transferrin to Milli-Q water or Au NPs did not change the intake behavior of the mosquitoes.

#### **4.6.2 The intake and metabolism of Au NP, BSA-Eu, and Iodine ion in mosquitoes**

As has been discussed above, the food composition will affect the intake behavior of mosquitoes. Here the food mixture was 60  $\mu\text{L}$  per vial with a composition of 29  $\mu\text{L}$  blood + 1  $\mu\text{L}$  KI (Iodine concentration 254 mg/mL) + 10  $\mu\text{L}$  Au NPs (Au concentration 7 mg/mL) + 20  $\mu\text{L}$  BSA-Eu (BSA concentration 30 mg/mL). Feeding was conducted on more than 14 vials of mosquitoes with 20 mosquitoes per vial. After feeding, anesthetizing treatment with the flow of CO<sub>2</sub> was conducted and only those mosquitoes which have intake the food mixture judged from the color of the abdomen were collected and then transferred to clean vials. Afterward, 2 vials of mosquitoes were marked with timepoint 0 and were stored for 1 hour at -20 °C and afterward digested for ICP-MS measurement. While the other vials of mosquitoes were reared with a fructose pad as food and incubated for 1 d, 2 d, 3 d, 4 d, 5 d, and 6 d respectively, and all the vials of mosquitoes were marked with their corresponding incubation days. More fructose was added to keep the fructose pad humid during the incubation time. During these days, all the mosquitoes were fed on fructose, and on each day, 2 vials of mosquitoes marked with this timepoint were anesthetized with the flow of CO<sub>2</sub> and stored for 1 hour at -20 °C and then digested for ICP-MS measurement. The 2 vials of mosquitoes marked with timepoint 6 d were starved 12 h before 6th day and then at 6th d were fed 30 min with 60  $\mu\text{L}$  food mixture composed of 30  $\mu\text{L}$  blood + 1  $\mu\text{L}$  NaBr (Br concentration 160 mg/mL) + 29  $\mu\text{L}$  Milli-Q water, then these mosquitoes were remarked as refeeding mosquitoes. These refeeding mosquitoes were also anesthetized with a flow of CO<sub>2</sub> and stored for 1 hour at -20 °C and then digested for ICP-MS measurement. Mosquitoes at all timepoints were digested for ICP-MS measurement following the same protocol. During the sample digestion, every mosquito was

firstly incubated overnight in 100  $\mu\text{L}$   $\text{HNO}_3$  (aq, 67 wt%) and afterward 200  $\mu\text{L}$   $\text{HCl}$  (aq, 35 wt%) was added to form Aqua Regia to further digest the Au NPs and BSA-Eu in the mosquitoes. Then this digested liquid was diluted with a certain volume of 2% V/V  $\text{HCl}$  (prepared by mixing 2 mL 35 wt.%  $\text{HCl}$  aq. With 98 mL Milli-Q water) and afterward filtered with 0.22  $\mu\text{m}$  PES filter membrane and measured with ICP-MS.

It must be paid enough attention to that there are many polyatomic interferences for the measurement of Br by ICP-MS. For example, the existence of  $40\text{Ar}39\text{K}^+$ ,  $31\text{P}16\text{O}3^+$ ,  $38\text{Ar}40\text{Ar}1\text{H}^+$  will be recognized as  $79\text{Br}$  by the ICP-MS and  $32\text{S}16\text{O}31\text{H}^+$ ,  $40\text{Ar}40\text{Ar}1\text{H}^+$ ,  $33\text{S}16\text{O}3^+$  will be recognized as  $81\text{Br}$  [165, 166]. Considering the detection limit of ICP-MS for Au, Eu, and I, the mass of Au, Eu, and I per mosquito below 0.01, 0.001, and 0.01  $\mu\text{g}$  can be regarded as zero respectively.

Table 4-7 Information about mosquitoes detected at timepoint 0 d in three individual experiments<sup>a</sup>

Exp erim ent NO.	Concentration element in food mixture, [mg/mL]			Mass of element detected in per mosquitoes, [ $\mu\text{g}$ ]			The volume of food sucked by per mosquito, [ $\mu\text{L}$ ]		
	$C_{(\text{Au}, \text{food})}$	$C_{(\text{Eu}, \text{food})}$	$C_{(\text{Iodine}, \text{food})}$	$m_{(\text{Au}, \text{int})}$	$m_{(\text{Eu}, \text{int})}$	$m_{(\text{I}, \text{int})}$	$V_{(\text{Au}, \text{int})}$	$V_{(\text{Eu}, \text{int})}$	$V_{(\text{I}, \text{int})}$
Jun. exp1	1.167	0.067	4.233	$1.11 \pm 0.54$	$0.17 \pm 0.08$	$2.28 \pm 1.34$	$0.95 \pm 0.46$	$2.47 \pm 1.43$	$0.54 \pm 0.32$
Jun. exp2	1.167	0.032	4.233	$1.70 \pm 0.80$	$0.07 \pm 0.03$	$2.60 \pm 1.10$	$1.46 \pm 0.68$	$2.18 \pm 1.04$	$0.61 \pm 0.26$
Aug exp1	1.167	0.133	4.233	$2.83 \pm 0.91$	$0.30 \pm 0.08$	$2.36 \pm 1.27$	$2.43 \pm 0.78$	$2.22 \pm 0.57$	$0.56 \pm 0.30$

<sup>a</sup>In Table 4-7,  $m_{(\text{Au}, \text{int})}$  and  $m_{(\text{Eu}, \text{int})}$  refer to the detected Au and Eu mass per mosquito assuming that all Au NPs and Eu-transferrin which were drunken by mosquito were detected.  $V_{(\text{Au}, \text{int})}$  and  $V_{(\text{Eu}, \text{int})}$  were calculated as :  $V_{(\text{Au}, \text{int})} = m_{(\text{Au}, \text{int})}/C_{(\text{Au}, \text{food})}$ ,  $V_{(\text{Eu}, \text{int})} = m_{(\text{Eu}, \text{int})}/C_{(\text{Eu}, \text{food})}$ . This calculation is based on the assumption that the mosquito did not choose which food component it likes and just suck the whole food as its initial composition was.

From Table 4-7, we can see that  $V_{(\text{I}, \text{int})}$  and  $V_{(\text{Au}, \text{int})}$ ,  $V_{(\text{Eu}, \text{int})}$  were not completely the same, which is different from the presented data of  $V_{(\text{Au}, \text{int})}$ ,  $V_{(\text{Eu}, \text{int})}$  for condition 0, 1 and 3 in Table 4-6. According to the t-test conducted by excel, there is always a significant difference between  $V_{(\text{I}, \text{int})}$  and  $V_{(\text{Au}, \text{int})}$ ,  $V_{(\text{Eu}, \text{int})}$  in all these three individual experiments presented in Table 4-7, and the  $V_{(\text{I}, \text{int})}$  is always much lower than  $V_{(\text{Au}, \text{int})}$ ,  $V_{(\text{Eu}, \text{int})}$ . During the 30 min feeding time and also

transportation time, we can observe the mosquito excretion, and also even after some time at -20 °C, mosquitoes can still be alive during the transportation at RT and we can also see excretion during this transportation time, which is before ICP-MS sample digestion. Thus we can infer that the detected low  $V_{(I,int)}$  and  $m_{(I,int)}$  per mosquito was because of the fast excretion of Iodine happening during this 30 mins feeding time and also sample transportation time, which can also induce the faster excretion of Iodine compared to Au NP and BSA-Eu. When comparing  $V_{(Au,int)}$  to  $V_{(Eu,int)}$ , according to the t-test conducted by excel, there is no significant difference between  $V_{(Au,int)}$  and  $V_{(Eu,int)}$  in Jun. exp2 and Aug exp1, which matches our assumption that the intake volume of Au NP and BSA-Eu are the same and the mosquito just sucked the food component as its initial composition and also the excretion of the Au NP and BSA-Eu by mosquito did not happen in timepoint 0 d sample. But the  $V_{(Eu,int)}$  is significantly higher than  $V_{(Au,int)}$  in Jun. exp1, which is opposed to our assumption.

In Table 4-7, all the feeding parameters in Jun. exp1, Jun. exp2, and Aug. exp1 were almost the same just except for two differences. 1st parameter is the Eu concentration in the food mixture which varies in these three individual experiments. This is because three batches of BSA-Eu were used respectively in these three individual experiments and the labeling efficiency of Eu to BSA is different in these three batches. The concentration of BSA-Eu in the food mixture is always 6.13 mg/mL, while Eu concentration is 0.067, 0.032, and 1.133 mg/mL respectively in Jun exp1, Jun. exp2, and Aug. exp1. 2nd parameter is that the refeeding at 6th d in Aug. exp1 is conducted in a completely new vial without excretions inside, while in Jun. exp1 and Jun. exp2 the refeeding at 6th d was just conducted in the old vial where the mosquitoes were incubated during the former 5 days.

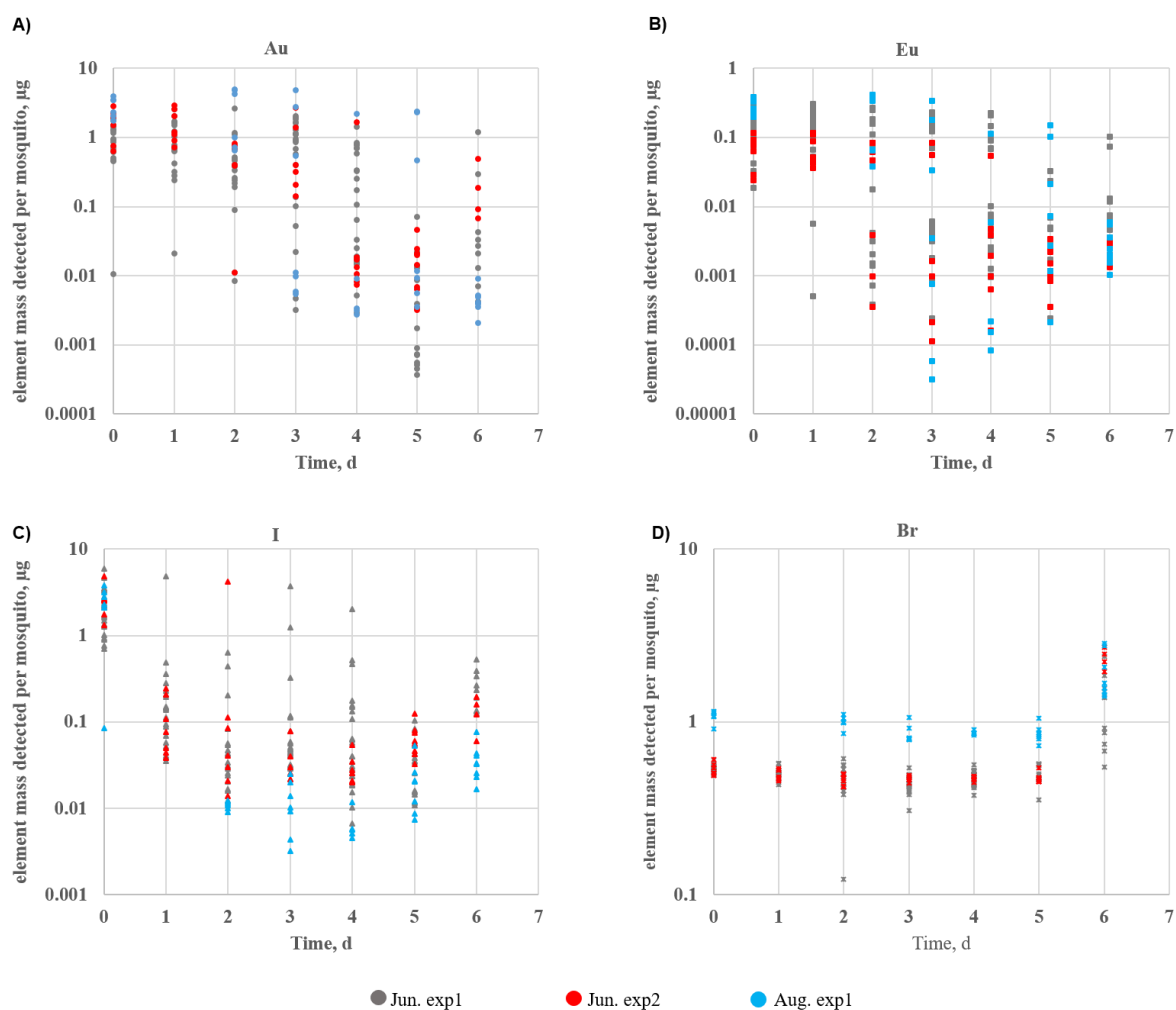


Figure 4-3 mass of Au, Eu, I, and Br detected per mosquito by ICP-MS after each timepoint. A), B), C), and D) refer to Au, Eu, I, and Br respectively. And each color refers to one individual experiment with the gray meaning Jun. exp1, the red meaning Jun. exp2 and the blue meaning Aug. exp1. In Aug. exp1 there was only one mosquito collected at timepoint 1d and the treatment of this mosquito was not successful and thus not presented.

Table 4-8 mass of Au, Eu, I, and Br detected per control mosquito by ICP-MS after each timepoint.

Time, [d]	Mass of element detected in per mosquitoes, [ $\mu\text{g}$ ]			
	$m_{(\text{Au,int})}$	$m_{(\text{Eu,int})}$	$m_{(\text{I,int})}$	$m_{(\text{Br,int})}$
0	$0.0174 \pm 0.0139$	$4.2 * 10^{(-6)} \pm 1.2 * 10^{(-6)}$	$0.0181 \pm 0.0261$	$1.0826 \pm 0.1331$
3	$0.0082 \pm 0.0051$	$6.1 * 10^{(-6)} \pm 2.8 * 10^{(-6)}$	$0.0137 \pm 0.0123$	$0.9179 \pm 0.0872$
6	$0.0046 \pm 0.0025$	$3.6 * 10^{(-6)} \pm 1.3 * 10^{(-6)}$	$0.0030 \pm 0.0007$	$1.0956 \pm 0.0651$

According to Figure 4-3, for the Au NPs, at timepoint 0 d, the mass of Au per mosquito detected by ICP-MS was higher than  $1 \mu\text{g}$  for about 70% of the mosquitoes ignoring two special mosquitoes whose Au mass was lower than  $0.1 \mu\text{g}$ . Then at timepoint 1 d, in about half of the mosquitoes, the mass of Au was higher than  $1 \mu\text{g}$  and in another half of the mosquitoes, the

mass of Au was lower than 1  $\mu\text{g}$ . With time going, higher percentage of mosquitoes showed internalized Au mass lowered than 1  $\mu\text{g}$ . At timepoint 5 d, more than 70% of the mosquitoes showed Au mass lower than 0.1  $\mu\text{g}$ , and even in a certain percentage of the mosquitoes, the Au mass was lower than 0.01  $\mu\text{g}$  which is zero considering the detection limit of Au in ICP-MS. Then at timepoint 6 d, when mosquitoes were collected after the refeeding, a difference was shown in these three individual experiments. In Aug. exp1 all the mosquitoes showed no Au inside, while in Jun. exp1 and Jun. exp2 still a quantity of Au was detected. Besides, Jun. exp1 and Jun. exp2 the Au in mosquitoes at timepoint 6 d were detected to be higher than the Au mass at timepoint 5 d. These two findings can be proof that the mosquitoes sucked also their excretion attached to the vial which contains Au when they suck the refeeding food mixture which contains no Au. Depending on these findings, we can infer that Au NP has been completely excreted after 6 d in all the mosquitoes if no refeeding was done.

The Eu mass detected per mosquito also decreased with the prolonging time just the same as Au. The difference between Au and Eu is that at timepoint 6 d, still a quantity of Eu remains inside mosquitoes judged from the mosquitoes in Aug. exp1, while Au has already been completely excreted.

The Iodine excretion speed is much higher than Au and Eu. At timepoint 0, almost all the mosquitoes showed Iodine mass higher than 0.7  $\mu\text{g}$ , while almost all the mosquitoes showed Iodine mass lower than 1  $\mu\text{g}$  at timepoint 1 d. And at timepoint 5 d, in Aug. exp1 almost all the mosquitoes showed Iodine mass lower than 0.1  $\mu\text{g}$ , which was close to the Iodine level in Control mosquitoes, while in Jun. exp1 and Jun. exp2 still a quantity of Iodine higher than 0.1  $\mu\text{g}$  was detected. Besides, Jun. exp1 and Jun. exp2 the Iodine in mosquitoes at timepoint 6 d was detected to be higher than the Iodine mass at timepoint 5 d. These two findings can be proof that the mosquitoes sucked also their excretion attached to the vial when they suck the refeeding food mixture which contains no Iodine and that Iodine has been completely excreted after 5 d in all the mosquitoes if no refeeding was done.

## 5. Summary and Outlook

### 5.1 The uptake of different size Au NP/NRs in Hela cells in different incubation systems

When analyzing the effect of NP/NR size and shape on the internalization of Au element mass per cell, it can be concluded that the uptake amount of ‘bigger Au NP/NR’ (50 nm, 100 nm Au NPs, and 100 nm Au NR) is much higher than ‘smaller Au NP/NR’ (5 nm, 25 nm Au NPs, and 40 nm Au NRs) in Static, Dynamic and Fluid system, but the internalization Au in terms of Au NPs number per cell is in a contrary trend. This can be attributed to the competition between these three factors: 1. higher Au concentration at the bottom of the flask in 50 nm, 100 nm Au NP and 100 nm Au NR in Static incubation because of sedimentation induced by gravity. 2. The initial concentration of 5 nm, 25 nm Au NPs in terms of Au element is much lower than the 50 nm, 100 nm Au NP and 100 nm Au NR according to ICP-MS rather than calculation according to UV-vis. 3. The wrapping time needed for the endocytosis of smaller Au NPs is shorter than the bigger Au NPs. 4. The periodic shaking in the Dynamic system and continuous uni-directional flow in the Fluid system took away the Au NPs before they have been truly “eaten” by the cells. 5. The molar mass of ‘bigger Au NP/NR’ (50 nm, 100 nm Au NP, 100 nm Au NR) is hundreds of times the molar mass of ‘smaller Au NP/NR’ (5 nm, 25 nm Au NP, 40 nm Au NR), meaning the uptake of single ‘bigger Au NP/NR’ can bring in large amount of Au mass inside cells.

The difference between the internalized Au mass per cell of ‘bigger Au NP/NR’ (50 nm, 100 nm Au NP, 100 nm Au NR) and the internalized Au mass per cell of ‘smaller Au NP/NR’ (5 nm, 25 nm Au NP, 40 nm Au NR) has become smaller when the incubation system changed from Static, Dynamic to Fluid, Suspension. This can be attributed to the bigger adverse effect of periodic shaking and continuous uni-directional flow on the uptake of larger Au NPs/NRs (50 nm, 100 nm Au NP, 100 nm Au NR) compared to the smaller Au NPs/NRs (5 nm, 25 nm Au NP, 40 nm Au NR). Since the bigger Au NPs need a longer time to be eaten by the cells, their uptake is more likely to be adversely affected by the Au NP movement.

Besides, it is much harder for Au NPs/NRs to adhere to cells in the unidirectional flow in the Fluid system compared to the Dynamic system, which can be revealed by the largely decreased uptake of 50 nm and 100 nm Au NPs in the Fluid system compared to Dynamic system.

It is a special phenomenon that in a Suspension system, the internalized Au mass per cell of bigger Au NP/NRs (50 nm, 100 nm Au NP, 100 nm Au NR) is no longer higher than the internalized Au mass per cell of small Au NP/NRs (5 nm, 25 nm Au NP, 40 nm Au NR) and in some cases, the uptake of the 5 nm Au NP can be even higher than the uptake of 100 nm Au NR in terms of Au element mass, which is completely different from the common trend presented in Static, Dynamic and Fluid system. The comparison between the suspension system and to dynamic system confirmed the important role of the Hela cell status in the uptake behavior. In the suspension system, the Hela cells gradually formed a tumor sphere with a lower contact possibility between Hela cells and Au NPs, which is a larger challenge for bigger Au NP/NRs (50 nm, 100 nm Au NP, 100 nm Au NR) compared to small Au NP/NRs (5 nm, 25 nm Au NP, 40 nm Au NR) considering the higher Brownian motion speed of small Au NP/NRs and some small holes existing in the Hela tumor spheres.

Besides, in all 4 systems, the uptake amount of the 6 sizes of Au NP all followed the same concentration-dependent and time-dependent trend, which is in accordance with many previous reports.

## **5.2 The uptake of different size Au NPs in RBCs**

For the 4 nm Au NPs, the internalized Au mass per cell kept the same when the RBCs cell density changed from  $10^7$  cell/mL to  $2 \times 10^7$  cell/mL, which is because the total Au NPs amount is more than 10 times the amount of internalized Au NP and because the volume occupied per cell far exceeded the actual volume of a RBC itself and the large amount of Au NPs in the volume occupied per cell can diffuse through Brownian motion to the cell nearby area after the depletion of cell nearby Au NPs, thus the Au NPs near cells are always more than excess even though the cell density was increased.

4, 25, and 50 nm Au NPs all experienced the same concentration-dependent uptake behavior, which is also in accordance with the findings in uptake in Hela cells. And when it comes to the effect of size on the uptake of Au NP, it can be found that the uptake of Au NP in terms of Au element mass per cell for the 4 nm Au NP is much larger than the 25 and 50 nm Au NP, which means this size-dependent uptake difference can be even enlarged if the uptake amount is in terms of Au NP number per cell. This is completely opposite to the general trend previously reported that the uptake of 'bigger Au NP/NR' in adherent cells are often higher than 'smaller Au NP/NR' in term of Au mass per cell. This is because the RBCs is suspension cell and the 50 nm Au NP can sediment to the bottom of the plate because of gravity, thus the actual Au

mass concentration at the bottom exceeded the saturation of the cell, while the actual Au mass concentration at the distance far from the bottom was much lower than the initial concentration, which results in the low uptake. Besides, the 5 nm has a higher Brownian motion speed compared to 25 and 50 nm, and thus has a higher opportunity to touch the RBCs, which results in the highest uptake.

### **5.3 Ingestion and metabolism of Au NPs in mosquito**

The optimized food mixture for mosquitoes to ensure reproducible and stable ingestion behavior and also enough strong signal of Au and Eu has been achieved. Then after feeding, the I ions showed the fastest excretion speed compared to 4nm Au NPs and BSA-Eu, and according to our observation, the excretion of I ions even starts immediately after the feeding. For the Au NP, at timepoint 0 d, almost 70% of the mosquitoes showed internalized Au higher than 1  $\mu\text{g}$  ignoring two special mosquitoes whose Au mass was lower than 0.1  $\mu\text{g}$ . Then at timepoint 1 d, in about half of the mosquitoes, the mass of Au was higher than 1  $\mu\text{g}$  and in another half of the mosquitoes, the mass of Au was lower than 1  $\mu\text{g}$ . This percentage of mosquitoes whose internalized Au is lower than 1  $\mu\text{g}$  increased with the time going and at timepoint 5 d, more than 70% of the mosquitoes showed Au mass lower than 0.1  $\mu\text{g}$  and even in a certain percentage of the mosquitoes, the Au mass was lower than 0.01  $\mu\text{g}$  which can be regarded as zero considering the detection limit of Au in ICP-MS. Then at timepoint 6 d, all Au NP has been completely excreted after 6 d in all the mosquitoes if no refeeding was done. If the refeeding food mixed with the excretion in the vial, the excretions can be again ingested by the mosquitoes revealed by the higher Au detected in mosquitoes in “Jun. exp1 and Jun. exp2” compared to the Au amount detected at timepoint 5 and also the no Au detected for the mosquitoes after refeeding in “Aug. exp1” where the old excretion has been cleaned.

The Eu mass detected per mosquito also decreased with the prolonging time just the same as Au. The difference between Au and Eu is that at timepoint 6 d, still a quantity of Eu remains inside mosquitoes judged from the mosquitoes in the experiment “Aug. exp1”, while Au has already been completely excreted.

The Iodine excretion speed is much higher than Au and Eu. At timepoint 0, almost all the mosquitoes showed an Iodine mass higher than 0.7  $\mu\text{g}$ , while almost all the mosquitoes showed an Iodine mass lower than 1  $\mu\text{g}$  at timepoint 1 d. And timepoint 5 d, almost all the mosquitoes showed Iodine mass lower than 0.1  $\mu\text{g}$ , which was close to the Iodine level in Control mosquitoes, meaning the Iodine has been completely excreted after 5 d in all the mosquitoes if



no refeeding was done. The detection of Iodine also revealed that the mosquitoes can ingest the excretion if the excretion was mixed with the refeeding food mixture.

## **5.4 The novelties of our study**

1) The design of the Dynamic system where the sedimentation of ‘bigger Au NP/NRs’ (50, 100 nm Au NPs and 100 nm Au NRs) have been destroyed helps to explain the size-dependent uptake with the initial Au concentration difference and the endocytosis route, endocytosis wrapping time and energy difference between different sizes Au NPs.

2) The design of the Fluid system simulated the actual bloodstream and provided a reference for the in vivo uptake behavior of different size Au NPs when the Au NPs were dispersed in the bloodstream. Besides, the continuous flow in the Fluid system also destroyed the sedimentation of larger Au NP/NRs (50, 100 nm Au NPs and 100 nm Au NRs) and revealed the fact that the continuous flow decreased the contact possibility between ‘bigger Au NP/NRs’ (50, 100 nm Au NPs) and Hela cells to a larger extent compared to ‘smaller Au NP/NRs’.

3) Our study confirmed the optimized size of 4-5 nm Au NPs for the uptake in suspended cell lines based on the higher uptake of 4 nm Au in terms of Au mass per cell in RBCs compared to 25 and 50 nm Au NPs and the different sizes Au NP/NRs uptake in suspended Hela cells.

4) An optimized food composition of Au NPs, Eu-BSA, Iodine and blood was achieved for the mosquito with full engorgement and the ingestion composition was just the same as the initial food mixture composition. Our study confirmed the fastest excretion of Iodine ions compared to Au NPs and BSA-Eu in mosquitoes and also the full excretion of Au NPs and Iodine ions after 6d while remaining of BSA-Eu in mosquitoes was still detected.

## **5.5 Future perspectives**

1) The designed initial Au concentration of all sizes of Au NPs should rely on the ICP-MS measurement rather than calculated from the UVvis considering the error in the calculated molar mass of Au NP owing to the approximate solid sphere model.

2) The flow speed and the shear stress can be adjusted to simulate the bloodstream in different regions such as the vessels surrounding the tumor.

3) When the uptake behavior of Au NPs in RBCs was investigated, the hemolysis should be also analyzed, which is an important physiological index for the RBCs condition.

4) X-ray Fluorescence Imaging with higher resolution should be used to detect the translocation of different size Au NPs in the organs of mosquitoes.

## 6. References

1. Fan, L.Y., et al., *Gold nanoparticles enhance antibody effect through direct cancer cell cytotoxicity by differential regulation of phagocytosis*. Nature Communications, 2021. **12**(1).
2. Radaic, A., et al., *Phosphatidylserine-Gold Nanoparticles (PS-AuNP) Induce Prostate and Breast Cancer Cell Apoptosis*. Pharmaceutics, 2021. **13**(7).
3. Kang, N., et al., *Magnetic targeting core/shell Fe<sub>3</sub>O<sub>4</sub>/Au nanoparticles for magnetic resonance/photoacoustic dual-modal imaging*. Materials Science and Engineering C-Materials for Biological Applications, 2019. **98**: p. 545-549.
4. Wang, Y.C., et al., *Radioluminescent Gold Nanocages with Controlled Radioactivity for Real-Time in Vivo Imaging*. Nano Letters, 2013. **13**(2): p. 581-585.
5. Wang, Y.H., et al., *Simulations and Experimental Study of Individual Au Nanoparticle Using Photothermal Heterodyne Imaging (PHI)*. Ieee Transactions on Instrumentation and Measurement, 2022. **71**.
6. Alexeree, S., et al., *A novel synthesis of a chlorophyll b-gold nanoconjugate used for enhancing photodynamic therapy: In vitro study*. Photodiagnosis and Photodynamic Therapy, 2021. **35**.
7. Pantiusenko, I.V., et al., *Development of Bacteriochlorophyll a-Based Near-Infrared Photosensitizers Conjugated to Gold Nanoparticles for Photodynamic Therapy of Cancer*. Biochemistry-Moscow, 2015. **80**(6): p. 752-762.
8. Yang, Y.M., et al., *Intracellular gold nanoparticle aggregation and their potential applications in photodynamic therapy*. Chemical Communications, 2014. **50**(55): p. 7287-7290.
9. Mallick, S., et al., *Silica Coated Gold Nanorods for Imaging and Photo-Thermal Therapy of Cancer Cells*. Journal of Nanoscience and Nanotechnology, 2013. **13**(5): p. 3223-3229.
10. Christie, C., et al., *Photothermal Therapy Employing Gold Nanoparticle-Loaded Macrophages as Delivery Vehicles: Comparing the Efficiency of Nanoshells Versus Nanorods*. Journal of Environmental Pathology Toxicology and Oncology, 2017. **36**(3): p. 229-235.
11. Kostevsek, N., et al., *Hybrid FePt/SiO<sub>2</sub>/Au nanoparticles as a theranostic tool: in vitro photo-thermal treatment and MRI imaging*. Nanoscale, 2018. **10**(3): p. 1308-1321.
12. Zeng, J.F., et al., *Preparation and Photo-thermal Properties of Thermo-sensitive Injectable Hydrogels Based on Chitosan and Au Nanoparticles*. Acta Polymerica Sinica, 2018(10): p. 1297-1306.
13. Guan, Z.P., et al., *Simultaneous Imaging and Selective Photothermal Therapy through Aptamer-Driven Au Nanosphere Clustering*. Journal of Physical Chemistry Letters, 2019. **10**(2): p. 183-188.
14. Safari, D., et al., *Gold nanoparticles as carriers for a synthetic Streptococcus pneumoniae type 14 conjugate vaccine*. Nanomedicine, 2012. **7**(5): p. 651-662.
15. Dings, R.P.M., M. Cannon, and K.B. Vang, *Design of Gold Nanoparticles in Dendritic Cell-Based Vaccines*. Particle & Particle Systems Characterization, 2018. **35**(9).
16. Escudero-Francos, M.A., et al., *Cellular Uptake and Tissue Biodistribution of Functionalized Gold Nanoparticles and Nanoclusters*. Journal of Biomedical Nanotechnology, 2017. **13**(2): p. 167-179.
17. Singh, L., et al., *Intracellular localization of gold nanoparticles with targeted delivery in MT-4 lymphocytes*. Advances in Natural Sciences-Nanoscience and Nanotechnology, 2016. **7**(4).

18. Huang, X.H., et al., *Plasmonic photothermal therapy (PPTT) using gold nanoparticles*. *Lasers in Medical Science*, 2008. **23**(3): p. 217-228.
19. Vines, J.B., et al., *Gold Nanoparticles for Photothermal Cancer Therapy*. *Frontiers in Chemistry*, 2019. **7**.
20. Ramezanzadeh, E., et al., *Evaluation of EGFR-targeted gold/gold sulfide (GGS) nanoparticles as a theranostic agent in photothermal therapy*. *Materials Research Express*, 2018. **5**(12).
21. Li, Z., et al., *Transporting carriers for intracellular targeting delivery via non-endocytic uptake pathways*. *Drug delivery*, 2017. **24**(sup1): p. 45-55.
22. Behzadi, S., et al., *Cellular uptake of nanoparticles: journey inside the cell*. *Chemical Society Reviews*, 2017. **46**(14): p. 4218-4244.
23. Verma, A. and F. Stellacci, *Effect of surface properties on nanoparticle–cell interactions*. *small*, 2010. **6**(1): p. 12-21.
24. Wang, T., et al., *Cellular uptake of nanoparticles by membrane penetration: a study combining confocal microscopy with FTIR spectroelectrochemistry*. *ACS nano*, 2012. **6**(2): p. 1251-1259.
25. Kaksonen, M. and A.J.N.r.M.c.b. Roux, *Mechanisms of clathrin-mediated endocytosis*. 2018. **19**(5): p. 313-326.
26. Rothberg, K.G., et al., *Caveolin, a protein component of caveolae membrane coats*. 1992. **68**(4): p. 673-682.
27. Xiang, S., et al., *Uptake mechanisms of non-viral gene delivery*. 2012. **158**(3): p. 371-378.
28. Jaumouillé, V. and S. Grinstein, *Receptor mobility, the cytoskeleton, and particle binding during phagocytosis*. *Current opinion in cell biology*, 2011. **23**(1): p. 22-29.
29. Flannagan, R.S., V. Jaumouillé, and S. Grinstein, *The cell biology of phagocytosis*. *Annual Review of Pathology: Mechanisms of Disease*, 2012. **7**: p. 61-98.
30. Canton, J., D. Neculai, and S. Grinstein, *Scavenger receptors in homeostasis and immunity*. *Nature Reviews Immunology*, 2013. **13**(9): p. 621-634.
31. He, B., et al., *Increased cellular uptake of peptide-modified PEGylated gold nanoparticles*. *Biochemical and Biophysical Research Communications*, 2017. **494**(1-2): p. 339-345.
32. Rothen-Rutishauser, B., et al., *Quantification of gold nanoparticle cell uptake under controlled biological conditions and adequate resolution*. *Nanomedicine*, 2014. **9**(5): p. 607-621.
33. Hao, X., et al., *Caveolae-mediated endocytosis of biocompatible gold nanoparticles in living HeLa cells*. *Journal of Physics-Condensed Matter*, 2012. **24**(16).
34. Yang, L.X., L. Shang, and G.U. Nienhaus, *Mechanistic aspects of fluorescent gold nanocluster internalization by live HeLa cells*. *Nanoscale*, 2013. **5**(4): p. 1537-1543.
35. Jiang, L.Q., et al., *Co-disposition of chitosan nanoparticles by multi types of hepatic cells and their subsequent biological elimination: the mechanism and kinetic studies at the cellular and animal levels*. *International Journal of Nanomedicine*, 2019. **14**: p. 6035-6060.
36. Chatterjee, M., et al., *Development of 6-Thioguanine conjugated PLGA nanoparticles through thioester bond formation: Benefits of electrospray mediated drug encapsulation and sustained release in cancer therapeutic applications*. *Materials Science and Engineering C-Materials for Biological Applications*, 2020. **114**.
37. Chithrani, B.D. and W.C.J.N.I. Chan, *Elucidating the mechanism of cellular uptake and removal of protein-coated gold nanoparticles of different sizes and shapes*. 2007. **7**(6): p. 1542-1550.

38. Chithrani, B.D., A.A. Ghazani, and W.C.J.N.I. Chan, *Determining the size and shape dependence of gold nanoparticle uptake into mammalian cells*. 2006. **6**(4): p. 662-668.
39. Kim, J., J.C. Sunshine, and J.J.J.B.c. Green, *Differential polymer structure tunes mechanism of cellular uptake and transfection routes of poly ( $\beta$ -amino ester) polyplexes in human breast cancer cells*. 2014. **25**(1): p. 43-51.
40. Tu, Z., et al., *Combination of surface charge and size controls the cellular uptake of functionalized graphene sheets*. 2017. **27**(33): p. 1701837.
41. Chu, Z., et al., *Cellular uptake, evolution, and excretion of silica nanoparticles in human cells*. 2011. **3**(8): p. 3291-3299.
42. Caraglia, M., et al., *Tumour-Specific Uptake of Anti-Cancer Drugs: The Future is Here*. *Current Drug Metabolism*, 2012. **13**(1): p. 4-21.
43. Karim, M.E., R. Rosli, and E.H. Chowdhury, *Systemic Delivery of Nanoformulations of Anti-cancer Drugs with Therapeutic Potency in Animal Models of Cancer*. *Current Cancer Therapy Reviews*, 2016. **12**(3): p. 204-220.
44. Rizwanullah, M., et al., *Phytochemical based nanomedicines against cancer: current status and future prospects*. *Journal of Drug Targeting*, 2018. **26**(9): p. 731-752.
45. Dhar, S., et al., *Biocompatible gellan gum-reduced gold nanoparticles: cellular uptake and subacute oral toxicity studies*. *Journal of Applied Toxicology*, 2011. **31**(5): p. 411-420.
46. Uribe-Querol, E. and C. Rosales, *Phagocytosis: Our Current Understanding of a Universal Biological Process*. *Frontiers in Immunology*, 2020. **11**.
47. Swanson, J.A., *Shaping cups into phagosomes and macropinosomes*. *Nature reviews Molecular cell biology*, 2008. **9**(8): p. 639-649.
48. Rosales, C. and E. Uribe-Querol, *Phagocytosis: a fundamental process in immunity*. *BioMed research international*, 2017. **2017**.
49. Rattanapinyopituk, K., et al., *Demonstration of the Clathrin- and Caveolin-Mediated Endocytosis at the Maternal-Fetal Barrier in Mouse Placenta after Intravenous Administration of Gold Nanoparticles*. *Journal of Veterinary Medical Science*, 2014. **76**(3): p. 377-387.
50. MacParland, S.A., et al., *Phenotype Determines Nanoparticle Uptake by Human Macrophages from Liver and Blood*. *Acs Nano*, 2017. **11**(3): p. 2428-2443.
51. Chakraborty, R., D. Leshem-Lev, and D. Fixler. *Differential uptake of gold-nanorods promotes identification of M1/M2 subtype of macrophage by flow cytometry*. in *Symposium on Nanoscale Imaging, Sensing, and Actuation for Biomedical Applications, held at SPIE BiOS Conference*. 2020. San Francisco, CA.
52. Davis, J. and V.J.J.o.B.C. Bennett, *Human erythrocyte clathrin and clathrin-uncoating protein*. 1985. **260**(27): p. 14850-14856.
53. Janetanakit, W., et al., *Gold-Embedded Hollow Silica Nanogolf Balls for Imaging and Photothermal Therapy*. *Acs Applied Materials & Interfaces*, 2017. **9**(33): p. 27533-27543.
54. Atukorale, P.U., et al., *Influence of the glycocalyx and plasma membrane composition on amphiphilic gold nanoparticle association with erythrocytes*. *Nanoscale*, 2015. **7**(26): p. 11420-11432.
55. Sahoo, K., et al., *Molecular and Biocompatibility Characterization of Red Blood Cell Membrane Targeted and Cell-Penetrating-Peptide-Modified Polymeric Nanoparticles*. *Molecular Pharmaceutics*, 2017. **14**(7): p. 2224-2235.
56. Abo-Zeid, Y. and M.C. Garnett, *Polymer nanoparticle as a delivery system for ribavirin: Do nanoparticle avoid uptake by Red Blood Cells?* *Journal of Drug Delivery Science and Technology*, 2020. **56**.

57. Ding, L., et al., *Size, Shape, and Protein Corona Determine Cellular Uptake and Removal Mechanisms of Gold Nanoparticles*. *Small*, 2018. **14**(42).
58. Rejman, J., et al., *Size-dependent internalization of particles via the pathways of clathrin- and caveolae-mediated endocytosis*. 2004. **377**(1): p. 159-169.
59. Gustafson, H.H., et al., *Nanoparticle uptake: the phagocyte problem*. *Nano today*, 2015. **10**(4): p. 487-510.
60. Shukla, R., et al., *Biocompatibility of gold nanoparticles and their endocytotic fate inside the cellular compartment: A microscopic overview*. *Langmuir*, 2005. **21**(23): p. 10644-10654.
61. Ma, X., et al., *Colloidal gold nanoparticles induce changes in cellular and subcellular morphology*. *ACS nano*, 2017. **11**(8): p. 7807-7820.
62. Wu, M.Y., et al., *Size-dependent cellular uptake and localization profiles of silver nanoparticles*. *International Journal of Nanomedicine*, 2019. **14**: p. 4247-4259.
63. Yang, Y., et al., *Size-Dependent Transmembrane Transport of Gold Nanocages*. *ACS Omega*, 2020. **5**(17): p. 9864-9869.
64. Krpetic, Z., et al., *Phagocytosis of Biocompatible Gold Nanoparticles*. *Langmuir*, 2010. **26**(18): p. 14799-14805.
65. Hadji, H. and K. Bouchemal, *Effect of micro- and nanoparticle shape on biological processes*. *Journal of Controlled Release*, 2021.
66. Huang, X.L., et al., *The effect of the shape of mesoporous silica nanoparticles on cellular uptake and cell function*. *Biomaterials*, 2010. **31**(3): p. 438-448.
67. Meng, H., et al., *Aspect ratio determines the quantity of mesoporous silica nanoparticle uptake by a small GTPase-dependent macropinocytosis mechanism*. *ACS nano*, 2011. **5**(6): p. 4434-4447.
68. Champion, J.A. and S. Mitragotri, *Shape induced inhibition of phagocytosis of polymer particles*. *Pharmaceutical research*, 2009. **26**(1): p. 244-249.
69. Rayavarapu, R.G., et al., *In vitro toxicity studies of polymer-coated gold nanorods*. 2010. **21**(14): p. 145101.
70. Huff, T.B., et al., *Controlling the cellular uptake of gold nanorods*. 2007. **23**(4): p. 1596-1599.
71. Nativo, P., I.A. Prior, and M.J.A.n. Brust, *Uptake and intracellular fate of surface-modified gold nanoparticles*. 2008. **2**(8): p. 1639-1644.
72. Liu, Y., et al., *Synthesis, stability, and cellular internalization of gold nanoparticles containing mixed peptide- poly (ethylene glycol) monolayers*. 2007. **79**(6): p. 2221-2229.
73. Li, Y. and N.A. Monteiro-Riviere, *Mechanisms of cell uptake, inflammatory potential and protein corona effects with gold nanoparticles*. *Nanomedicine*, 2016. **11**(24): p. 3185-3203.
74. Cheng, X.J., et al., *Protein Corona Influences Cellular Uptake of Gold Nanoparticles by Phagocytic and Nonphagocytic Cells in a Size-Dependent Manner*. *ACS Applied Materials & Interfaces*, 2015. **7**(37): p. 20568-20575.
75. Chauhan, V.P., et al., *Delivery of molecular and nanoscale medicine to tumors: transport barriers and strategies*. *Annu Rev Chem Biomol Eng*, 2011. **2**(1): p. 281-298.
76. Dewhirst, M.W. and T.W. Secomb, *Transport of drugs from blood vessels to tumour tissue*. *Nature Reviews Cancer*, 2017. **17**(12): p. 738-750.
77. Gao, Y., et al., *Advances in mathematical models of the active targeting of tumor cells by functional nanoparticles*. *Computer Methods and Programs in Biomedicine*, 2020. **184**: p. 105106.
78. Tan, J., A. Thomas, and Y. Liu, *Influence of red blood cells on nanoparticle targeted delivery in microcirculation*. *Soft matter*, 2012. **8**(6): p. 1934-1946.

79. Sohrabi, S., et al., *Numerical simulation of particle transport and deposition in the pulmonary vasculature*. Journal of biomechanical engineering, 2014. **136**(12): p. 121010.
80. Müller, K., D.A. Fedosov, and G. Gompper, *Margination of micro-and nano-particles in blood flow and its effect on drug delivery*. Scientific reports, 2014. **4**(1): p. 1-8.
81. Shah, S., et al., *Modeling particle shape-dependent dynamics in nanomedicine*. Journal of nanoscience and nanotechnology, 2011. **11**(2): p. 919-928.
82. Li, Y., et al., *Multiscale modeling and uncertainty quantification in nanoparticle-mediated drug/gene delivery*. Computational Mechanics, 2014. **53**(3): p. 511-537.
83. Liu, Y., S. Shah, and J. Tan, *Computational modeling of nanoparticle targeted drug delivery*. Reviews in Nanoscience and Nanotechnology, 2012. **1**(1): p. 66-83.
84. Tan, J., et al., *The influence of size, shape and vessel geometry on nanoparticle distribution*. Microfluidics and nanofluidics, 2013. **14**(1): p. 77-87.
85. Tan, J., et al., *Coupled particulate and continuum model for nanoparticle targeted delivery*. Computers & structures, 2013. **122**: p. 128-134.
86. Lee, T.-R., et al., *On the near-wall accumulation of injectable particles in the microcirculation: smaller is not better*. Scientific reports, 2013. **3**(1): p. 1-8.
87. Decuzzi, P., et al., *Intravascular delivery of particulate systems: does geometry really matter?* Pharmaceutical research, 2009. **26**(1): p. 235-243.
88. Hyakutake, T. and S. Nagai, *Numerical simulation of red blood cell distributions in three-dimensional microvascular bifurcations*. Microvascular research, 2015. **97**: p. 115-123.
89. Breitner, E.K., et al., *Implementation of physiological fluids to provide insight into the characterization, fate, and biological interactions of silver nanoparticles*. Nanotechnology, 2018. **29**(25): p. 254001.
90. Braun, N.J., et al., *Implementation of a dynamic co-culture model abated silver nanoparticle interactions and nanotoxicological outcomes in vitro*. Nanomaterials, 2021. **11**(7): p. 1807.
91. Lu, R.X.Z., et al., *Heart-on-a-Chip Platform for Assessing Toxicity of Air Pollution Related Nanoparticles*. Advanced Materials Technologies, 2021. **6**(2).
92. Mathur, A., et al., *Human iPSC-based cardiac microphysiological system for drug screening applications*. Scientific reports, 2015. **5**(1): p. 1-7.
93. Qiu, Y., et al., *Microvasculature-on-a-chip for the long-term study of endothelial barrier dysfunction and microvascular obstruction in disease*. Nature biomedical engineering, 2018. **2**(6): p. 453-463.
94. Kayal, S. and R.V. Ramanujan, *Anti-cancer drug loaded iron-gold core-shell nanoparticles (Fe@ Au) for magnetic drug targeting*. Journal of nanoscience and nanotechnology, 2010. **10**(9): p. 5527-5539.
95. Almeida, J.P.M., et al., *In vivo biodistribution of nanoparticles*. Nanomedicine, 2011. **6**(5): p. 815-835.
96. Li, M., et al., *Physiologically based pharmacokinetic modeling of nanoparticles*. ACS Nano **4**, 6303–6317 (2010).
97. Alexis, F., et al., *Factors affecting the clearance and biodistribution of polymeric nanoparticles*. 2008. **5**(4): p. 505-515.
98. Owens III, D.E. and N.A.J.I.j.o.p. Peppas, *Opsonization, biodistribution, and pharmacokinetics of polymeric nanoparticles*. 2006. **307**(1): p. 93-102.
99. Moghimi, S.M., A.C. Hunter, and J.C.J.P.r. Murray, *Long-circulating and target-specific nanoparticles: theory to practice*. 2001. **53**(2): p. 283-318.
100. Lin, Z., et al., *Pharmacokinetics of metallic nanoparticles*. 2015. **7**(2): p. 189-217.

101. De Jong, W.H., et al., *Particle size-dependent organ distribution of gold nanoparticles after intravenous administration*. 2008. **29**(12): p. 1912-1919.
102. Sonavane, G., et al., *Biodistribution of colloidal gold nanoparticles after intravenous administration: effect of particle size*. 2008. **66**(2): p. 274-280.
103. Balasubramanian, S.K., et al., *Biodistribution of gold nanoparticles and gene expression changes in the liver and spleen after intravenous administration in rats*. 2010. **31**(8): p. 2034-2042.
104. Semmler-Behnke, M., et al., *Biodistribution of 1.4- and 18-nm gold particles in rats*. 2008. **4**(12): p. 2108-2111.
105. Sun, G., et al., *Facile, efficient approach to accomplish tunable chemistries and variable biodistributions for shell cross-linked nanoparticles*. 2008. **9**(7): p. 1997-2006.
106. Frigell, J., et al., *<sup>68</sup>Ga-labeled gold glyconanoparticles for exploring blood–brain barrier permeability: preparation, biodistribution studies, and improved brain uptake via neuropeptide conjugation*. 2014. **136**(1): p. 449-457.
107. Hirn, S., et al., *Particle size-dependent and surface charge-dependent biodistribution of gold nanoparticles after intravenous administration*. 2011. **77**(3): p. 407-416.
108. Malugin, A. and H.J.J.o.A.T.A.I.J. Ghandehari, *Cellular uptake and toxicity of gold nanoparticles in prostate cancer cells: a comparative study of rods and spheres*. 2010. **30**(3): p. 212-217.
109. Sindhvani, S., et al., *Three-dimensional optical mapping of nanoparticle distribution in intact tissues*. 2016. **10**(5): p. 5468-5478.
110. Tan, J., et al., *The influence of size, shape and vessel geometry on nanoparticle distribution*. 2013. **14**(1): p. 77-87.
111. Cho, E.C., Q. Zhang, and Y.N. Xia, *The effect of sedimentation and diffusion on cellular uptake of gold nanoparticles*. *Nature Nanotechnology*, 2011. **6**(6): p. 385-391.
112. Feliu, N., et al., *Quantitative Particle-Cell Interaction: Some Basic Physicochemical Pitfalls*. *Langmuir*, 2017. **33**(27): p. 6639-6646.
113. Han, J., et al., *Acute and chronic shear stress differently regulate endothelial internalization of nanocarriers targeted to platelet-endothelial cell adhesion molecule-1*. 2012. **6**(10): p. 8824-8836.
114. Khan, O.F. and M.V.J.B.m. Sefton, *Endothelial cell behaviour within a microfluidic mimic of the flow channels of a modular tissue engineered construct*. 2011. **13**(1): p. 69-87.
115. Nagy, J.A., H.F.J.C. Dvorak, and e. metastasis, *Heterogeneity of the tumor vasculature: the need for new tumor blood vessel type-specific targets*. 2012. **29**(7): p. 657-662.
116. Hühn, J., et al., *Selected Standard Protocols for the Synthesis, Phase Transfer, and Characterization of Inorganic Colloidal Nanoparticles*. *Chemistry of Materials*, 2017. **29**(1): p. 399-461.
117. Brust, M., et al., *Synthesis of thiol-derivatised gold nanoparticles in a two-phase liquid–liquid system*. 1994(7): p. 801-802.
118. Lin, C.A.J., et al., *Design of an amphiphilic polymer for nanoparticle coating and functionalization*. 2008. **4**(3): p. 334-341.
119. Thanh, N.T., N. Maclean, and S.J.C.r. Mahiddine, *Mechanisms of nucleation and growth of nanoparticles in solution*. 2014. **114**(15): p. 7610-7630.
120. Viswanatha, R., et al., *Growth mechanism of nanocrystals in solution: ZnO, a case study*. 2007. **98**(25): p. 255501.
121. Yin, Y. and A.P.J.N. Alivisatos, *Colloidal nanocrystal synthesis and the organic–inorganic interface*. 2005. **437**(7059): p. 664-670.



122. Bastús, N.G., J. Comenge, and V.J.L. Puentes, *Kinetically controlled seeded growth synthesis of citrate-stabilized gold nanoparticles of up to 200 nm: size focusing versus Ostwald ripening*. 2011. **27**(17): p. 11098-11105.
123. Ye, X., et al., *Using binary surfactant mixtures to simultaneously improve the dimensional tunability and monodispersity in the seeded growth of gold nanorods*. 2013. **13**(2): p. 765-771.
124. del Pino, P., et al., *Basic Physicochemical Properties of Polyethylene Glycol Coated Gold Nanoparticles that Determine Their Interaction with Cells*. *Angewandte Chemie-International Edition*, 2016. **55**(18): p. 5483-5487.
125. Roy, S., et al., *Lysosomal Proton Buffering of Poly(ethylenimine) Measured In Situ by Fluorescent pH-Sensor Microcapsules*. *ACS Nano*, 2020. **14**(7): p. 8012-8023.
126. Sun, X., et al., *Tracking stem cells and macrophages with gold and iron oxide nanoparticles—The choice of the best suited particles*. 2019. **15**: p. 267-279.
127. Cohen, L.S. and G.P. Studzinski, *CORRELATION BETWEEN CELL ENLARGEMENT AND NUCLEIC ACID AND PROTEIN CONTENT OF HELA CELLS IN UNBALANCED GROWTH PRODUCES BY INHIBITORS OF DNA SYNTHESIS*. *Journal of Cellular Physiology*, 1967. **69**(3): p. 331-+.
128. Rivera-Gil, P., et al., *The Challenge To Relate the Physicochemical Properties of Colloidal Nanoparticles to Their Cytotoxicity*. *Accounts of Chemical Research*, 2013. **46**(3): p. 743-749.
129. van Oss, C.J.J.O.D.S.A., *A review of "Intermolecular and Surface Forces, Jacob N. Israelachvili. Academic Press, London, 1991. Pp. xxi+ 450; hardbound, \$49.95. 1992.* **13**(6): p. 718-719.
130. Zhang, F., et al., *Ion and pH Sensing with Colloidal Nanoparticles: Influence of Surface Charge on Sensing and Colloidal Properties*. *Chemphyschem*, 2010. **11**(3): p. 730-735.
131. Bao, G. and X.R.J.P.o.t.N.A.o.S. Bao, *Shedding light on the dynamics of endocytosis and viral budding*. 2005. **102**(29): p. 9997-9998.
132. Deserno, M. and W.M.J.T.J.o.P.C.B. Gelbart, *Adhesion and wrapping in colloid-vesicle complexes*. 2002. **106**(21): p. 5543-5552.
133. Gao, H., W. Shi, and L.B.J.P.o.t.N.A.o.S. Freund, *Mechanics of receptor-mediated endocytosis*. 2005. **102**(27): p. 9469-9474.
134. Tzlil, S., et al., *A statistical-thermodynamic model of viral budding*. 2004. **86**(4): p. 2037-2048.
135. Xia, Y., et al., *Novel functionalized selenium nanoparticles for enhanced anti-hepatocarcinoma activity in vitro*. 2015. **10**(1): p. 1-14.
136. Hanada, S., et al., *Cell-based in vitro blood-brain barrier model can rapidly evaluate nanoparticles' brain permeability in association with particle size and surface modification*. 2014. **15**(2): p. 1812-1825.
137. Liu, X.S., et al., *Minimizing nonspecific phagocytic uptake of biocompatible gold nanoparticles with mixed charged zwitterionic surface modification*. *Journal of Materials Chemistry*, 2012. **22**(5): p. 1916-1927.
138. Yan, H., et al., *Influence of the chirality of carbon nanodots on their interaction with proteins and cells*. 2021. **12**(1): p. 1-14.
139. Win, K.Y. and S.-S.J.B. Feng, *Effects of particle size and surface coating on cellular uptake of polymeric nanoparticles for oral delivery of anticancer drugs*. 2005. **26**(15): p. 2713-2722.
140. Antonelli, A., et al., *Red blood cells as carriers in magnetic particle imaging*. *Biomedical Engineering-Biomedizinische Technik*, 2013. **58**(6): p. 517-525.

141. Lau, I.P., et al., *In vitro effect of CTAB- and PEG-coated gold nanorods on the induction of eryptosis/erythroptosis in human erythrocytes*. *Nanotoxicology*, 2012. **6**(8): p. 847-856.
142. Jiang, Q., et al., *Erythrocyte-cancer hybrid membrane-camouflaged melanin nanoparticles for enhancing photothermal therapy efficacy in tumors*. *Biomaterials*, 2019. **192**: p. 292-308.
143. Piao, J.G., et al., *Erythrocyte Membrane Is an Alternative Coating to Polyethylene Glycol for Prolonging the Circulation Lifetime of Gold Nanocages for Photothermal Therapy*. *ACS Nano*, 2014. **8**(10): p. 10414-10425.
144. Rao, L., et al., *Synthetic nanoparticles camouflaged with biomimetic erythrocyte membranes for reduced reticuloendothelial system uptake*. *Nanotechnology*, 2016. **27**(8).
145. Zhou, G., et al., *Quantitative analysis of gold and carbon nanoparticles in mammalian cells by flow cytometry light scattering*. *Journal of Nanoparticle Research*, 2017. **19**(2).
146. Wang, S.H., et al., *Dose dependent distribution and aggregation of gold nanoparticles within human lung adeno-carcinoma cells*. *RSC Advances*, 2015. **5**(119): p. 98309-98317.
147. Hemingway, J.J.P.T.o.t.R.S.B.B.S., *The role of vector control in stopping the transmission of malaria: threats and opportunities*. 2014. **369**(1645): p. 20130431.
148. Mnzava, A.P., et al., *Implementation of the global plan for insecticide resistance management in malaria vectors: progress, challenges and the way forward*. 2015. **14**(1): p. 1-9.
149. Ranson, H., et al., *Pyrethroid resistance in African anopheline mosquitoes: what are the implications for malaria control?* 2011. **27**(2): p. 91-98.
150. Ardanuy, M., et al., *Preparation of durable insecticide cotton fabrics through sol-gel treatment with permethrin*. *Surface & Coatings Technology*, 2014. **239**: p. 132-137.
151. Aziz, A., *A comparative study and characterization of Azadirachta indica mediated nano-insecticide and ethanolic extract against mosquito vectors - Arabian and Indian strains*. *Entomological Research*, 2021. **51**(11): p. 559-567.
152. Benelli, G., *On a Magical Mystery Tour of Green Insecticide Research: Current Issues and Challenges*. *Molecules*, 2020. **25**(21).
153. Duarte, J.L., et al., *Botanical insecticide-based nanosystems for the control of Aedes (Stegomyia) aegypti larvae*. *Environmental Science and Pollution Research*, 2020. **27**(23): p. 28737-28748.
154. Parthiban, E., et al., *Biocompatible green synthesized silver nanoparticles impact on insecticides resistant developing enzymes of dengue transmitted mosquito vector*. *SN Applied Sciences*, 2019. **1**(10).
155. Zhang, Y.F., et al., *Self-assembled mixed micelle loaded with natural pyrethrins as an intelligent nano-insecticide with a novel temperature-responsive release mode*. *Chemical Engineering Journal*, 2019. **361**: p. 1381-1391.
156. Paquette, C.C., et al., *Biodistribution and trafficking of hydrogel nanoparticles in adult mosquitoes*. 2015. **9**(5): p. e0003745.
157. Hecker, H.J.C. and t. research, *Structure and function of midgut epithelial cells in Culicidae mosquitoes (Insecta, Diptera)*. 1977. **184**(3): p. 321-341.
158. Piermarini, P.M., et al., *Malpighian tubules as novel targets for mosquito control*. 2017. **14**(2): p. 111.
159. Schwarz, G., et al., *DOTA based metal labels for protein quantification: a review*. 2014. **29**(2): p. 221-233.
160. Sosabowski, J.K. and S.J.J.N.p. Mather, *Conjugation of DOTA-like chelating agents to peptides and radiolabeling with trivalent metallic isotopes*. 2006. **1**(2): p. 972-976.

161. Briegel, H.J.J.o.i.p., *Mosquito reproduction: incomplete utilization of the blood meal protein for oögenesis*. 1985. **31**(1): p. 15-21.
162. Briegel, H.J.J.o.i.p., *Protein catabolism and nitrogen partitioning during oögenesis in the mosquito Aedes aegypti*. 1986. **32**(5): p. 455-462.
163. Briegel, H.J.J.o.i.p., *Metabolic relationship between female body size, reserves, and fecundity of Aedes aegypti*. 1990. **36**(3): p. 165-172.
164. France, K.R. and C.J.J.o.I.P. Judson, *Nitrogen partitioning and blood meal utilization by Aedes aegypti (Diptera Culicidae)*. 1979. **25**(11): p. 841-846.
165. Tan, S.H. and G.J.A.S. Horlick, *Background spectral features in inductively coupled plasma/mass spectrometry*. 1986. **40**(4): p. 445-460.
166. Vanhoe, H.J.J.o.t.e., e.i. health, and disease, *A review of the capabilities of ICP-MS for trace element analysis in body fluids and tissues*. 1993. **7**(3): p. 131-139.
167. Haiss, W., Thanh, N. T., Aveyard, J., & Fernig, D. G. (2007). Determination of size and concentration of gold nanoparticles from UV– Vis spectra. *Analytical chemistry*, **79**(11), 4215-4221.

## 7. Publications

1. Roy, S., Liu, Z., Sun, X., Gharib, M., Yan, H., **Huang, Y.**, & ...Parak, W. J. (2019). Assembly and degradation of inorganic nanoparticles in biological environments. *Bioconjugate Chemistry*, 30(11), 2751-2762.
2. Sanchez-Cano C, Alvarez-Puebla RA, Abendroth JM, Beck T, Blick R, Cao Y, Caruso F, Chakraborty I, Chapman HN, Chen C, Cohen BE, Conceição ALC, Cormode DP, Cui D, Dawson KA, Falkenberg G, Fan C, Feliu N, Gao M, Gargioni E, Glüer CC, Grüner F, Hassan M, Hu Y, **Huang Y**, Huber S, Huse N, Kang Y, Khademhosseini A, Keller TF, Körnig C, Kotov NA, Koziej D, Liang XJ, Liu B, Liu S, Liu Y, Liu Z, Liz-Marzán LM, Ma X, Machicote A, Maison W, Mancuso AP, Megahed S, Nickel B, Otto F, Palencia C, Pascarelli S, Pearson A, Peñate-Medina O, Qi B, Rädler J, Richardson JJ, Rosenhahn A, Rothkamm K, Rübhausen M, Sanyal MK, Schaak RE, Schlemmer HP, Schmidt M, Schmutzler O, Schotten T, Schulz F, Sood AK, Spiers KM, Staufer T, Stemer DM, Stierle A, Sun X, Tsakanova G, Weiss PS, Weller H, Westermeier F, Xu M, Yan H, Zeng Y, Zhao Y, Zhao Y, Zhu D, Zhu Y, Parak WJ. X-ray-Based Techniques to Study the Nano-Bio Interface. *ACS Nano*. 2021 Mar 23;15(3):3754-3807. doi: 10.1021/acsnano.0c09563. Epub 2021 Mar 2. PMID: 33650433; PMCID: PMC7992135.
3. Kang, Y., Nack, L. M., Liu, Y., Qi, B., **Huang, Y.**, Liu, Z., ... & Parak, W. J. (2022). Quantitative considerations about the size dependence of cellular entry and excretion of colloidal nanoparticles for different cell types. *ChemTexts*, 8(1), 1-8.
4. A significant part of this work is in preparation for submission: Yalan Huang, Xing Sun, Sabine Vidal-Y-Sy, Christian Gorzelanny, Neus Feliu, Wolfgang Parak, Cellular Uptake of Nanoparticles: the Impact of the exposure conditions.

## 8. Acknowledgements

Sincere thanks should be given to my supervisors Prof. Wolfgang J. Parak, and Dr. Neus Feliu for the continuous assistance and support of my doctorate studies in Center for Hybrid Nanostructure (CHyN), Chemistry department in Hamburg University.

Firstly, I would express my sincere thanks to Prof. Wolfgang J. Parak for allowing me to study in his group during my PhD period. It is an interdisciplinary group with free access to many advanced scientific instruments and it is my great honor to become a member of his group. Besides, thanks to his great support and professional guidance on my Ph.D. projects.

And I will also thank Dr. Neus Feliu for offering me continuous help on my Ph.D. projects and for all her patient discussion and warm caring all the time.





I would like to thank Yang Liu for helping me with the ICP-MS measurement. And I want to thank Marta Gallego for the TEM measurement. And I want to thank Xing Sun for the cooperation work in the uptake of Au NP/NRs in Static, Dynamic, and Fluid systems. And I want to thank Arne Krüger for the Red Blood Cells uptake experiments. I want to thank Dr. Stephanie Jansen and Dr. Anna Heitmann for the operation with the mosquitoes. And I also want to thank Bing Qi for the measurement of the standard curve for the BSA concentration calculation based on the Coomassie assay.


















I want to express sincere thanks to my parents, who always encourage me and also take care of me all the time.

I want to thank all my colleagues and my friends for their help with the lab instruments maintenance and lab items supply.







## 9. List of hazardous substances

Chemical	GHS Symbol	Hazardous statement	Precautionary statement
Dulbecco's modified eagle medium		Not hazardous substance or mixture	
Penicillin/streptomycin		Not hazardous substance or mixture	
Fetal bovine serum		Not hazardous substance or mixture	
Resazurin		Not hazardous substance or mixture	
Phosphate buffered saline		Not hazardous substance or mixture	
0.05% trypsin/EDTA		Not hazardous substance or mixture	
Bovine serum albumin		Not a hazardous substance or mixture	
Sodium chloride		Not a hazardous substance or mixture	
Europium(III) chloride		Not a hazardous substance or mixture	
poly(isobutylene-altmaleic anhydride)		Not a hazardous substance or mixture	
Sodium citrate dihydrate C <sub>6</sub> H <sub>5</sub> Na <sub>3</sub> O <sub>7</sub> · 2H <sub>2</sub> O		Not a hazardous substance or mixture	
Tetraoctylammonium bromide		Not a hazardous substance or mixture	
RPMI 1640		Not a hazardous substance or mixture	
Sodium Bromide		Not a hazardous substance or mixture	
Fructose		Not a hazardous substance or mixture	
Gold(III) chloride trihydrate HAuCl <sub>4</sub> · 3H <sub>2</sub> O	 - Danger	H314, H317	P260, P264, P272, P280, P301, P330, P331, P303, P361, P353, P304, P340, P310, P305, P351,

				P338, P310, P333, P313, P362, P364, P405, P501
Poly(ethylene glycol) methyl ether thiol CH <sub>3</sub> O(CH <sub>2</sub> CH <sub>2</sub> O) <sub>n</sub> CH <sub>2</sub> CH <sub>2</sub> SH	 warning	H315, H319, H335		P261, P264, P271, P280, P302+P352, P304+P340+P312, P305+P351+P338, P333+P313, P337+P313, P362+P364, P403+P233, P405, P501
Dodecylamine CH <sub>3</sub> (CH <sub>2</sub> ) <sub>11</sub> NH <sub>2</sub>	 Danger	H304, H335, H410	H314, H373,	P260, P264, P271, P273, P280, P301+P310, P301+P330+P331, P303+P361+P353, P304+P340+P310, P305+P351+P338+P310, P314, P363, P391, P403+P233, P405, P501
Chloroform CHCl <sub>3</sub>	 Danger	H302, H319, H336, H361, H412	H315, H331, H351, H372,	P201, P202, P260, P264, P270, P271, P273, P280, P301+P312+P330, P302+P352, P304+P340+P338, P308+P313, P332+P313, P337+P313, P362+P364, P403+P233, P405, P501
Sodium hydroxide NaOH	 Danger	H290, H402	H314,	P234, P260, P264, P273, P280, P301+P330+P331, P303+P361+P353, P304+P340+P310, P305+P351+P338, P337+P313, P363, P390, P405, P501

Tetrahydrofuran C <sub>4</sub> H <sub>8</sub> O	   Danger	H225, H302, H319, H335, H336, H351,	P201, P202, P210, P233, P240, P241, P243, P261, P264, P270, P271, P280, P301+P312+P330, P303+P361+P353, P304+P340+P312, P305+P351+P338, P308+P313, P337+P313, P370+P378, P403+P233, P403+P235, P405, P501
Ethanol C <sub>2</sub> H <sub>6</sub> O	  Danger	H225, H319	P210, P305+P351+P338, P337+P313, P403+P235
Sodium borohydride	    Danger	H260,H301,H314 ,H318,H360FD	P231+P232, P260, P280, P303+P361+P353, P304+P340+P310, P305+P351+P338,
Toluene	   Danger	H225, H304, H315, H336, H 361d, H373, H412	P202, P210, P273, P301+P310, P303+P361+P353, P331
Hydrochloric Acid	  Danger	H2901, H314, H335	P234, P261, P271, P280, P303+P361+P353, P305+P350+P338
1-dodecanethiol	   Danger	H314, H317	P261, P272, P280, P303+P361+P353, P305+P351+P338



Methanol	   Danger	H225, H301+H311+H331, H370	P210, P233, P280, P301+P310, P303+P361+P353, P304+P340+P311
Potassium iodide	 Danger	H372	P260, P264, P270, P314, P501
Coomassie (Bradford) Protein Assay Kit	  Warning	H290, H315, H319, H371	P234, P260P264, P302+P352, P305+P351+P338, P308+P311

## Declaration on Oath

I hereby declare that this doctoral dissertation is my own work and that I have not used any sources other than the acknowledged resources and aids.

Date, 24. April. 2023

Signature 